

# Intraspecific predator interference promotes biodiversity in ecosystems

Ju Kang<sup>1†</sup>, Shijie Zhang<sup>2,3†</sup>, and Xin Wang<sup>1\*</sup>

1.School of Physics, Sun Yat-sen University, Guangzhou 510275, China

2.School of Mathematics, Sun Yat-sen University, Guangzhou 510275, China

3.Department of Mechanical Engineering, Massachusetts Institute of Technology, Cambridge, MA 02139, USA

†These authors contributed equally to this work

\*Corresponding author. E-mail: wangxin36@mail.sysu.edu.cn

Explaining biodiversity is a fundamental issue in ecology. A long-standing puzzle lies in the paradox of the plankton: many species of plankton feeding on a limited type of resources coexist, apparently flouting Competitive Exclusion Principle (CEP), which holds that the number of predator (consumer) species cannot exceed that of the resources at steady state. Here we present a mechanistic model, and show that the intraspecific interference among the consumers enables strikingly a plethora of consumer species to coexist at constant population densities with only one or a handful of resource species. The facilitated biodiversity is resistant to stochasticity, either with stochastic simulation algorithm or individual-based modeling. Our model naturally explains the classical experiments that invalidate CEP, quantitatively illustrates the universal S shape pattern of the rank-abundance curves across a wide range of ecological communities, and can be broadly used to resolve the mystery of biodiversity in many natural ecosystems.

## I. INTRODUCTION

The most prominent feature of life on Earth is its remarkable species diversity: countless macro- and micro-species fill every corner on land and in the water [1–4]. In tropical forests, thousands of plant and vertebrate species coexist [2]. Within only a gram of soil, the number of microbial species is estimated to be 2,000-18,000 [4]. In the photic zone of the world ocean, there are roughly 150,000 eukaryotic plankton species [3]. Explaining the astonishing biodiversity is a major focus in ecology [1]. A great challenge stems from the well-known Competitive Exclusion Principle (CEP): two species competing for a single type of resources cannot coexist at constant population densities [5, 6], or generically, the number of consumers species cannot exceed that of resources at steady state [7, 8]. On the contrary, in the paradox of plankton, a limited type of resources support hundreds or more coexisting species of phytoplankton [9]. Then, how can plankton and many other organisms somehow liberate the constraint of CEP?

Early since MacArthur and Levin proposed the classical mathematical proof for CEP in the 1960s [7], various mechanisms have been put forward to overcome the limit set by CEP [10]. Some suggest that the system never approaches steady state where the CEP applies, due to temporal variations [9, 11], spatial heterogeneity [12], or species' self-organized dynamics [13, 14]. Others consider factors such as toxin [15], cross feeding [16, 17], spatial circulation [18, 19], kill the winner [20], pack hunting [21], collective behavior [22], metabolic trade-offs [23, 24], co-evolution [25], and other complex interactions among the species [26–31]. However, questions remain as to what determines species diversity in nature, especially for quasi-well-mixed systems such as that for the plankton [1, 32].

In this work, we present a mechanistic model of predator interference that extends the classical Beddington-DeAngelis (B-D) phenomenological model [26, 27] with a detailed consideration of the pairwise encounter. Through forming the intraspecific interference pair that effectively constitutes a negative feedback loop, a wide range of consumer species can coexist with only one or few types of resources. The coexistence state is resistant to stochasticity and hence can be realized in practice. Our model is broadly applicable and can be used to explain biodiversity in many ecosystems. In particular, it naturally explains species coexistence in classical experiments that invalidate CEP [33, 34], and quantitatively illustrates the S shape pattern of the rank-abundance curves in an extensive spectrum of ecological communities, ranging from the communities of ocean plankton [35, 36], river fishes [37], rainforest birds [38, 39], bats [40], butterflies [41], to those of desert bees [42] and lizards [37].

## II. RESULTS

### A. A generic model of pairwise encounter

Predator interference, i.e., the temporary pairwise encounter among consumer individuals such as a staring contest or a fight, is commonly described by the B-D model [26, 27]. From the mechanistic perspective, however, the functional response of the B-D model can be formally derived from the consumption between a consumer species and a resource species without involving any form of predator interference [21, 43] (see SI Sec. IIB for details). To resolve this issue, we consider a generic mechanistic model of pairwise encounter. Specifically,  $S_C$  consumer species  $\{C_1, \dots, C_{S_C}\}$  competing for  $S_R$  resource species  $\{R_1, \dots, R_{S_R}\}$ . The consumers are biotic, while the resources can be either biotic or abiotic. For simplicity, we assume that all species are motile

and each moves at a certain speed, namely,  $v_{C_i}$  for consumer species  $C_i$  ( $i = 1, \dots, S_C$ ) and  $v_{R_l}$  for resource species  $R_l$  ( $l = 1, \dots, S_R$ ). For abiotic resources, they cannot propel themselves, yet may passively drift due to environmental factors. Each consumer is free to feast on one or multiple types of resources, while consumers do not directly interact with one another other than pairwise encounters.

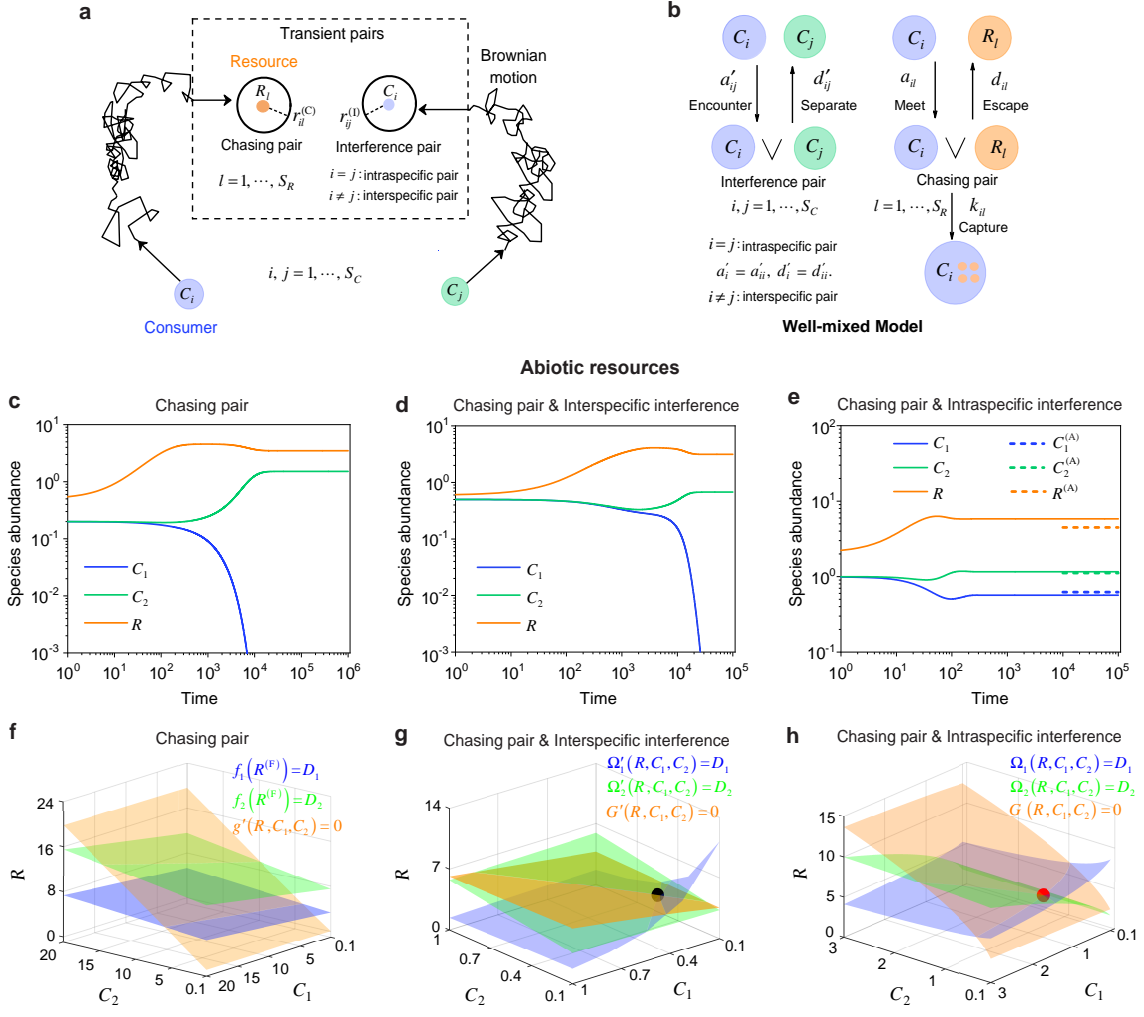


Figure 1. A model of pairwise encounter may naturally break Competitive Exclusion Principle (CEP). (a-b) A generic model of  $S_C$  consumer species competing for  $S_R$  resource species with pairwise encounter. (a) A consumer individual  $C_i$  moves randomly in space. It can form a chasing pair with a resource  $R_l$  when their distance is less than  $r_{il}^{(C)}$ , and form an interference pair with another consumer  $C_j$  when their distance is less than  $r_{ij}^{(I)}$ . (b) The well-mixed model of (a). (c-h) A simple case of two consumer species ( $S_C = 2$ ) feeding on one abiotic resource species ( $S_R = 1$ ). (c-e) Time courses of the species abundances in different scenarios. (f-h) Positive solutions to the steady-state equations:  $\dot{R} = 0$  (orange surface),  $\dot{C}_1 = 0$  (blue surface),  $\dot{C}_2 = 0$  (green surface). (c, f) In the scenario involving only chasing pair, the green and blue surfaces in (f) are parallel, and thus the consumer species cannot coexist at steady state (see (c) for time courses). (d, g) In the scenario involving chasing pair and interspecific interference, the three surfaces in (g) are unparallel and hence share a common point (shown in black). Yet this fixed point is unstable, and thus the consumer species still cannot coexist at steady state (see (d) for time courses). (e, h) In the scenario involving chasing pair and intraspecific interference, all surfaces in (h) are unparallel and therefore intersect at one point (shown in red). This fixed point is stable, and hence the consumer species may coexist at steady state (see (e) for time courses). The dotted lines in (e) are the analytical solutions of the species abundances at steady state (marked with superscript “(A)”) calculated from Eqs. S41 and S44. See SI Sec. VIII for simulation details.

Then, we proceed to explicitly consider the population structure of the consumers and resources: some are wandering around freely, taking Brownian motions; others are encountering with one another, forming ephemeral entangled pairs. Specifically, when a consumer individual  $C_i$  and a resource  $R_l$  get close in space within a distance of  $r_{il}^{(C)}$  (Figure 1a), the consumer can chase the resource and form a chasing pair, denoted as  $C_i^{(P)} \vee R_l^{(P)}$  (Figure 1b), where the superscript “(P)” represents pair. The resource can either escape with rate  $d_{il}$  or be caught and consumed by the consumer with rate  $k_{ij}$ . Meanwhile, when a  $C_i$  individual encounters another consumer  $C_j$  ( $j = 1, \dots, S_C$ ) of the same ( $i = j$ ) or a different ( $i \neq j$ ) species within a distance of  $r_{ij}^{(I)}$  (Figure 1a), they

can stare to, fight against or play with each other and thus form an interference pair, denoted as  $C_i^{(P)} \vee C_j^{(P)}$  (Figure 1b). The paired state is evanescent, two consumers separate from each other with rate  $d'_{il}$ . For simplicity, we assume that all  $r_{il}^{(C)}$  and  $r_{ij}^{(I)}$  are identical respectively, i.e.,  $\forall i, j, l, r_{il}^{(C)} = r^{(C)}$  and  $r_{ij}^{(I)} = r^{(I)}$ .

In a well-mixed system, the encounter rates among the species can be calculated with the mean-field approximation. For example, in a squared system with a length of  $L$ , the encounter rate between species  $C_i$  and  $R_l$  is  $a_{il} = 2r^{(C)}L^{-2}\sqrt{v_{C_i}^2 + v_{R_l}^2}$ , while that between species  $C_i$  and  $C_j$  is  $a'_{ij} = 2r^{(I)}L^{-2}\sqrt{v_{C_i}^2 + v_{C_j}^2}$  (see SI Sec. VII A and Figure S1 for details). Then, we can explicitly describe the population dynamics of the system. For clarity, we classify the scenarios into cases involving different types of pairwise encounters. Specifically, for a system involving only chasing pair:

$$\begin{cases} \dot{x}_{il} = a_{il}C_i^{(F)}R_l^{(F)} - (d_{il} + k_{il})x_{il}, \\ \dot{C}_i = \sum_{l=1}^{S_R} w_{il}k_{il}x_{il} - D_iC_i, \\ \dot{R}_l = g_l(\{R_l\}, \{x_i\}, \{C_i\}), i = 1, \dots, S_C, l = 1, \dots, S_R. \end{cases} \quad (1)$$

Here, the superscript “(F)” represents the populations that are freely wandering, while  $x_{il} \equiv C_i^{(P)} \vee R_l^{(P)}$  stands for the chasing pair.  $g_l$  is an unspecific function, while  $D_i$  and  $w_{il}$  are two constants, where  $D_i$  denotes the mortality rate of consumer  $C_i$ , and  $w_{il}$  is the mass conversion ratio [21] from resource  $R_l$  to consumer  $C_i$ . With the integration of intraspecific predator interference, we combine Eq. 1 and the following equation:

$$\dot{y}_i = a'_i[C_i^{(F)}]^2 - d'_iy_i, i = 1, \dots, S_C, \quad (2)$$

where  $a'_i = a'_{ii}$ ,  $d'_i = d'_{ii}$ , and  $y_i \equiv C_i^{(P)} \vee C_i^{(P)}$  represents the intraspecific interference pair. For a system involving chasing pair and interspecific interference, we combine Eq. 1 with the following equation:

$$\dot{z}_{ij} = a'_{ij}C_i^{(F)}C_j^{(F)} - d'_{ij}z_{ij}, i, j = 1, \dots, S_C, i \neq j, \quad (3)$$

where  $z_{ij} \equiv C_i^{(P)} \vee C_j^{(P)}$  stands for the interspecific interference pair. In the case where chasing pair and both intra- and inter-specific interference are all relevant, we combine Eqs. 1-3, and the populations of consumers and resources are given by  $C_i = C_i^{(F)} + \sum_l x_{il} + 2y_i + \sum_{j \neq i} z_{ij}$  and  $R_l = R_l^{(F)} + \sum_i x_{il}$ , respectively.

Generically, the consumption and interference processes are much quicker compared to the birth and death processes [21], and thus in the derivation of the functional response,  $\mathcal{F}(R_l, C_i) \equiv k_{il}x_{il}/C_i$  by the definition, the consumption and interference processes are supposed to be in fast equilibrium (i.e.,  $\dot{x}_{il} = 0$ ,  $\dot{y}_i = 0$  and  $\dot{z}_{ij} = 0$  wherever applies). For scenarios involving all different types of pairwise encounters, we find that the functional response in the B-D model is a valid approximation only for a special case (Figures S2-S4, referring to SI Sec. II for the rigorous forms and derivation details) with  $d_{il} = 0$  and  $R_l \gg \sum_{i=1}^{S_C} C_i$  ( $i = 1, \dots, S_C, l = 1, \dots, S_R$ ).

In Eq. 1, the explicit form of function  $g_l$  is unspecified. To facilitate further analysis, we assume that the population dynamics of the resources follow the same construction rule as that in the MacArthur’s consumer-resource model [44, 45]. Then,

$$g_l(\{R_l\}, \{x_i\}, \{C_i\}) = \begin{cases} R_0^{(l)}R_l(1 - R_l/K_0^{(l)}) - \sum_{i=1}^{S_C} k_{il}x_{il}, & \text{for biotic resources,} \\ R_a^{(l)}(1 - R_l/K_0^{(l)}) - \sum_{i=1}^{S_C} k_{il}x_{il}, & \text{for abiotic resources.} \end{cases} \quad (4)$$

In the absence of consumers, biotic resources follow logistic population growth. Therefore,  $R_0^{(l)}$  and  $K_0^{(l)}$  represent the intrinsic growth rate and the carrying capacity of consumer species  $R_l$ , respectively. For abiotic resources,  $R_a^{(l)}$  stands for the external resource supply rate of  $R_l$ , and  $K_0^{(l)}$  is the abundance of  $R_l$  at steady state without consumers. In fact, using dimensional analysis, we can make all parameters dimensionless (see SI Sec. VI). For convenience, we use the same notations below, while all parameters are dimensionless unless otherwise specified. PNG

## B. Intraspecific predator interference facilitates species coexistence and breaks CEP

To clarify the specific mechanism that can facilitate species coexistence, we systematically investigate the scenarios involving different forms of pairwise encounters in a simple case of  $S_C = 2$ ,  $S_R = 1$ , i.e., two consumer species  $C_i$  ( $i = 1, 2$ ) competing for one resource species  $R_l$  ( $l = 1$ ). To simplify the notations, we omit the “ $l$ ” in the sub-/super-scripts since  $S_R = 1$ . For clarity, we assign each consumer species of unique competitiveness by

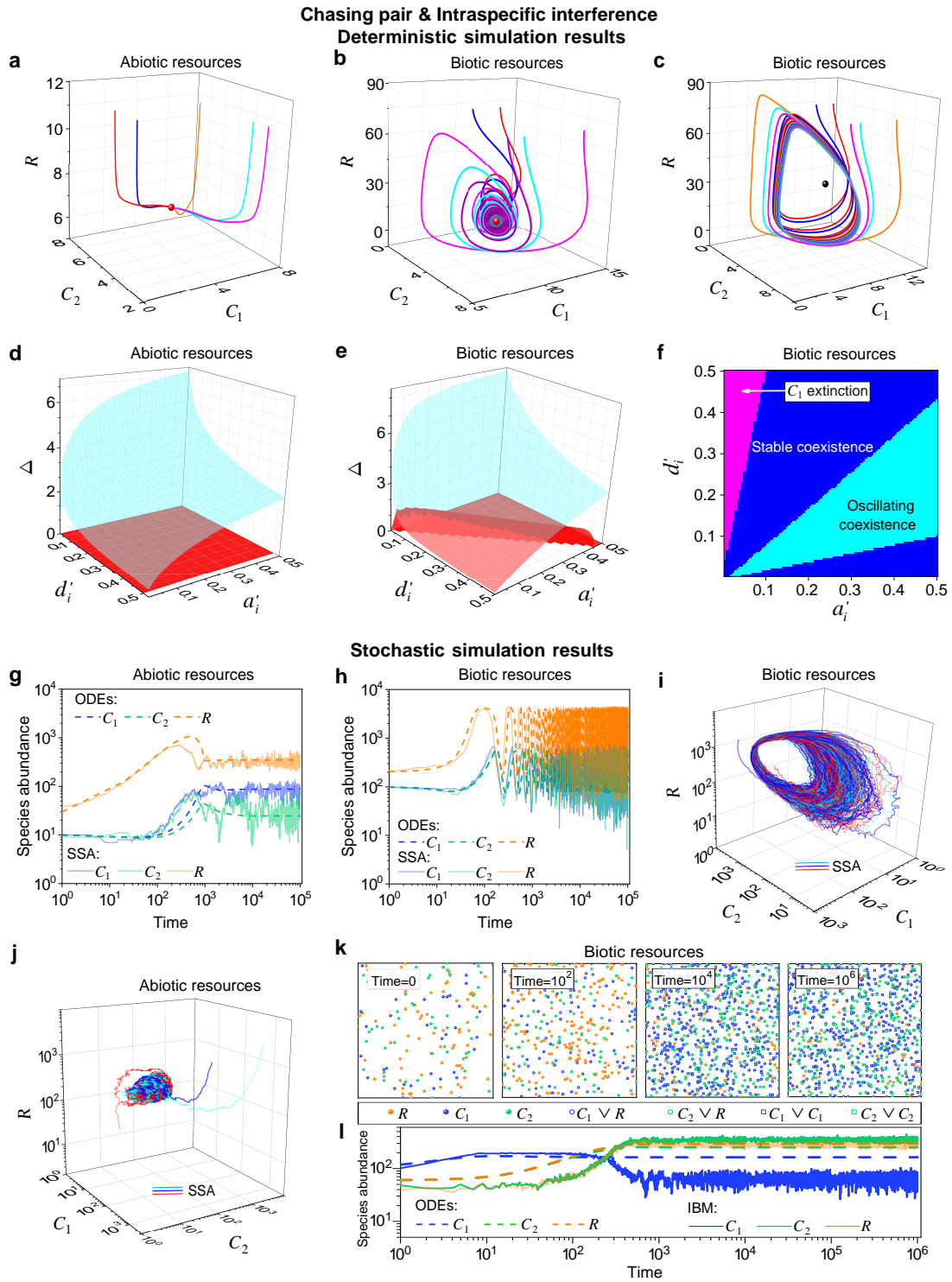


Figure 2. Intraspecific predator interference facilitates species coexistence regardless of stochasticity. Here we consider the case of  $S_C = 2$ ,  $S_R = 1$ . (a-c) Representative trajectories of species coexistence in the phase space simulated with ordinary differential equations (ODEs). (a-b) The fixed points (shown in red) are stable and globally attractive. (c) The fixed point (shown in black) is unstable, and all trajectories attract to a limit cycle. (d-e) 3D phase diagrams in the ODEs studies.  $D_i$  ( $i = 1, 2$ ) is the only parameter that varies with the two consumer species, and  $\Delta \equiv (D_1 - D_2)/D_2$  measures the competitive difference between the two species. The parameter region below the blue surface yet above the red surface represents stable coexistence. The region below the red surface and above  $\Delta = 0$  represents unstable fixed points, which may end in a limit cycle or  $C_1$  extinction. (f) An exemplified transection that corresponds to the  $\Delta = 1$  plane in (e). (g-h) Time courses of the species abundances simulated with ODEs or stochastic simulation algorithm (SSA). (i-j) Representative trajectories of species coexistence in the phase space simulated with SSA. (i) The stochastic limit cycle is stable. All species coexist in an oscillating way (see (h) for time courses). (j) The coexistence state is stable and globally attractive (see (g) for time courses). (k) Snapshots of the individual based modeling (IBM). (l) Time courses of the species abundances simulated with IBM. See SI Sec. VIII for simulation details.

the setting that the mortality rate  $D_i$  is the only parameter varying with the two consumer species, and define  $\Delta \equiv (D_1 - D_2)/D_2$  as the competitive difference.

First, we conduct the analysis in a deterministic framework with ordinary differential equations (ODEs). In the scenario involving only chasing pair, consistent with our previous study, consumer species can never coexist at steady state except for special parameter settings (sets of measure zero) [21]. In practice, if all species coexist, the steady-state equations of the consumer species ( $\dot{C}_i = 0$ ) yield  $f_i(R^{(F)}) \equiv R^{(F)}/(R^{(F)} + K_i) = D_i$  ( $i = 1, 2$ ), with  $K_i = (d_i + k_i)/a_i$ , which corresponds to two parallel surfaces in the  $(C_1, C_2, R)$  coordinate (Figure 1f, see also Figure S5a-b), making steady coexistence mission impossible (Figures 1c and S5c-d, see also S5a-b and Ref. [21] for details).

Meanwhile, in the scenario involving chasing pair and interspecific interference, if all species coexist, the steady-state equations of the species correspond to three non-parallel surfaces  $\Omega'_i(R, C_1, C_2) = D_i$  ( $i = 1, 2$ ),  $G'(R, C_1, C_2) = 0$  (Figures 1g, S6, see SI Sec. IV for details), which can intersect at a common point (fixed point). However, this fixed point is unstable (see Figure S6 and SI Sec. IV), and thus consumer species are still unable to coexist at constant population densities. With abiotic resources, one of the consumer species is doom to extinct (Figure 1d). Conversely, when the resources are biotic, both consumer species may coexist indefinitely with time series dynamics, namely, with periodic oscillation or quasi-periodic oscillation (Figure S7, ODEs results).

Next, we turn to the scenario involving chasing pair and intraspecific interference. Likewise, steady coexistence requires that three non-parallel surfaces  $\Omega_i(R, C_1, C_2) = D_i$  ( $i = 1, 2$ ),  $G(R, C_1, C_2) = 0$  (Figures 1h, S8a, b, see SI Sec. III for details) cross at a common point. Indeed, this naturally happens, and encouragingly the fixed point can be stable. Then, two consumer species can stably coexist at steady state with only one resource species, which obviously breaks CEP (Figures 1e, S9a). In fact, there exist one or multiple types of long-term coexisting patterns depending on the life form of the resources. With abiotic resources, the coexisting state is globally attractive (Figure 2a, d). When the resources are biotic, the coexisting state can be either globally attractive (Figure 2c) or unstable, and the population dynamics may end in a limit cycle (Figures 2c, S9b-c). In fact, for either life form of the resources, there exists a non-zero volume of parameter space where the two consumer species stably coexist at constant population densities (Figure 2d-f), demonstrating that the violation of CEP does not depend on special parameter settings.

We further consider the scenario involving chasing pair and both intra- and inter-specific interference (Figures S10-S12). Much as expected, the species coexistence behavior is very similar to that without interspecific interference.

### C. Intraspecific interference promotes biodiversity in the presence of stochasticity

To facilitate biodiversity in a real system, stochasticity naturally involves for its ubiquity in nature. However, recent studies show that stochasticity is prone to jeopardize species coexistence [25]. Influential mechanisms such as “kill the winner” fail when stochasticity is incorporated [25]. Consistent with this, we observe that two notable cases of oscillating coexistence [13, 14] turn into species extinction when stochasticity is introduced (Figure S13), where we simulate the models with stochastic simulation algorithm (SSA) [46] and adopt the same parameters as those in the original references [13, 14].

Then, we proceed to investigate the impact of stochasticity on the long-term coexisting behavior of our model using SSA. Specifically, in the scenario involving chasing pair and interspecific interference, the two consumer species fail to coexist along with stochasticity (Figure S7, SSA results). Conversely, in the scenario involving chasing pair and intraspecific interference, species may coexist indefinitely in the SSA simulations. To be more precise, they can either fluctuate around a globally attractive steady state (Figure 2g, j) or present sustainable stochastic oscillations in the vicinity of a stable limit cycle (Figure 2h-i). In fact, the parameter region for species coexistence in this scenario is rather similar between the SSA and ODEs studies (Figure S14). Finally, in the scenario involving chasing pair and both inter- and intra-specific interference, unsurprisingly, all species can coexist indefinitely in company with stochasticity (Figure S12).

To further mimic the time evolution in a real ecosystem, we resort to individual-based modeling (IBM) [47, 48], an essentially stochastic simulation method, which is widely used in ecology. The system is homogeneous, with a squared landscape of length  $L$  and periodic boundary conditions (see SI Sec. VII A for details). Likewise, we consider the case of  $S_C = 2$ ,  $S_R = 1$ . In the scenario involving chasing pair and intraspecific interference, snapshots of the system in the time evolution are shown in Figure 2k. By collecting species abundances in the time series, it is evident that the two consumer species can coexist for long with only one type of resources (Figure 2l). Taken together with the SSA simulation studies, it is obvious that intraspecific interference can promote species coexistence along with stochasticity.

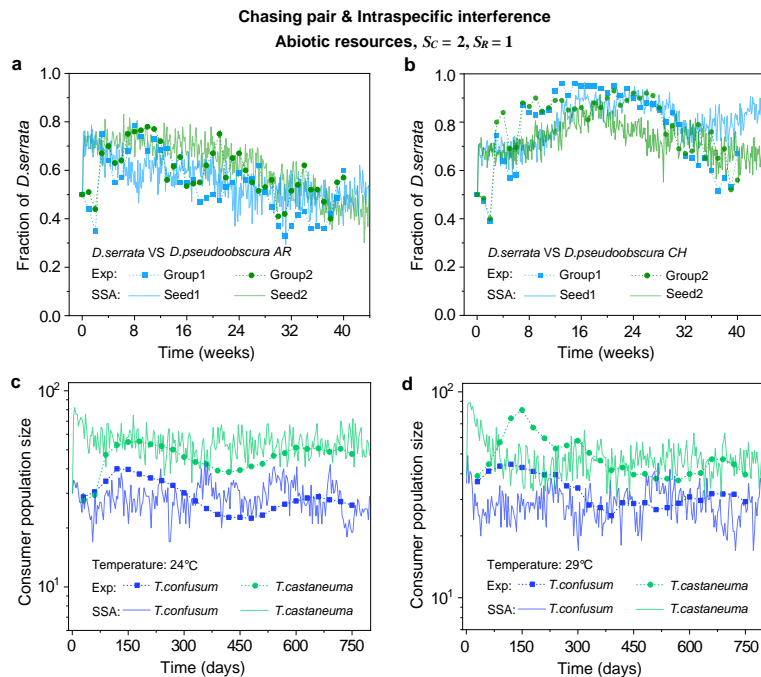


Figure 3. A model of intraspecific predator interference explains two classical experiments that invalidate CEP. Here, the solid icons represent the experimental data, which are connected by the dotted lines for the sake of visibility. The solid lines stand for the SSA simulation results. In all cases, two consumer species ( $S_C = 2$ ) coexist for long with only one type of resources ( $S_R = 1$ ). (a-b) In Ayala’s experiment [33], two *Drosophila* species (consumers), *D. serrata* and *D. pseudoobscura*, compete for the same type of abiotic resources within a laboratory bottle. (c-d) In Park’s experiment [34], two *Tribolium* species, *T. confusum* and *T. castaneum*, compete for the same food (flour). See SI Sec. VIII for simulation details. See also Figures S14-S16.

#### D. Comparison with experimental studies that reject CEP

Two classical studies [33, 34] reported that, in their respective laboratory systems, two species of insects coexisted for roughly years or more with only one type of resources. Specifically, Francisco Ayala observed that two species of flies, *Drosophila serrata* and *Drosophila pseudoobscura*, coexisted for more than 40 weeks (duration of the experiment) when competing for the same abiotic resources in a bottle with serial transfer (resource supply) [33]. Likewise, Thomas Park found that two species of beetles, *Tribolium confusum* and *Tribolium castaneum*, coexisted for more than two years (duration of the experiment) when competing for the same type of food (flour) [34]. Evidently, these two experiments [33, 34] are not compatible with CEP, while factors such as temporal variations, spatial heterogeneity, cross-feeding, pack hunting, etc. are clearly not involved in such systems. As intraspecific fighting is prevalent among insects [49], especially for *Drosophila* [50, 51], we apply the model involving chasing pair and intraspecific interference to simulate the two systems. Overall, our stochastic simulation results (with SSA) show good consistency with those of the experiments (Figure 3, see also Figures S14-S16). The fluctuations in experimental time series can be mainly account by stochasticity.

#### E. A handful of resource species can support an unexpected wide range of consumer species regardless of stochasticity

To resolve the puzzle stated in the paradox of the plankton, we proceed to analyze the generic case that  $S_C$  consumers species competing for  $S_R$  resource species (with  $S_C > S_R$ ) within the scenario involving chasing pair and intraspecific interference. The population dynamics is described by Eqs. 1, 2, 4. As with the cases above, each consumer species is assigned of unique competitiveness through a distinctive  $D_i$  ( $i = 1, \dots, S_C$ ).

Strikingly, a plethora of consumer species may coexist at steady state with only one resource species ( $S_C \gg 1$ ,  $S_R = 1$ ) in the ODEs simulations, and crucially, the facilitated biodiversity can still be maintained in the stochastic simulations (with SSA). The long-term coexistence behavior are exemplified in Figures 4 and S17-S26, involving resource species that are biotic or abiotic, and simulations with or without stochasticity. The number of consumer species in long-term coexistence can be up to hundreds or more (Figures 4, S18-S19). To mimic the real ecosystems, we further analyze the cases with more than one type of resources, such as systems with  $S_R = 3$  ( $S_C \gg S_R$ ). Just like the case of  $S_R = 1$  ( $S_C \gg S_R$ ), an extensive range of consumer species may coexist indefinitely regardless of stochasticity (Figures 4, S18, S22-S26, ).

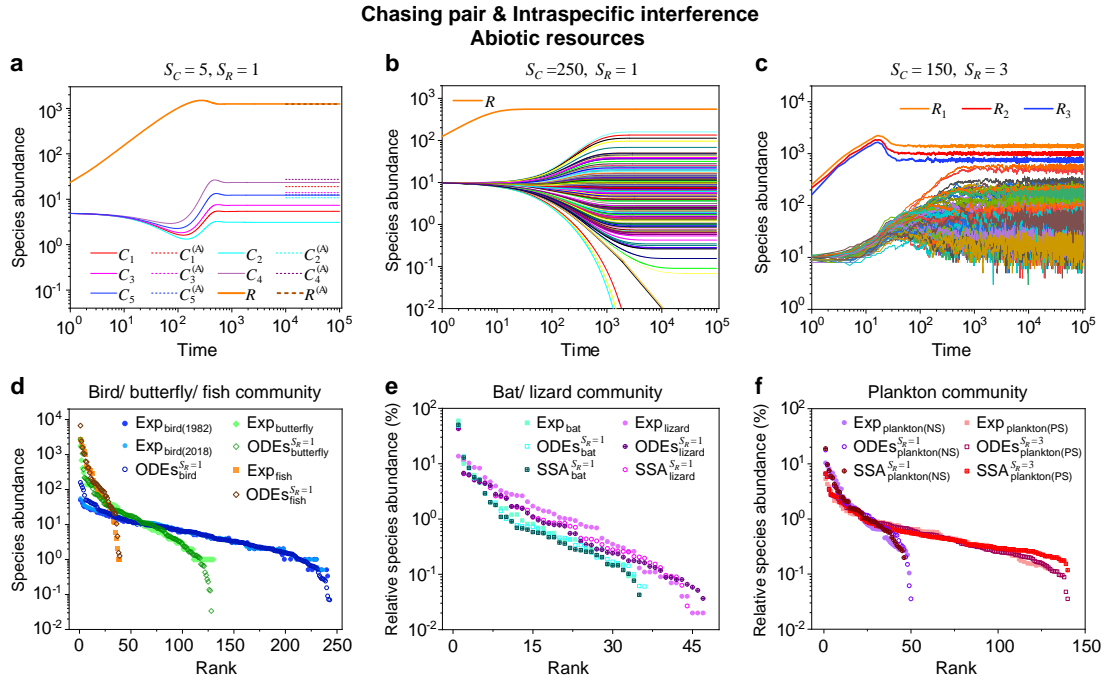


Figure 4. A model of intraspecific predator interference illustrates the S shape pattern of the species' rank-abundance curves across different ecological communities. (a-c) Intraspecific interference enables a wide range of consumer species ( $S_C \gg S_R$ ) to coexist with only one or a handful of resources species regardless of stochasticity. (a, b) Time courses of the species abundances simulated with ODEs. The dashed lines in (a) are the analytical steady-state solutions (marked with superscript “(A)”) calculated from Eqs. S52-S64. (c) Time courses of the species abundances simulated with SSA. (d-f) Species' rank-abundance curves for various communities. The solid icons represent the experimental data (marked with “Exp”) reported in existing studies [35, 37–42], while the hollow icons and those with “+” center are the ODEs and SSA results constructed from timestamp  $t = 1.0 \times 10^5$  in the time series, respectively. The bird community data were collected longitudinally within the same Amazonian region in 1982 and 2018 [38, 39], while the plankton community data were obtained separately from the Norwegian Sea (NS) and Pacific Station (PS) [35]. In the model settings for each ecological system ( $S_C \gg S_R$ ,  $S_R = 1$  or 3), the mortality rate  $D_i$  ( $i = 1, \dots, S_C$ ) is the only parameter varying with the consumer species, which was randomly sampled from a Gaussian distribution. In the Kolmogorov–Smirnov test, the probabilities ( $p$  values) that the simulation results and the corresponding experimental data come from the same distributions are:  $p_{\text{ODEs}}^{\text{bird}(1982)} = 0.17$ ,  $p_{\text{ODEs}}^{\text{bird}(2018)} = 0.26$ ,  $p_{\text{ODEs}}^{\text{butterfly}} = 0.70$ ,  $p_{\text{ODEs}}^{\text{fish}} = 0.88$ ;  $p_{\text{ODEs}}^{\text{bat}} = 0.42$ ,  $p_{\text{SSA}}^{\text{bat}} = 0.48$ ,  $p_{\text{ODEs}}^{\text{lizard}} = 0.96$ ,  $p_{\text{SSA}}^{\text{lizard}} = 0.54$ ;  $p_{\text{ODEs}}^{\text{plankton(NS)}} = 0.46$ ,  $p_{\text{SSA}}^{\text{plankton(NS)}} = 0.37$ ,  $p_{\text{ODEs}}^{\text{plankton(PS)}} = 0.20$ ,  $p_{\text{SSA}}^{\text{plankton(PS)}} = 0.06$ . With a significance threshold of 0.05, none of the  $p$  values suggest there exists a statistically significant difference. See SI Sec. VIII for simulation details and the Shannon entropies. See also Figures S19-S26.

When the population size of each resource species are much larger than the total population of consumers (i.e.,  $R_l \gg \sum_{i=1}^{S_C} C_i$ , with  $l = 1, 2, \dots, S_R$ ), if all resource species are biotic, or if there are only one type of resources ( $S_R = 1$ ), the steady-state population of each consumer and resource species can be obtained analytically (see SI Sec. IIIB for details). In fact, the analytical solutions are highly consistent with the numerical results (Figures 1e, 4a, S8c-d and S18a-b), and can even quantitatively predict the coexistence region of the parameter space (Figure S8e-f).

## F. The S shape pattern of the rank-abundance curves in a broad range of ecological communities

A prominent feature of biodiversity is that the species' rank-abundance curves follow a universal S shape pattern in the linear-log plots across a broad spectrum of ecological communities. This has been exemplified in reports ranging from communities of ocean plankton worldwide [35, 36], tropical river fishes from Argentina [37], forest bats of Trinidad [40], rainforest trees [42], birds [38, 39], butterflies [41] in Amazonia, to those of desert bees [42] in Utah and lizards from South Australia [37]. In the specific case of Amazonian bird community at Jatun Sacha, the population structure and rank-abundance curve remain largely unaltered over a period of thirty decades or more [38, 39]. Regarding the plankton communities, samples collected worldwide follow highly similar distributions and rank-abundance curves [35, 36]. Nevertheless, questions remain as to what bring about the universal pattern of rank-abundance curves across different communities.

Previously, this pattern was mostly explained by the neutral theory [42], which requires special parameter settings that all consumer species share identical fitness. To resolve this issue, we apply the model involving

chasing pair and intraspecific interference to simulate the ecological communities, where one ( $S_R = 1$ ) or three ( $S_R = 3$ ) types of resources support a large number of consumer species ( $S_C \gg S_R$ ). In each model system, the mortality rates of consumer species follow a Gaussian distribution where the coefficient of variance (CV) was taken around 0.3.

Remarkably, for a broad array of the ecological communities, the rank-abundance curves obtained from the long-term coexisting state of both the ODEs and SSA simulation studies agree quantitatively with those of experiments (Figure 4d-f, see also Figures S19, S20, S22, S24 and S26), sharing roughly equal Shannon entropies and mostly being regarded as identical distributions in the Kolmogorov–Smirnov statistical test (with a significance threshold of 0.05). Still, there is a noticeable discrepancy between the experimental data and SSA studies in terms of the species' absolute abundances (e.g., Figure S19c): those with experimental abundances less than 10 tend to extinct in the SSA simulations. This is due to the fact that the recorded individuals in an experimental sample are just a tiny portion of that in the real ecological system, whereas the species population size in a natural community is certainly much larger than 10.

### III. DISCUSSIONS

The conflict between the CEP and biodiversity, exemplified by the paradox of the plankton [9], is a long-standing puzzle in ecology. Although many mechanisms have been proposed to overcome the limit set by CEP [9–31], it is still unclear how can plankton and many other organisms flout CEP and maintain biodiversity in quasi-well-mixed natural ecosystems. To address this issue, we investigate a mechanistic model with detailed consideration of the pairwise encounter, especially the formation of chasing pair and interference pair. Using numerical simulations combined with mathematical analysis, we identify that the intraspecific interference among the consumer individuals can promote a wide range of consumer species to coexist indefinitely with only one or a handful of resource species. In fact, species coexistence in our model is robust to parameter perturbations and stochasticity. There is a non-zero volume of parameter region for species' steady coexistence (see Figures 2d-f, S10a-c for the ODEs results), which can still be largely maintained in the stochastic simulations (Figure S14). By applying the above analysis to real ecological systems, remarkably, our model naturally explains two classical experiments that reject the CEP [33, 34] (Figure 3), and quantitatively illustrates the universal S shape pattern of the rank-abundance curves for a broad range of ecological communities [35–39, 41, 42] (Figures 4, S19, S20, S22, S24 and S26).

Intuitively, the mechanism of how intraspecific interference facilitates species coexistence can be understood from the underlying feedback loop. Specifically, for consumer species of higher competitiveness and thus with more individuals in an ecological community, e.g., species  $C_i$ , a larger portion of  $C_i$  individuals are then engaged in the intraspecific interference pair which are temporarily absent from hunting (Figure S27a-b). Consequently, there would be a smaller fraction of  $C_i$  within the chasing pair (Figure S27a-b), which effectively forms a self-inhibiting negative feedback loop (Figure S27c). This feedback loop results in an overall balance among the consumer species, and thus promotes biodiversity.

In fact, predator interference has been introduced long ago in the classical B-D phenomenological model [26, 27], yet the functional response of B-D model involving intraspecific interference can be formally derived from the scenario involving only chasing pair without predator interference [21, 43] (see Eq. S8). By extending the B-D model from the mechanistic perspective, we reconcile the conflict and show that B-D model corresponds to a special case of our mechanistic model yet without the escape rate (Figures S2-S4, see SI Sec. II for details).

Finally, our model can be widely used to explain biodiversity in many ecosystems. In practice, many more factors are potentially involved, and special attention is required to disentangle confounding factors. In microbial systems, cross-feeding is commonly involved [16, 17], and species' preference for food is shaped by the evolution course and environmental history [52]. It is still highly challenging to fully explain how organisms evolve and maintain biodiversity in diverse ecosystems.

### ACKNOWLEDGMENTS

We thank Roy Kishony, Eric D. Kelsic and Fan Zhong for helpful discussions. This work was supported by National Natural Science Foundation of China (Grant No.12004443), Guangzhou Municipal Innovation Fund (Grant No.202102020284) and the Hundred Talents Program of Sun Yat-sen University.

### AUTHOR CONTRIBUTIONS

X.W. conceived and designed the project, supervised the study, developed the model, carried out the theoretical analysis, and wrote the paper. J.K. carried out the numerical simulations, analyzed the data, contributed to modeling together with the theoretical analysis, and wrote the paper. S.J.Z developed the code for SSA and IBM simulations.

## COMPETING INTERESTS

The authors declare no competing interests.

## REFERENCES

- 
- [1] Elizabeth Pennisi. What determines species diversity? *Science*, 309(5731):90-90, 2005.
  - [2] Carina Hoorn, Frank P. Wesselingh, H. Ter Steege, M.A. Bermudez, A. Mora, J. Sevink, Isabel Sanmarín, A. Sanchez-Meseguer, C.L. Anderson, J.P. Figueiredo, C. Jaramillo, D. Riff, F. R. Negri, H. Hooghiemstra, J. Lundberg, T. Stadler, T. Särkinen, and A. Antonelli. Amazonia through time: Andean uplift, climate change, landscape evolution, and biodiversity. *Science*, 330(6006):927-931, 2010.
  - [3] Colomban De Vargas, Stéphane Audic, Nicolas Henry, Johan Decelle, Frédéric Mahé, Ramiro Logares, Enrique Lara, Cédric Berney, Noan Le Bescot, Ian Probert, Margaux Carmichael, Julie Poulain, Sarah Romac, Sébastien Colin, Jean-Marc Aury, Lucie Bittner, Samuel Chaffron, Micah Dunthorn, Stefan Engelen, Olga Flegontova, Lionel Guidi, Aleš Horák, Olivier Jaillon, Gipsi Lima-Mendez, Julius Lukeš, Shruti Malviya, Raphael Morard, Matthieu Mulot, Eleonora Scalco, Raffaele Siano, Flora Vincent, Adriana Zingone, Céline Dimier, Marc Picheral, Sarah Searson, Stefanie Kandels-Lewis, Tara Oceans Coordinators, Silvia G Acinas, Peer Bork, Chris Bowler, Gabriel Gorsky, Nigel Grimsley, Pascal Hingamp, Daniele Iudicone, Fabrice Not, Hiroyuki Ogata, Stéphane Pesant, Jeroen Raes, Michael E. Sieracki, Sabrina Speich, Lars Stemmann, Shinichi Sunagawa, Jean Weissenbach, Patrick Wincker, and Eric Karsenti. Eukaryotic plankton diversity in the sunlit ocean. *Science*, 348(6237):1261605, 2015.
  - [4] Rolf Daniel. The metagenomics of soil. *Nature Reviews Microbiology*, 3:470-478, 2005.
  - [5] F Gause, G. *The struggle for existence*. The Williams & Wilkins Company, Baltimore, 1934.
  - [6] Garrett Hardin. The competitive exclusion principle. *Science*, 131(3409):1292-1297, 1960.
  - [7] Robert MacArthur and Richard Levins. Competition, habitat selection, and character displacement in a patchy environment. *Proceedings of the National Academy of Sciences of the United States of America*, 51(6):1207-1210, 1964.
  - [8] Simon A Levin. Community equilibria and stability, and an extension of the competitive exclusion principle. *The American Naturalist*, 104(939):413-423, 1970.
  - [9] G Evelyn Hutchinson. The paradox of the plankton. *The American Naturalist*, 95(882):137-145, 1961.
  - [10] Peter Chesson. Mechanisms of maintenance of species diversity. *Annual Review of Ecology and Systematics*, 31(1):343-366, 2000.
  - [11] Richard Levins. Coexistence in a variable environment. *The American Naturalist*, 114(6):765-783, 1979.
  - [12] Simon A. Levin. Dispersion and population interactions. *The American Naturalist*, 108(960):207-228, 1974.
  - [13] Arthur L Koch. Competitive coexistence of two predators utilizing the same prey under constant environmental conditions. *Journal of Theoretical Biology*, 44(2):387-395, 1974.
  - [14] Jef Huisman and Franz J Weissing. Biodiversity of plankton by species oscillations and chaos. *Nature*, 402(6760):407-410, 1999.
  - [15] Tamás LCzárán, Rolf F Hoekstra, and Ludo Pagie. Chemical warfare between microbes promotes biodiversity. *Proceedings of the National Academy of Sciences of the United States of America*, 99(2):786-790, 2002.
  - [16] Akshit Goyal and Sergei Maslov. Diversity, stability, and reproducibility in stochastically assembled microbial ecosystems. *Physical Review Letters*, 120(15):158102, 2018.
  - [17] Joshua E Goldford, Nanxi Lu, Djordje Bajić, Sylvie Estrela, Mikhail Tikhonov, Alicia Sanchez-Gorostiaga, Daniel Segrè, Pankaj Mehta, and Alvaro Sanchez. Emergent simplicity in microbial community assembly. *Science*, 361(6401):469-474, 2018.
  - [18] Paula Villa Martín, Aleš Buček, Thomas Bourguignon, and Simone Pigolotti. Ocean currents promote rare species diversity in protists. *Science advances*, 6(29):eaaz9037, 2020.
  - [19] Deepak Gupta, Stefano Garlaschi, Samir Suweis, Sandro Azaele, and Amos Maritan. Effective resource competition model for species coexistence. *Physical Review Letters*, 127(20):208101, 2021.
  - [20] T Frede Thingstad. Elements of a theory for the mechanisms controlling abundance, diversity, and biogeochemical role of lytic bacterial viruses in aquatic systems. *Limnology and Oceanography*, 45(6):1320-1328, 2000.
  - [21] Xin Wang and Yang-Yu Liu. Overcome competitive exclusion in ecosystems. *iScience*, 23(4):101009, 2020.
  - [22] Benjamin D Dalziel, Mark Novak, James R Watson, and Stephen P Ellner. Collective behaviour can stabilize ecosystems. *Nature Ecology & Evolution*, 5(10):1435-1440, 2021.
  - [23] Anna Posfai, Thibaud Taillefumier, and Ned S Wingreen. Metabolic trade-offs promote diversity in a model ecosystem. *Physical Review Letters*, 118(2):028103, 2017.
  - [24] Benjamin G Weiner, Anna Posfai, and Ned S Wingreen. Spatial ecology of territorial populations. *Proceedings of the National Academy of Sciences of the United States of America*, 116(36):17874-17879, 2019.
  - [25] Chi Xue and Nigel Goldenfeld. Coevolution maintains diversity in the stochastic "kill the winner" model. *Physical Review Letters*, 119(26):268101, 2017.
  - [26] John R Beddington. Mutual interference between parasites or predators and its effect on searching efficiency. *The Journal of Animal Ecology*, 44(1):331-340, 1975.
  - [27] Donald Lee DeAngelis, RA Goldstein, and Robert V O'Neill. A model for tropic interaction. *Ecology*, 56(4):881-892, 1975.

- [28] Roger Arditi and Lev R Ginzburg. Coupling in predator-prey dynamics: ratio-dependence. *Journal of Theoretical Biology*, 139(3):311-326, 1989.
- [29] Eric D Kelsic, Jeffrey Zhao, Kalin Vetsigian, and Roy Kishony. Counteraction of antibiotic production and degradation stabilizes microbial communities. *Nature*, 521(7553):516-519, 2015.
- [30] Jacopo Grilli, György Barabás, Matthew J Michalska-Smith, and Stefano Allesina. Higher-order interactions stabilize dynamics in competitive network models. *Nature*, 548(7666):210-213, 2017.
- [31] Christoph Ratzke, Julien Barrere, and Jeff Gore. Strength of species interactions determines biodiversity and stability in microbial communities. *Nature Ecology & Evolution*, 4(3):376-383, 2020.
- [32] Shinichi Sunagawa, Silvia G Acinas, Peer Bork, Chris Bowler, Damien Eveillard, Gabriel Gorsky, Lionel Guidi, Daniele Iudicone, Eric Karsenti, Fabien Lombard, Hiroyuki Ogata, Stephane Pesant, Matthew B. Sullivan, Patrick Wincker, and Coloman de Vargas. Tara oceans: towards global ocean ecosystems biology. *Nature Reviews Microbiology*, 18(8):428-445, 2020.
- [33] Francisco J Ayala. Experimental invalidation of the principle of competitive exclusion. *Nature*, 224(5224):1076-1079, 1969.
- [34] Thomas Park. Experimental studies of interspecies competition ii. temperature, humidity, and competition in two species of tribolium. *Physiological Zoology*, 27(3):177-238, 1954.
- [35] Jed A. Fuhrman, Joshua A. Steele, Ian Hewson, Michael S. Schwalbach, Mark V. Brown, Jessica L. Green, and James H. Brown. A latitudinal diversity gradient in planktonic marine bacteria. *Proceedings of the National Academy of Sciences*, 105(22):7774-7778, 2008.
- [36] Shruti Malviya Coloman De Vargas Eric Karsenti Chris Bowler Enrico Ser-Giacomi, Lucie Zinger and Silvia De Monte. Ubiquitous abundance distribution of non-dominant plankton across the global ocean. *Nature Ecology & Evolution*, 2(2):1243-1249, 2018.
- [37] Martin L. Cody and Jeffrey A. Smallwood. *Long-term studies of vertebrate communities*. Academic Press, 1996.
- [38] John Terborgh, Scott K. Robinson, Theodore A. Parker III, Charles A. Munn, and Nina Pierpont. Structure and organization of an amazonian forest bird community. *Ecological Monographs*, 60(2):213-238, 1990.
- [39] Ari Martinez, Jose Ponciano, Juan Gomez, Thomas Valqui, Jorge Novoa, Ettore Camerlenghi, Blaine Carnes, Eliseo Parra, John Fitzpatrick, Scott K. Robinson, Jacob Socolar, and John Terborgh. The structure and organization of an amazonian bird community remains little changed after nearly four decades. *Authorea Preprints*, 2021.
- [40] F. M. Clarke and Lvra Racey. Life after logging: post-logging recovery of a neotropical bat community. *Journal of Applied Ecology*, 42(2):409-420, 2005.
- [41] Philip J. Devries, Debra Murray, and Russell Lande. Species diversity in vertical, horizontal, and temporal dimensions of a fruit-feeding butterfly community in an ecuadorian rainforest. *Biological journal of the Linnean Society*, 62(3):343-364, 1997.
- [42] Stephen P. Hubbell. *The Unified Neutral Theory of Biodiversity and Biogeography*. Princeton University Press, 2001.
- [43] Gert Huisman and Rob J De Boer. A formal derivation of the "beddington" functional response. *Journal of Theoretical Biology*, 185(3):389-400, 1997.
- [44] Robert MacArthur. Species packing and competitive equilibrium for many species. *Theoretical Population Biology*, 1(1):1-11, 1970.
- [45] Peter Chesson. Macarthur's consumer-resource model. *Theoretical Population Biology*, 37(1):26-38, 1990.
- [46] Daniel T Gillespie. Stochastic simulation of chemical kinetics. *Annu. Rev. Phys. Chem.*, 58:35-55, 2007.
- [47] Volker Grimm and Steven F Railsback. *Individual-based modeling and ecology*. Princeton university press, 2013.
- [48] Kalin Vetsigian. Diverse modes of eco-evolutionary dynamics in communities of antibiotic-producing microorganisms. *Nature Ecology & Evolution*, 1(1):1-9, 2017.
- [49] Jacobus J Boomsma, Boris Baer, and Jürgen Heinze. The evolution of male traits in social insects. *Annu. Rev. Entomol.*, 50:395-420, 2005.
- [50] Heiko Dankert, Liming Wang, Eric D Hoopfer, David J Anderson, and Pietro Perona. Automated monitoring and analysis of social behavior in drosophila. *Nature Methods*, 6(4):297-303, 2009.
- [51] Selby Chen, Ann Yeelin Lee, Nina M Bowens, Robert Huber, and Edward A Kravitz. Fighting fruit flies: a model system for the study of aggression. *Proceedings of the National Academy of Sciences of the United States of America*, 99(8):5664-5668, 2002.
- [52] Xin Wang, Kang Xia, Xiaojing Yang, and Chao Tang. Growth strategy of microbes on mixed carbon sources. *Nature Communications*, 10(1):1279, 2019.
- [53] Richard T Holmes, Thomas W Sherry, and Franklin W Sturges. Bird community dynamics in a temperate deciduous forest: Long-term trends at hubbard brook. *Ecological Monographs*, 56(3):201-220, 1986.

# Supplementary Information

## I. THE CLASSICAL PROOF OF COMPETITIVE EXCLUSION PRINCIPLE (CEP)

In the 1960s, MacArthur and Levin [7, 8] put forward the classical mathematical proof of CEP. We rephrase their idea in the simple case of  $S_C = 2$  and  $S_R = 1$ , i.e., two consumer species  $C_1$  and  $C_2$  competing for one resource species  $R$ . In practice, this proof can be generalized into higher dimensions with several consumer and resource species. The population dynamics of the system can be described as follows:

$$\begin{cases} \dot{C}_i = C_i(f_i(R) - D_i), & i = 1, 2; \\ \dot{R} = g(R, C_1, C_2). \end{cases} \quad (\text{S1})$$

Here  $C_i$  and  $R$  represent the population abundances of consumers and resources, respectively, while the functional forms of  $f_i(R)$  and  $g(R, C_1, C_2)$  are unspecific.  $D_i$  stands for the mortality rate of the species  $C_i$ . If all consumer species can coexist at steady state, then  $f_i(R)/D_i = 1$  ( $i = 1, 2$ ). In a 2-D representation, this requires that three lines  $y = f_i(R)/D_i$  ( $i = 1, 2$ ) and  $y = 1$  share a common point, which is commonly impossible unless the model parameters satisfy special constraint (sets of Lebesgue measure zero). In a 3-D representation, the two planes corresponding to  $f_i(R)/D_i = 1$  ( $i = 1, 2$ ) are parallel, and hence do not share a common point (Figure S5a-b, see also Ref. [21] for details).

## II. COMPARISON OF THE FUNCTIONAL RESPONSE WITH BEDDINGTON-DEANGELIS (B-D) MODEL

### A. B-D model

In 1975, Beddington proposed a mathematical model [26] to describe the influence of predator interference on the functional response with hand-waving derivations. In the same year, DeAngelis and his colleagues considered a related question and put forward a similar model [27]. Essentially, both models are phenomenological, and they were called B-D model in the subsequent studies. In practice, the B-D model can be extended into scenarios involving different types of pairwise encounters with Beddington's modelling method. In this section, we systematically compare the functional response in B-D model with that of our mechanistic model in all the relevant scenarios.

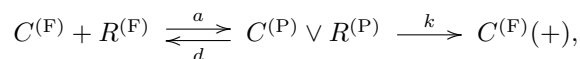
Recalling Beddington's analysis, the model [26] consists of one consumer species  $C$  and one resource species  $R$  ( $S_C = 1, S_R = 1$ ). In a well-mixed system, an individual consumer meets a resource with rate  $a$ , while encounters another consumer with rate  $a'$ . There are two other phenomenological parameters in this model, namely, the handling time  $t_h$  and the wasting time  $t_w$ . Both can be determined by specifying the scenario and using statistical physics modeling analysis. In fact, Beddington analyzed the searching efficiency  $\Xi_{\text{B-D}}$  rather than the functional response  $\mathcal{F}_{\text{B-D}}$ , yet both can be reciprocally derived with  $\Xi_{\text{B-D}} \equiv \mathcal{F}_{\text{B-D}}/R$ . Here  $R$  stands for the population abundance of the resources, and the specific form of  $\Xi_{\text{B-D}}$  is [26]:

$$\Xi_{\text{B-D}}(R, C) = \frac{a}{1 + at_h R + a't_w C'}, \quad (\text{S2})$$

where  $C' = C - 1$ , and  $C$  stands for the population abundance of the consumes. Generally,  $C \gg 1$ , and thus  $C' \approx C$ .

### B. Scenario involving only chasing pair

Here we consider the scenario involving only chasing pair for the simple case with one consumer species  $C$  and one resource species  $R$  ( $S_C = 1, S_R = 1$ ). When an individual consumer is chasing a resource, they form a chasing pair:



where the superscript “(F)” stands for populations that are freely wandering, and “(+)” signifies gaining biomass (we count  $C^{(\text{F})}(+)$  as  $C^{(\text{F})}$ ).  $C^{(\text{P})} \vee R^{(\text{P})}$  represents chasing pair (where “(P)” signifies pair), denoted as  $x$ .  $a$ ,  $d$  and  $k$  stand for encounter rate, escape rate and capture rate, respectively. Hence, the total number of consumers and resources are  $C \equiv C^{(\text{F})} + x$  and  $R \equiv R^{(\text{F})} + x$ . Then, the population dynamics of the system follows:

$$\begin{cases} \dot{x} = aC^{(\text{F})}R^{(\text{F})} - (k + d)x, \\ \dot{C} = wx - DC, \\ \dot{R} = g(R, x, C). \end{cases} \quad (\text{S3})$$

Here the functional form of  $g(R, x, C)$  is unspecified, while  $D$  and  $w$  represent the mortality rate of the consumer species and biomass conversion ratio [21], respectively. Since consumption process is generically much faster than the birth/death process, in deriving the functional response, the consumption process is supposed to be in fast equilibrium (i.e.,  $\dot{x} = 0$ ). Then, we can solve for  $x$  with:

$$x^2 - (R + C + K)x + RC = 0, \quad (\text{S4})$$

where  $K = \frac{k+d}{a}$ , and then,

$$x = \frac{2RC}{(R + C + K)} \frac{1}{\left(1 + \sqrt{1 - \frac{4RC}{(R+C+K)^2}}\right)}. \quad (\text{S5})$$

By definition, the functional response and search efficiency are:

$$\mathcal{F}_{\text{CP}}(R, C) = \frac{kx}{C}, \quad (\text{S6a})$$

$$\Xi_{\text{CP}}(R, C) = \frac{kx}{RC}. \quad (\text{S6b})$$

Hence, we obtain the functional response and search efficiency in this chasing-pair scenario:

$$\mathcal{F}_{\text{CP}}(R, C)_{(1)} = k \frac{(R + C + K)}{2C} \left(1 - \sqrt{1 - \frac{4RC}{(R + C + K)^2}}\right), \quad (\text{S7a})$$

$$\Xi_{\text{CP}}(R, C)_{(1)} = k \frac{(R + C + K)}{2RC} \left(1 - \sqrt{1 - \frac{4RC}{(R + C + K)^2}}\right). \quad (\text{S7b})$$

Since  $\frac{4RC}{(R+C+K)^2} < 4\frac{C}{R} \ll 1$ , using first order approximations in Eq. S7, we obtain  $\sqrt{1 - \frac{4RC}{(R+C+K)^2}} \approx 1 - \frac{2RC}{(R+C+K)^2}$ . Then the functional response and search efficiency are:

$$\mathcal{F}_{\text{CP}}(R, C)_{(2)} = k \frac{R}{R + C + K}, \quad (\text{S8a})$$

$$\Xi_{\text{CP}}(R, C)_{(2)} = \frac{k}{R + C + K}. \quad (\text{S8b})$$

Evidently, there is no predator interference within the chasing-pair scenario, yet the functional response form is identical to the B-D model involving intraspecific interference (see Eq. S2). Meanwhile, using first order approximations in the denominator of Eq. S5, we have  $x \approx \frac{RC}{(R+C+K) - \frac{RC}{(R+C+K)}}$ . Hence,

$$\mathcal{F}_{\text{CP}}(R, C)_{(3)} = k \frac{R}{(R + C + K) - \frac{RC}{(R+C+K)}}, \quad (\text{S9a})$$

$$\Xi_{\text{CP}}(R, C)_{(3)} = \frac{k}{(R + C + K) - \frac{RC}{(R+C+K)}}. \quad (\text{S9b})$$

In the case that  $R \gg C$ , then  $R \gg C > x = R - R^{(F)}$ . By applying  $R \approx R^{(F)}$  in Eq. S3, we obtain  $x \approx \frac{RC}{R+K}$ . Then,

$$\mathcal{F}_{\text{CP}}(R, C)_{(4)} = k \frac{R}{R + K}, \quad (\text{S10a})$$

$$\Xi_{\text{CP}}(R, C)_{(4)} = \frac{k}{R + K}. \quad (\text{S10b})$$

To compare these functional responses with that of the B-D model, we determine the parameters  $t_h$  and  $t_w$  in the B-D model by calculating their ensemble average values in a stochastic framework. Using the properties of waiting time distribution in the Poisson process, we obtain  $\langle t_h \rangle = \frac{1}{k}$  and  $\langle t_w \rangle = \frac{1}{d'}$  (in the chasing-pair scenario,  $a' = 0$ ). By substituting these calculations into Eq. S2, we have

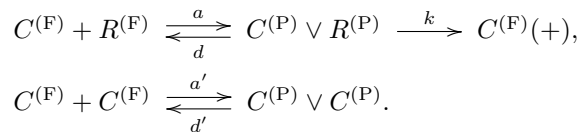
$$\Xi_{\text{CP}}^{\text{B-D}}(R, C) = \frac{a}{1 + Ra/k} = \frac{k}{k/a + R}, \quad (\text{S11a})$$

$$\mathcal{F}_{\text{CP}}^{\text{B-D}}(R, C) = \frac{kR}{k/a + R}. \quad (\text{S11b})$$

In the special case with  $d = 0$  and  $R \gg C$ , the B-D model is consistent with our mechanistic model:  $\Xi_{\text{B-D}}(R, C) = \Xi_{\text{CP}}(R, C)_{(4)}$ . Outside the special region, however, the discrepancy can be considerably large (see Figure S2 for the comparison).

### C. Scenario involving chasing pair and intraspecific interference

Here we consider the scenario with additional involvement of intraspecific interference in the simple case of  $S_C = 1$  and  $S_R = 1$ :



Here  $C^{(P)} \vee C^{(P)}$  stands for the intraspecific predator interference pair, denoted as  $y$ ;  $a'$  and  $d'$  represent the encounter rate and separation rate of the interference pair, respectively. Then, the total population of consumers and resources are  $C \equiv C^{(F)} + x + 2y$  and  $R \equiv R^{(F)} + x$ . Hence the population dynamics of the consumers and resources can be described as follows:

$$\begin{cases} \dot{x} = aC^{(F)}R^{(F)} - (k+d)x, \\ \dot{y} = a'[C^{(F)}]^2 - d'y, \\ \dot{C} = wkx - DC, \\ \dot{R} = g(R, x, C). \end{cases} \quad (\text{S12})$$

The consumption process and interference process are supposed to be in fast equilibrium (i.e.,  $\dot{x} = 0, \dot{y} = 0$ ), then we can solve for  $x$  with:

$$x^3 + \phi_2 x^2 + \phi_1 x + \phi_0 = 0, \quad (\text{S13})$$

where  $\phi_0 = -CR^2$ ,  $\phi_1 = 2CR + KR + R^2$ ,  $\phi_2 = 2\beta K^2 - K - C - 2R$ , with  $\beta = a'/d'$ . The discriminant of Eq. S13 (denoted as  $\Lambda$ ) is

$$\Lambda = -4\psi^3 - 27\varphi^2, \quad (\text{S14})$$

with  $\psi = \phi_1 - (\phi_2)^2/3$  and  $\varphi = \phi_0 - \phi_1\phi_2/3 + 2(\phi_2)^3/27$ . When  $\Lambda < 0$ , there are one real solution  $x_{(1)}$  and two complex solutions  $x_{(2)}, x_{(3)}$ , which are

$$x_{(1)} = \theta_1 + \theta_2 - \phi_2/3, x_{(2)} = \omega\theta_1 + \omega^2\theta_2 - \phi_2/3, x_{(3)} = \omega^2\theta_1 + \omega\theta_2 - \phi_2/3, \quad (\text{S15})$$

where  $\omega = -1/2 + i\sqrt{3}/2$  ( $i$  stands for the imaginary unit),  $\theta_1 = (-\varphi/2 + \sqrt{-\Lambda/108})^{1/3}$ , and  $\theta_2 = (-\varphi/2 - \sqrt{-\Lambda/108})^{1/3}$ . On the other hand, when  $\Lambda > 0$ , there are three real solutions  $x_{(1)}, x_{(2)}$ , and  $x_{(3)}$ , which are

$$x_{(1)} = \psi' \cos \varphi' - \phi_2/3, x_{(2)} = \psi' \cos(\varphi' + \frac{2\pi}{3}) - \phi_2/3, x_{(3)} = \psi' \cos(\varphi' + \frac{4\pi}{3}) - \phi_2/3, \quad (\text{S16})$$

where  $\psi' = (-4\psi/3)^{1/2}$  and  $\varphi' = \arccos(-(-\psi/3)^{-3/2}\varphi/2)/3$ . Note that  $x \in [0, \min(R, C)]$ , then we obtain the exact feasible solution of  $x$  (denoted as  $x_{\text{ext}}$ ), and hence the functional response and search efficiency are

$$\mathcal{F}_{\text{intra}}(R, C)_{(1)} = \frac{kx_{\text{ext}}}{C}, \quad (\text{S17a})$$

$$\Xi_{\text{intra}}(R, C)_{(1)} = \frac{kx_{\text{ext}}}{RC}. \quad (\text{S17b})$$

In the case of  $R \gg C$ , then  $R - R^{(F)} = x < C \ll R$ , and thus  $R^{(F)} \approx R$ . Still, the consumption process is supposed to be in fast equilibrium (i.e.,  $\dot{x} = 0, \dot{y} = 0$ ), and then we obtain

$$x \approx \frac{RC}{\sqrt{[\frac{1}{2}(K+R)]^2 + 2C\beta K^2 + \frac{1}{2}(K+R)}}. \quad (\text{S18})$$

Consequently,

$$\mathcal{F}_{\text{intra}}(R, C)_{(2)} = k \frac{R}{\sqrt{[\frac{1}{2}(K+R)]^2 + 2C\beta K^2 + \frac{1}{2}(K+R)}}, \quad (\text{S19a})$$

$$\Xi_{\text{intra}}(R, C)_{(2)} = k \frac{1}{\sqrt{[\frac{1}{2}(K+R)]^2 + 2C\beta K^2 + \frac{1}{2}(K+R)}}. \quad (\text{S19b})$$

When  $\beta \ll \frac{1}{8C}$  or  $8\beta C/(1+R/K)^2 \ll 1$ , using first order approximations in the denominator of Eq. S18, we have

$$x \approx \frac{RC}{(K+R) + \frac{2K}{(1+R/K)}\beta C}, \quad (\text{S20})$$

and then,

$$\mathcal{F}_{\text{intra}}(R, C)_{(3)} = k \frac{R}{(K+R) + \frac{2K}{(1+R/K)}\beta C}, \quad (\text{S21a})$$

$$\Xi_{\text{intra}}(R, C)_{(3)} = k \frac{1}{(K+R) + \frac{2K}{(1+R/K)}\beta C}. \quad (\text{S21b})$$

In the case that  $8\beta C/(1+R/K)^2 \gg 1$ , using first order approximations in Eq. S18, we obtain

$$x \approx \frac{RC}{K\sqrt{2C\beta} + \frac{(K+R)^2}{8K\sqrt{2C\beta}} + \frac{1}{2}(K+R)}, \quad (\text{S22})$$

and thus,

$$\mathcal{F}_{\text{intra}}(R, C)_{(4)} = k \frac{R}{K\sqrt{2C\beta} + \frac{(K+R)^2}{8K\sqrt{2C\beta}} + \frac{1}{2}(K+R)}, \quad (\text{S23a})$$

$$\Xi_{\text{intra}}(R, C)_{(4)} = k \frac{1}{K\sqrt{2C\beta} + \frac{(K+R)^2}{8K\sqrt{2C\beta}} + \frac{1}{2}(K+R)}. \quad (\text{S23b})$$

Meanwhile, the B-D model only fits to the cases with  $d = 0$ . By calculating the average values of  $t_h$  and  $t_w$  in the stochastic framework, we have  $\langle t_h \rangle = \frac{1}{k}$ ,  $\langle t_w \rangle = \frac{1}{d}$ . Thus, we obtain the searching efficiency and functional response in the B-D model:

$$\Xi_{\text{intra}}^{\text{B-D}}(R, C) = \frac{a}{1 + \frac{a}{k}R + \frac{a'}{d}C} = \frac{a}{1 + R/K|_{d=0} + \beta C}, \quad (\text{S24a})$$

$$\mathcal{F}_{\text{intra}}^{\text{B-D}}(R, C) = \frac{aR}{1 + R/K|_{d=0} + \beta C}. \quad (\text{S24b})$$

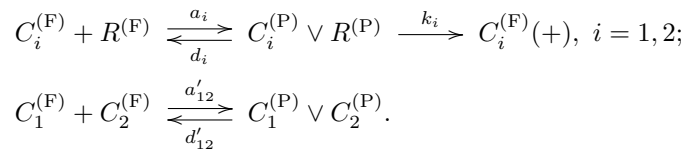
Overall, the searching efficiency (and the functional response) of the B-D model is quite different from either the rigorous form  $\Xi_{\text{intra}}(R, C)_{(1)}$ , the quasi rigorous form  $\Xi_{\text{intra}}(R, C)_{(2)}$ , or the more simplified forms  $\Xi_{\text{intra}}(R, C)_{(3)}$  and  $\Xi_{\text{intra}}(R, C)_{(4)}$  (Figure S3). Still, there is a region where the discrepancies can be small, namely  $d \approx 0$  and  $R \gg C$  (Figure S3). Intuitively, when  $\beta \ll \frac{1}{8C}$  and  $d = 0$ , then  $\Xi_{\text{intra}}(R, C)_{(3)} = \frac{a}{1 + \frac{a}{k}R + \frac{a'}{(1+R/K)}\beta C}$ .

Consequently, if  $R/K_i = x/C_i^{(F)} < 1$ , then  $\frac{2}{(1+R/K_i)} \in [1, 2]$ . In this case, the difference between  $\Xi_{\text{intra}}^{\text{B-D}}(R, C)$  and  $\Xi_{\text{intra}}(R, C)_{(3)}$  is small.

In fact, the above analysis also applies to cases with more than one types of consumer species (i.e., for cases with  $S_C > 1$ ).

#### D. Scenario involving chasing pair and interspecific interference

Next, we consider the scenario involving chasing pair and interspecific interference in the case of  $S_C = 2$  and  $S_R = 1$ :



Here  $C_1^{(P)} \vee C_2^{(P)}$  stands for the interspecific interference pair, denoted as  $z$ ;  $a'_{12}$  and  $d'_{12}$  represent the encounter rate and separation rate of the interference pair, respectively. Then, the total population of consumers and resources are  $C_i \equiv C_i^{(F)} + x_i + z$  and  $R \equiv R^{(F)} + x_1 + x_2$ . The population dynamics of the consumers and resources follows:

$$\begin{cases} \dot{x}_i = a_i C_i^{(F)} R^{(F)} - (k_i + d_i) x_i, \quad i = 1, 2; \\ \dot{z} = a'_{12} C_1^{(F)} C_2^{(F)} - d'_{12} z, \\ \dot{C}_i = w_i k_i x_i - D_i C_i, \\ \dot{R} = g(R, x_1, x_2, C_1, C_2). \end{cases} \quad (\text{S25})$$

where the functional form of  $g(R, x_1, x_2, C_1, C_2)$  is unspecified, while  $D_i$  and  $w_i$  represents the mortality rates of the two consumers species and biomass conversion ratios. Still, the consumption/interference process is supposed to be in fast equilibrium, i.e.,  $\dot{x}_i = 0, \dot{z} = 0$ . In the case that  $R \gg C_1 + C_2 > x_1 + x_2$ , by applying  $R^{(F)} \approx R$ , we obtain

$$x_1 \approx \frac{2C_1(R/K_2 + 1)R/K_1}{\sqrt{[\gamma(C_2 - C_1) + (\frac{R}{K_1} + 1)(\frac{R}{K_2} + 1)]^2 + 4\gamma C_1(\frac{R}{K_1} + 1)(\frac{R}{K_2} + 1) + \gamma(C_2 - C_1) + (\frac{R}{K_1} + 1)(\frac{R}{K_2} + 1)}}, \quad (\text{S26a})$$

$$x_2 \approx \frac{2C_2(R/K_1 + 1)R/K_2}{\sqrt{[\gamma(C_1 - C_2) + (\frac{R}{K_1} + 1)(\frac{R}{K_2} + 1)]^2 + 4\gamma C_2(\frac{R}{K_1} + 1)(\frac{R}{K_2} + 1) + \gamma(C_1 - C_2) + (\frac{R}{K_1} + 1)(\frac{R}{K_2} + 1)}}. \quad (\text{S26b})$$

Then, the searching efficiencies and functional responses are:

$$\Xi_1^{\text{inter}}(R, C_1, C_2)_{(1)} = \frac{2k_1(R/K_2 + 1)/K_1}{\gamma(C_2 - C_1) + (\frac{R}{K_1} + 1)(\frac{R}{K_2} + 1) + \sqrt{[\gamma(C_2 - C_1) + (\frac{R}{K_1} + 1)(\frac{R}{K_2} + 1)]^2 + 4\gamma C_1(\frac{R}{K_1} + 1)(\frac{R}{K_2} + 1)}}, \quad (\text{S27a})$$

$$\Xi_2^{\text{inter}}(R, C_1, C_2)_{(1)} = \frac{2k_2(R/K_1 + 1)/K_2}{\gamma(C_1 - C_2) + (\frac{R}{K_1} + 1)(\frac{R}{K_2} + 1) + \sqrt{[\gamma(C_1 - C_2) + (\frac{R}{K_1} + 1)(\frac{R}{K_2} + 1)]^2 + 4\gamma C_2(\frac{R}{K_1} + 1)(\frac{R}{K_2} + 1)}}, \quad (\text{S27b})$$

$$\mathcal{F}_1^{\text{inter}}(R, C_1, C_2)_{(1)} = \frac{2k_1(R/K_2 + 1)R/K_1}{\gamma(C_2 - C_1) + (\frac{R}{K_1} + 1)(\frac{R}{K_2} + 1) + \sqrt{[\gamma(C_2 - C_1) + (\frac{R}{K_1} + 1)(\frac{R}{K_2} + 1)]^2 + 4\gamma C_1(\frac{R}{K_1} + 1)(\frac{R}{K_2} + 1)}}, \quad (\text{S27c})$$

$$\mathcal{F}_2^{\text{inter}}(R, C_1, C_2)_{(1)} = \frac{2k_2(R/K_1 + 1)R/K_2}{\gamma(C_1 - C_2) + (\frac{R}{K_1} + 1)(\frac{R}{K_2} + 1) + \sqrt{[\gamma(C_1 - C_2) + (\frac{R}{K_1} + 1)(\frac{R}{K_2} + 1)]^2 + 4\gamma C_2(\frac{R}{K_1} + 1)(\frac{R}{K_2} + 1)}}. \quad (\text{S27d})$$

Since  $\frac{4\gamma^2 C_1 C_2}{[\gamma C_1 + \gamma C_2 + (\frac{R}{K_1} + 1)(\frac{R}{K_2} + 1)]^2} < 1$ , by applying first order approximation to the denominator of Eq. S26, we obtain:

$$x_1 \approx \frac{C_1 R}{(R + K_1) + \frac{\gamma K_1 K_2 C_2}{(R + K_2)} - \frac{\gamma^2 K_1 K_2 C_1 C_2}{[\gamma(C_1 + C_2) + (\frac{R}{K_1} + 1)(\frac{R}{K_2} + 1)](R + K_2)}}, \quad (\text{S28a})$$

$$x_2 \approx \frac{C_2 R}{(R + K_2) + \frac{\gamma K_1 K_2 C_1}{(R + K_1)} - \frac{\gamma^2 K_1 K_2 C_1 C_2}{[\gamma(C_1 + C_2) + (\frac{R}{K_1} + 1)(\frac{R}{K_2} + 1)](R + K_1)}}. \quad (\text{S28b})$$

and the searching efficiencies and functional responses are

$$\Xi_1^{\text{inter}}(R, C_1, C_2)_{(2)} = \frac{k_1}{(R + K_1) + \frac{\gamma K_1 K_2 C_2}{(R + K_2)} - \frac{\gamma^2 K_1 K_2 C_1 C_2}{[\gamma(C_1 + C_2) + (\frac{R}{K_1} + 1)(\frac{R}{K_2} + 1)](R + K_2)}}, \quad (\text{S29a})$$

$$\Xi_2^{\text{inter}}(R, C_1, C_2)_{(2)} = \frac{k_2}{(R + K_2) + \frac{\gamma K_1 K_2 C_1}{(R + K_1)} - \frac{\gamma^2 K_1 K_2 C_1 C_2}{[\gamma(C_1 + C_2) + (\frac{R}{K_1} + 1)(\frac{R}{K_2} + 1)](R + K_1)}}. \quad (\text{S29b})$$

$$\mathcal{F}_1^{\text{inter}}(R, C_1, C_2)_{(2)} = \frac{k_1 R}{(R + K_1) + \frac{\gamma K_1 K_2 C_2}{(R + K_2)} - \frac{\gamma^2 K_1 K_2 C_1 C_2}{[\gamma(C_1 + C_2) + (\frac{R}{K_1} + 1)(\frac{R}{K_2} + 1)](R + K_2)}}, \quad (\text{S29c})$$

$$\mathcal{F}_2^{\text{inter}}(R, C_1, C_2)_{(2)} = \frac{k_2 R}{(R + K_2) + \frac{\gamma K_1 K_2 C_1}{(R + K_1)} - \frac{\gamma^2 K_1 K_2 C_1 C_2}{[\gamma(C_1 + C_2) + (\frac{R}{K_1} + 1)(\frac{R}{K_2} + 1)](R + K_1)}}. \quad (\text{S29d})$$

Likewise, the B-D model only fits to cases with  $d = 0$ . By calculating the average values in a stochastic framework, we obtain  $\langle t_h^i \rangle = \frac{1}{k_i}, \langle t_w^i \rangle = \frac{1}{d_{12}^i}$  ( $i = 1, 2$ ). Then, we obtain the searching efficiencies in the B-D model:

$$\Xi_1^{\text{B-D (inter)}}(R, C_1, C_2) = \frac{a_1}{1 + \frac{a_1}{k_1} R + \frac{a_{12}^1}{d_{12}^1} C_2} = \frac{a_1}{1 + R/K_1 |_{d=0} + \gamma C_2}, \quad (\text{S30a})$$

$$\Xi_2^{\text{B-D (inter)}}(R, C_1, C_2) = \frac{a_2}{1 + \frac{a_2}{k_2} R + \frac{a_{12}^2}{d_{12}^2} C_1} = \frac{a_2}{1 + R/K_2 |_{d=0} + \gamma C_1}. \quad (\text{S30b})$$

Consequently, the functional responses in the B-D model are:

$$\mathcal{F}_1^{\text{B-D (inter)}}(R, C_1, C_2) = \frac{a_1 R}{1 + R/K_1 |_{d=0} + \gamma C_2}, \quad (\text{S31a})$$

$$\mathcal{F}_2^{\text{B-D (inter)}}(R, C_1, C_2) = \frac{a_2 R}{1 + R/K_2 |_{d=0} + \gamma C_1}. \quad (\text{S31b})$$

Evidently, the searching efficiencies in the B-D model are overall different from either the quasi rigorous form  $\Xi_i(R, C_1, C_2)_1$ , or the simplified form  $\Xi_i(R, C_1, C_2)_2$  (Figure S4). Still, the discrepancy can be small when  $d \approx 0$  and  $R \gg C$  (Figure S4). Intuitively, when  $\gamma \ll \min(C_1^{-1}, C_2^{-1})$ , we have

$$\Xi_1^{\text{inter}}(R, C_1, C_2)_{(2)} \approx \frac{a_1}{(1 + \frac{a_1}{k_1}R) + \frac{\gamma C_2}{R/K_2+1}}, \quad (\text{S32a})$$

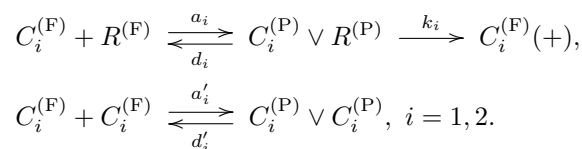
$$\Xi_2^{\text{inter}}(R, C_1, C_2)_{(2)} \approx \frac{a_2}{(1 + \frac{a_2}{k_2}R) + \frac{\gamma C_1}{R/K_1+1}}. \quad (\text{S32b})$$

Thus, if  $R/K_i = x_i/C_i^{(\text{F})} < 1$  ( $i = 1, 2$ ), then  $\frac{1}{1+R/K_i} \in [0.5, 1]$ . In this case, the difference between  $\Xi_i^{\text{B-D (inter)}}(R, C_1, C_2)$  and  $\Xi_i^{\text{inter}}(R, C_1, C_2)_{(2)}$  is small.

### III. SCENARIO INVOLVING CHASING PAIR AND INTRASPECIFIC INTERFERENCE

#### A. Two consumers species competing for one resource species

We consider the scenario involving chasing pair and intraspecific interference in the simple case of  $S_C = 2$  and  $S_R = 1$ :



Here, the variables and parameters are just extended from the case of  $S_C = 1$  and  $S_R = 1$  (see Sec. II C). The total number of consumers and resources are  $C_i \equiv C_i^{(\text{F})} + x_i + 2y_i$  and  $R \equiv R^{(\text{F})} + \sum_{i=1}^2 x_i$ . Hence, the population dynamics of the consumers and resources can be described as follows:

$$\begin{cases} \dot{x}_i = a_i C_i^{(\text{F})} R^{(\text{F})} - (k_i + d_i)x_i, \quad i = 1, 2; \\ \dot{y}_i = a'_i [C_i^{(\text{F})}]^2 - d'_i y_i, \\ \dot{C}_i = w_i k_i x_i - D_i C_i, \\ \dot{R} = g(R, x_1, x_2, C_1, C_2). \end{cases} \quad (\text{S33})$$

The functional form of  $g(R, x_1, x_2, C_1, C_2)$  is unspecified. For simplicity, we define  $K_i \equiv (d_i + k_i)/a_i$ ,  $\alpha_i \equiv D_i/(w_i k_i)$ , and  $\beta_i \equiv a'_i/d'_i$  ( $i = 1, 2$ ). At steady state, from  $\dot{x}_i = 0$ ,  $\dot{y}_i = 0$ , we have

$$\begin{cases} x_i = C_i^{(\text{F})} R^{(\text{F})} / K_i, \quad i = 1, 2; \\ y_i = \beta_i [C_i^{(\text{F})}]^2. \end{cases} \quad (\text{S34})$$

Note that  $C_i \equiv C_i^{(\text{F})} + x_i + 2y_i$ , and  $R \equiv R^{(\text{F})} + \sum_{i=1}^2 x_i$ . Then,

$$R^{(\text{F})} = R / (1 + C_1^{(\text{F})} / K_1 + C_2^{(\text{F})} / K_2), \quad (\text{S35a})$$

$$C_i = C_i^{(\text{F})} + R^{(\text{F})} C_i^{(\text{F})} / K_i + 2\beta_i [C_i^{(\text{F})}]^2, \quad i = 1, 2. \quad (\text{S35b})$$

By substituting Eq. S35a into Eq. S35b, we have

$$C_2^{(\text{F})} = \frac{K_2}{K_1} \left[ \frac{R C_1^{(\text{F})}}{C_1 - C_1^{(\text{F})} - 2\beta_1 [C_1^{(\text{F})}]^2} - K_1 - C_1^{(\text{F})} \right], \quad (\text{S36a})$$

$$(C_2 - C_2^{(\text{F})} - 2\beta_2 [C_2^{(\text{F})}]^2) (1 + C_1^{(\text{F})} / K_1 + C_2^{(\text{F})} / K_2) = R C_2^{(\text{F})} / K_2. \quad (\text{S36b})$$

Then, we can present  $C_i^{(\text{F})}$  with  $C_1$ ,  $C_2$  and  $R$  ( $i = 1, 2$ ). By further combining with Eqs. S34, S35a and S36a, we express  $R^{(\text{F})}$ ,  $x_i$ , and  $y_i$  using  $C_1$ ,  $C_2$  and  $R$ . In particular, for  $x_i$ , we have:

$$x_i = u_i(R, C_1, C_2), \quad i = 1, 2. \quad (\text{S37})$$

If all species coexist, then the steady-state equations of  $\dot{C}_i = 0$  ( $i = 1, 2$ ) and  $\dot{R} = 0$  are:

$$\begin{cases} \Omega_1(R, C_1, C_2) - D_1 = 0, \\ \Omega_2(R, C_1, C_2) - D_2 = 0, \\ G(R, C_1, C_2) = 0, \end{cases} \quad (\text{S38})$$

where  $G(R, C_1, C_2) \equiv g(R, u_1(R, C_1, C_2), u_2(R, C_1, C_2), C_1, C_2)$ , and  $\Omega_i(R, C_1, C_2) \equiv \frac{w_i k_i}{C_i} u_i(R, C_1, C_2)$ . In practice, Eq. S38 corresponds to three unparallel surfaces, which share a common point (Figures 1h and S8a-b). Importantly, the fixed point can be stable, and hence two consumer species may coexist at constant population densities.

### 1. Stability analysis and a Hopf bifurcation

We use linear stability analysis to study the local stability of the fixed point. Specifically, for an arbitrary fixed point  $E(x_1, x_2, y_1, y_2, C_1, C_2, R)$ , only when all the eigenvalues (defined as  $\lambda_i, i = 1, \dots, 7$ ) of the Jacobian matrix at point  $E$  own negative real parts would the point be locally stable.

Here we identify that when the separation rate  $d'$  ( $d' = d'_1 = d'_2$ ) of the interference-pair increases in the vicinity of the critical value  $d'_c$ , the population dynamics of the system transits from a stable fixed point into a stable limit cycle (Figure S9c-d, see also Figure S9a-b). In particular, the amplitude of the oscillation gradually increases with the bifurcation parameter  $d'$ . More quantitatively, the amplitude is proportional to  $\sqrt{d' - d'_c}$  (Figure S9c), which clearly demonstrates a supercritical Hopf bifurcation.

To further investigate whether there exists a non-zero measure parameter region for species coexistence, we set  $D_i$  ( $i = 1, 2$ ) to be the only parameter that varies with species  $C_1$  and  $C_2$ , and then  $\Delta \equiv (D_1 - D_2)/D_2$  reflects the complete difference between the two consumer species. As shown in Figure 2d-e, the region below the blue surface and above the red surface corresponds to stable coexistence, while that below the red surface and above  $\Delta = 0$  corresponds to unstable fixed points. Above all, there exists a non-zero measure parameter region to promote species coexistence regardless the life form of the resources.

### 2. Analytical solutions of the species abundances at steady state

At steady state, since  $\dot{x}_i = \dot{y}_i = \dot{C}_i = 0$  ( $i = 1, 2$ ), then,

$$\begin{cases} x_i = \alpha_i C_i, \\ C_i^{(\text{F})} = K_i \alpha_i C_i / R^{(\text{F})}, \\ y_i = \beta_i (K_i \alpha_i C_i)^2 [R^{(\text{F})}]^{-2}. \end{cases} \quad (\text{S39})$$

Meanwhile,  $C_i = C_i^{(\text{F})} + x_i + 2y_i$ , and  $C_i, R > 0$  ( $i = 1, 2$ ). Then, we have

$$C_i = \frac{(1 - \alpha_i)[R^{(\text{F})}]^2 - K_i \alpha_i R^{(\text{F})}}{2\beta_i (K_i \alpha_i)^2}. \quad (\text{S40})$$

If the resource species owns a much larger population abundance than the consumers (i.e.,  $R \gg C_1 + C_2$ ), then  $R \gg x_1 + x_2$ , and  $R^{(\text{F})} \approx R$ . Thus,

$$C_i = \frac{(1 - \alpha_i)R^2 - K_i \alpha_i R}{2\beta_i (K_i \alpha_i)^2}. \quad (\text{S41})$$

By further assuming that the population dynamics of the resources follow identical construction rule as the MacArthur's consumer-resource model, we have

$$g(R, x_1, x_2, C_1, C_2) = \begin{cases} R_0 R (1 - R/K_0) - (k_1 x_1 + k_2 x_2), & \text{for biotic resources,} \\ R_a (1 - R/K_0) - (k_1 x_1 + k_2 x_2), & \text{for abiotic resources.} \end{cases} \quad (\text{S42})$$

Since  $\dot{R} = 0$ , then for biotic resources,

$$R = \frac{k_1/(2\beta_1 K_1) + k_2/(2\beta_2 K_2) + R_0}{\frac{k_1(1-\alpha_1)}{2\beta_1 \alpha_1 (K_1)^2} + \frac{k_2(1-\alpha_2)}{2\beta_2 \alpha_2 (K_2)^2} + \frac{R_0}{K_0}}. \quad (\text{S43})$$

For abiotic resources,

$$R = \frac{-\kappa_1 + \sqrt{\kappa_1^2 + 4\kappa_2 R_a}}{2\kappa_2}, \quad (\text{S44})$$

where  $\kappa_1 = \frac{R_a}{K_0} - \frac{k_1}{2\beta_1 K_1} - \frac{k_2}{2\beta_2 K_2}$  and  $\kappa_2 = \frac{k_1(1-\alpha_1)}{2\beta_1 \alpha_1 (K_1)^2} + \frac{k_2(1-\alpha_2)}{2\beta_2 \alpha_2 (K_2)^2}$ .

Eqs. S41, S43, S44 are the analytical solutions of species abundances at steady state when  $R \gg C_1 + C_2$ . As shown in Figure 1e, the analytical solutions agree well with the numerical results (the exact solutions). To conduct a systematic comparison for different model parameters, we assign  $D_i$  ( $i = 1, 2$ ) to be the only parameter varying with species  $C_1$  and  $C_2$  ( $D_1 > D_2$ ), and define  $\Delta \equiv (D_1 - D_2)/D_2$  as the competitive difference between the two consumer species. The comparison between analytical solutions and numerical results is shown in Figure S8c-d. Clearly, they are close to each other, exhibiting very good consistency for all cases regardless of the life form of the resources.

Furthermore, we test if the parameter region for species coexistence is predictable using the analytical solutions. Since  $D_i$  ( $i = 1, 2$ ) is the only parameter that varies with the two-consumer species, the supremum of the tolerated competitive difference for species coexistence (defined as  $\bar{\Delta}$ ) corresponds to the steady-state solutions that satisfy  $R, C_2 > 0$  and  $C_1 = 0^+$ , where  $0^+$  stands for the infinitesimal positive number. To calculate the analytical solutions at the upper surface of the coexistence region, where  $\Delta = \bar{\Delta}$  and  $C_1 = 0^+$ , we further combine Eq. S41 and then obtain (note that  $R > 0$ )

$$R = \frac{K_1 \alpha_1}{1 - \alpha_1}. \quad (\text{S45})$$

Meanwhile,

$$\alpha_1 = \alpha_2(\Delta + 1) = \alpha_2(\bar{\Delta} + 1). \quad (\text{S46})$$

For biotic resources, combining Eqs. S43, S45 and S46, we have

$$\bar{\Delta} = \frac{1 - (K/K_0 + 1)\alpha_2}{k/(2\beta KR_0) + (K/K_0 + 1)\alpha_2}, \quad (\text{S47})$$

where  $K = K_i$ ,  $k = k_i$ , and  $\beta = \beta_i$  ( $i = 1, 2$ ). For abiotic resources, combining Eqs. S44-S46, we have

$$\bar{\Delta} = \frac{1}{\alpha_2(K_1 \varpi + 1)} - 1, \quad (\text{S48})$$

where  $\varpi = \frac{1}{2}(\frac{1}{K_0} - \frac{k_2}{2R_a \beta_2 K_2}) + \frac{1}{2}\sqrt{(\frac{1}{K_0} - \frac{k_2}{2R_a \beta_2 K_2})^2 + 2\frac{k_2(1-\alpha_2)}{R_a \beta_2 \alpha_2 (K_2)^2}}$ . When  $R \gg C_1 + C_2$ , the comparison of  $\bar{\Delta}$  obtained from analytical solutions with that from numerical results (the exact solutions) are shown in Figure S8e-f, which overall exhibits good consistency.

## B. $S_C$ consumers species competing for $S_R$ resources species

Here we consider the scenario involving chasing pair and intraspecific interference for the generic case with  $S_C$  types of consumers and  $S_R$  types of resources. Then, the population dynamics of the system can be described as follows:

$$\begin{cases} \dot{x}_{il} = a_{il} C_i^{(F)} R_l^{(F)} - (k_{il} + d_{il}) x_{il}, \\ \dot{y}_i = a'_{ii} [C_i^{(F)}]^2 - d'_{ii} y_i, \\ \dot{C}_i = \sum_{l=1}^{S_R} w_{il} k_{il} x_{il} - D_i C_i, \\ \dot{R}_l = g_l(\{R_l\}, \{x_i\}, \{C_i\}), i = 1, \dots, S_C, l = 1, \dots, S_R. \end{cases} \quad (\text{S49})$$

Note that Eq. S49 is identical with Eqs. 1-2, and we use the same variables and parameters as that in the main text. Then, the populations of the consumers and resources are  $C_i = C_i^{(F)} + \sum_{l=1}^{S_R} x_{il} + 2y_i$  and  $R_l = R_l^{(F)} + \sum_{i=1}^{S_C} x_{il}$ . For convenience, we define  $K_{il} \equiv (d_{il} + k_{il})/a_{il}$ ,  $\alpha_{il} \equiv D_{il}/(k_{il} w_{il})$  and  $\beta_i \equiv a'_{ii}/d'_{ii}$  ( $i = 1, \dots, S_C, l = 1, \dots, S_R$ ).

1. Analytical solutions of species abundances at steady state

At steady state, from  $\dot{x}_{il} = 0$ ,  $\dot{y}_i = 0$ , and  $\dot{C}_i = 0$ , we have,

$$\begin{cases} x_{il} = C_i^{(F)} R_l^{(F)} / K_{il}, \\ y_i = \beta_i [C_i^{(F)}]^2, \\ C_i^{(F)} = \sum_{l=1}^{S_R} x_{il} / \alpha_{il} = \sum_{l=1}^{S_R} C_i^{(F)} R_l^{(F)} / (K_{il} \alpha_{il}). \end{cases} \quad (\text{S50})$$

Meanwhile  $C_i = C_i^{(F)} + \sum_{l=1}^{S_R} x_{il} + 2y_i$ , and note that  $C_i > 0$ , thus

$$C_i^{(F)} = \frac{1}{2\beta_i} \left[ -1 + \sum_{l=1}^{S_R} \left( \frac{1}{\alpha_{il}} - 1 \right) \frac{R_l^{(F)}}{K_{il}} \right]. \quad (\text{S51})$$

Combined with Eq. S51, and then

$$C_i = \sum_{l=1}^{S_R} \frac{R_l^{(F)}}{2\beta_i \alpha_{il} K_{il}} \left[ -1 + \sum_{l'=1}^{S_R} \left( \frac{1}{\alpha_{il'}} - 1 \right) \frac{R_{l'}^{(F)}}{K_{il'}} \right]. \quad (\text{S52})$$

We further assume that the specific function of  $g_l(\{R_l\}, \{x_i\}, \{C_i\})$  satisfies Eq. 4, i.e.,

$$g_l(\{R_l\}, \{x_i\}, \{C_i\}) = \begin{cases} R_0^{(l)} R_l (1 - R_l / K_0^{(l)}) - \sum_{i=1}^{S_C} k_{il} x_{il}, & \text{for biotic resources,} \\ R_a^{(l)} (1 - R_l / K_0^{(l)}) - \sum_{i=1}^{S_C} k_{il} x_{il}, & \text{for abiotic resources.} \end{cases} \quad (\text{S53})$$

For biotic resources, by combining Eqs. S50, S51 and S53, we have

$$R_0^{(l)} R_l (1 - \frac{R_l}{K_0^{(l)}}) = \sum_{i=1}^{S_C} \frac{k_{il}}{2\beta_i K_{il}} \left[ -1 + \sum_{l'=1}^{S_R} \left( \frac{1}{\alpha_{il'}} - 1 \right) \frac{R_{l'}^{(F)}}{K_{il'}} \right] R_l^{(F)}. \quad (\text{S54})$$

If the population abundance of each resource species is much more than the total population of all consumers (i.e.,  $R_l \gg \sum_{i=1}^{S_C} C_i, l = 1, \dots, S_R$ ), then  $R_l \gg \sum_{i=1}^{S_C} x_{il}$  and  $R_l^{(F)} \approx R_l$ . Since  $R_l > 0 (l = 1, \dots, S_R)$ , then

$$\sum_{l'=1}^{S_R} [\delta_{l,l'} \frac{R_0^{(l)}}{K_0^{(l)}} + \sum_{i=1}^{S_C} \frac{k_{il}}{2\beta_i K_{il} K_{il'}} \left( \frac{1}{\alpha_{il'}} - 1 \right)] R_{l'} = R_0^{(l)} + \sum_{i=1}^{S_C} \frac{k_{il}}{2\beta_i K_{il}}, \quad (\text{S55})$$

with  $\delta_{l,l'} = \begin{cases} 0, & l \neq l'. \\ 1, & l = l'. \end{cases}$  To present Eq. S55 in a matrix form, we define matrix  $\mathbf{A} \equiv [A_{sq}] \in \mathbb{R}^{S_R \times S_R}$  ( $\mathbb{R}$  stands for the real number field), with

$$A_{sq} = \delta_{s,q} \frac{R_0^{(s)}}{K_0^{(s)}} + \sum_{i=1}^{S_C} \frac{k_{is}}{2\beta_i K_{is} K_{iq}} \left( \frac{1}{\alpha_{iq}} - 1 \right), \quad s, q = 1, \dots, S_R, \quad (\text{S56})$$

and two arrays

$$\begin{cases} \mathbf{B} \equiv (R_0^{(1)} + \sum_{i=1}^{S_C} \frac{k_{i1}}{2\beta_i K_{i1}}, \dots, R_0^{(S_R)} + \sum_{i=1}^{S_C} \frac{k_{iS_R}}{2\beta_i K_{iS_R}})^T, \\ \mathbf{R} \equiv (R_1, \dots, R_{S_R})^T, \end{cases} \quad (\text{S57})$$

where ‘‘T’’ represents the transpose. Then, Eq. S55 can be written as

$$\mathbf{A} \cdot \mathbf{R} = \mathbf{B}. \quad (\text{S58})$$

We can solve for  $\mathbf{R}$ :

$$\mathbf{R} = \frac{\text{adj}(\mathbf{A})}{\det(\mathbf{A})} \cdot \mathbf{B}. \quad (\text{S59})$$

where  $\text{adj}(\mathbf{A})$  and  $\det(\mathbf{A})$  denote the adjugate matrix and determinant of  $\mathbf{A}$ , respectively. Next, we define  $\mathbf{C} \equiv (C_1, \dots, C_{S_C})$ . Note that  $R_l \approx R_l^{(\text{F})}$ , combined with Eq. S52, we have

$$\begin{cases} \mathbf{C} \equiv (C_1, \dots, C_{S_C}), \\ C_i = \sum_{l=1}^{S_R} \frac{R_l}{2\beta_i \alpha_{il} K_{il}} [-1 + \sum_{l'=1}^{S_R} (\frac{1}{\alpha_{il'}} - 1) \frac{R_{l'}}{K_{il'}}], i = 1, \dots, S_C. \end{cases} \quad (\text{S60})$$

Then, for biotic resources, Eqs. S59-S60 are the analytical solutions to the steady state species abundances when  $R_l \gg \sum_{i=1}^{S_C} C_i (l = 1, \dots, S_R)$ . On the other hand, for abiotic resource, by combining Eqs. S50, S51 and S53, we have

$$R_0^{(l)} (1 - \frac{R_l}{K_0^{(l)}}) = \sum_{i=1}^{S_C} \frac{k_{il}}{2\beta_i K_{il}} [-1 + \sum_{l'=1}^{S_R} (\frac{1}{\alpha_{il'}} - 1) \frac{R_{l'}^{(\text{F})}}{K_{il'}}] R_l^{(\text{F})}. \quad (\text{S61})$$

If  $R_l \gg \sum_{i=1}^{S_C} C_i (l = 1, \dots, S_R)$ , then  $R_l \gg \sum_{i=1}^{S_C} x_{il}$  and  $R_l^{(\text{F})} \approx R_l$ . Thus,

$$(\frac{R_0^{(l)}}{K_0^{(l)}} - \sum_{i=1}^{S_C} \frac{k_{il}}{2\beta_i K_{il}} + \sum_{l'=1}^{S_R} \sum_{i=1}^{S_C} \frac{k_{il}}{2\beta_i K_{il}} (\frac{1}{\alpha_{il'}} - 1) \frac{R_{l'}}{K_{il'}}) R_l = R_0^{(l)}, \quad (\text{S62})$$

with  $l = 1, \dots, S_R$ . Eq. S62 is a set of second-order algebraic differential equations, which is clearly solvable.

In fact, when  $S_R = 1, S_C \geq 1$ , and  $R_l \gg \sum_{i=1}^{S_C} C_i (l = 1)$ , we can explicitly present the analytical solution of the steady-state species abundances. To simplify the notations, we omit the “ $l$ ” in the sub-/super-scripts since  $S_R = 1$ . Then, for biotic resources,

$$\begin{cases} R = \frac{R_0 + \sum_{i=1}^{S_C} k_i / (2\beta_i K_i)}{\sum_{i=1}^{S_C} \frac{k_i (1 - \alpha_i)}{2\beta_i \alpha_i (K_i)^2} + \frac{R_0}{K_0}}, \\ C_i = \frac{1}{2\beta_i \alpha_i K_i} [(\frac{1}{\alpha_i} - 1) \frac{R}{K_i} - 1] R, i = 1, \dots, S_C. \end{cases} \quad (\text{S63})$$

For abiotic resources,

$$\begin{cases} R = \frac{-\gamma_1 + \sqrt{\gamma_1^2 + 4\gamma_2 R_0}}{2\gamma_2}, \\ C_i = \frac{1}{2\beta_i \alpha_i K_i} [(\frac{1}{\alpha_i} - 1) \frac{R}{K_i} - 1] R, i = 1, \dots, S_C. \end{cases} \quad (\text{S64})$$

Here  $\gamma_1 \equiv \frac{R_0}{K_0} - \sum_{i=1}^{S_C} \frac{k_i}{2\beta_i K_i}$  and  $\gamma_2 \equiv \sum_{i=1}^{S_C} \frac{k_i (1 - \alpha_i)}{2\beta_i \alpha_i (K_i)^2}$ .

#### IV. SCENARIO INVOLVING CHASING PAIR AND INTERSPECIFIC INTERFERENCE

Here we consider the scenario involving chasing pair and interspecific interference in the case of  $S_C = 2$  and  $S_R = 1$ , with all settings follow that depicted in Sec. II D. Then,  $C_i \equiv C_i^{(\text{F})} + x_i + z, R \equiv R^{(\text{F})} + x_1 + x_2$ , and the population dynamics follows (identical with Eq. S25):

$$\begin{cases} \dot{x}_i = a_i C_i^{(\text{F})} R^{(\text{F})} - (k_i + d_i) x_i, i = 1, 2; \\ \dot{z} = a'_{12} C_1^{(\text{F})} C_2^{(\text{F})} - d'_{12} z, \\ \dot{C}_i = w_i k_i x_i - D_i C_i, \\ \dot{R} = g(R, x_1, x_2, C_1, C_2). \end{cases} \quad (\text{S65})$$

Here the functional form of  $g(R, x_1, x_2, C_1, C_2)$  is unspecified. For convenience, we define  $K_i \equiv (d_i + k_i)/a_i$ ,  $\alpha_i \equiv D_i/(w_i k_i)$  ( $i = 1, 2$ ), and  $\gamma \equiv a'_{12}/d'_{12}$ . At steady state, from  $\dot{x}_i = 0$  ( $i = 1, 2$ ) and  $\dot{z} = 0$ , we have

$$\begin{cases} x_i = C_i^{(F)} R^{(F)} / K_i, i = 1, 2; \\ z = \gamma C_1^{(F)} C_2^{(F)}. \end{cases} \quad (\text{S66})$$

Note that  $C_i \equiv C_i^{(F)} + x_i + z$  and  $R \equiv R^{(F)} + x_1 + x_2$ , then,

$$\begin{cases} C_1 = C_1^{(F)} + R^{(F)} C_1^{(F)} / K_1 + \gamma C_1^{(F)} C_2^{(F)}, \\ C_2 = C_2^{(F)} + R^{(F)} C_2^{(F)} / K_2 + \gamma C_1^{(F)} C_2^{(F)}, \\ R = R^{(F)} (1 + C_1^{(F)} / K_1 + C_2^{(F)} / K_2). \end{cases} \quad (\text{S67})$$

Then, we can express  $C_1^{(F)}$ ,  $C_2^{(F)}$  and  $R^{(F)}$  with  $C_1, C_2$  and  $R$ . Combined with Eq. S66,  $x_i$  and  $z$  can also be expressed using  $C_1, C_2$  and  $R$ . In particular, for  $x_i$ , we have

$$x_i = u'_i(R, C_1, C_2), i = 1, 2. \quad (\text{S68})$$

If all species coexist, by defining  $\Omega'_i(R, C_1, C_2) \equiv \frac{w_i k_i}{C_i} u'_i(R, C_1, C_2)$ , then, the steady-state equations of  $\dot{C}_i = 0$  ( $i = 1, 2$ ) and  $\dot{R} = 0$  are:

$$\begin{cases} \Omega'_1(R, C_1, C_2) - D_1 = 0, \\ \Omega'_2(R, C_1, C_2) - D_2 = 0, \\ G'(R, C_1, C_2) = 0, \end{cases} \quad (\text{S69})$$

where  $G'(R, C_1, C_2) \equiv g(R, u'_1(R, C_1, C_2), u'_2(R, C_1, C_2), C_1, C_2)$ . Here, Eq. S69 corresponds to three unparallel surfaces and share a common point (Figures 1g and S6a-b). However, all the fixed points are unstable, and hence the consumer species cannot stably coexist at steady state (Figure 1d).

### A. Stability analysis of the coexistence behavior

In the scenario involving chasing pair and interspecific interference, all the fixed points are unstable (Figure S6e-f). For abiotic resources, the two consumer species cannot coexist for long (Figures 1d and S7a). For biotic resources, in the ODEs studies, both consumer species may coexist with oscillations (Figure S7c, e) or in a quasi periodic way (Figure S7d, f, see Figure S7g and h for the Lyapunov exponents and Poincare map). However, none of the coexisting states can be maintained along with stochasticity (Figure S7j, see Figure S7i for the ODEs counterpart).

### B. Analytical results of the fixed-point solution

We proceed to investigate the unstable fixed point where  $R, C_1, C_2 > 0$ . From  $\dot{x}_i = 0$  ( $i = 1, 2$ ),  $\dot{z} = 0$ ,  $\dot{C}_i = 0$ , and note that  $C_i \equiv C_i^{(F)} + x_i + z$ , we have

$$\begin{cases} C_i = K_i \alpha_i C_i (R^{(F)})^{-1} + \alpha_i C_i + z, i = 1, 2; \\ z = \gamma K_1 \alpha_1 K_2 \alpha_2 (R^{(F)})^{-2} C_1 C_2. \end{cases} \quad (\text{S70})$$

Since  $C_i > 0$ , then

$$\begin{cases} C_1 = \frac{(1-\alpha_2)[R^{(F)}]^2 - K_2 \alpha_2 R^{(F)}}{\gamma K_1 \alpha_1 K_2 \alpha_2}, \\ C_2 = \frac{(1-\alpha_1)[R^{(F)}]^2 - K_1 \alpha_1 R^{(F)}}{\gamma K_1 \alpha_1 K_2 \alpha_2}. \end{cases} \quad (\text{S71})$$

If  $R \gg C_1 + C_2$ , then  $R \gg x_1 + x_2$  and  $R^{(F)} \approx R$ , we have

$$\begin{cases} C_1 = \frac{(1-\alpha_2)R^2 - K_2 \alpha_2 R}{\gamma K_1 \alpha_1 K_2 \alpha_2}, \\ C_2 = \frac{(1-\alpha_1)R^2 - K_1 \alpha_1 R}{\gamma K_1 \alpha_1 K_2 \alpha_2}. \end{cases} \quad (\text{S72})$$

Still, we assume that the population dynamics of the resource species follows Eq. S42. At the fixed point,  $\dot{R} = 0$ . For biotic resources, we have

$$R_0 R \left(1 - \frac{R}{K_0}\right) = k_1 \alpha_1 C_1 + k_2 \alpha_2 C_2. \quad (\text{S73})$$

Substituting Eq. S72 into Eq. S73, and note that  $R > 0$ , then we can solve for  $R$

$$R = \frac{R_0 + \frac{k_1}{\gamma K_1} + \frac{k_2}{\gamma K_2}}{\frac{k_1 \alpha_1 + k_2 \alpha_2}{\gamma K_1 \alpha_1 K_2 \alpha_2} - \frac{k_1 + k_2}{\gamma K_1 K_2} + \frac{R_0}{K_0}}. \quad (\text{S74})$$

For abiotic resources, we have

$$R_a \left(1 - \frac{R}{K_0}\right) = k_1 \alpha_1 C_1 + k_2 \alpha_2 C_2. \quad (\text{S75})$$

Combined with Eq. S72, we can solve for  $R$

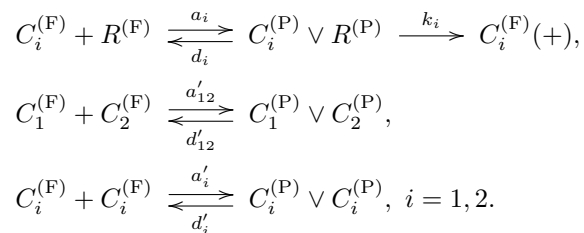
$$R = \frac{-\varrho_1 + \sqrt{\varrho_1^2 + 4\varrho_2 R_a}}{2\varrho_2}. \quad (\text{S76})$$

where  $\varrho_1 = \frac{R_a}{K_0} - \frac{k_1}{\gamma K_1} - \frac{k_2}{\gamma K_2}$  and  $\varrho_2 = \frac{k_1(1-\alpha_2)}{\gamma K_1 K_2 \alpha_2} + \frac{k_2(1-\alpha_1)}{\gamma K_1 K_2 \alpha_1}$ .

Eqs. S72, S74 and S76 are the analytical solutions of the fixed point when  $R \gg C_1 + C_2$ . As shown in Figure S6c-d, the analytical predictions agree well with the numerical results (the exact solutions).

## V. SCENARIO INVOLVING CHASING PAIR AND BOTH INTRA- AND INTER-SPECIFIC INTERFERENCE

Here we consider the scenario involving chasing pair and both intra- and inter-specific interference in the simple case of  $S_C = 2$  and  $S_R = 1$ :



We adopt the same notations as that depicted in Sec. III A and IV. Then,  $C_i \equiv C_i^{(\text{F})} + x_i + 2y_i + z$  and  $R \equiv R^{(\text{F})} + x_1 + x_2$ , and the population dynamics of the system can be described as follows:

$$\begin{cases} \dot{x}_i = a_i C_i^{(\text{F})} R^{(\text{F})} - (k_i + d_i) x_i, \\ \dot{z} = a'_{12} C_1^{(\text{F})} C_2^{(\text{F})} - d'_{12} z, \\ \dot{y}_i = a'_i [C_i^{(\text{F})}]^2 - d'_i y_i, \\ \dot{C}_i = w_i k_i x_i - D_i C_i, \\ \dot{R} = g(R, x_1, x_2, C_1, C_2), \quad i = 1, 2. \end{cases} \quad (\text{S77})$$

Here, the functional form of  $g(R, x_1, x_2, C_1, C_2)$  follows Eq. S42. For convenience, we define  $K_i \equiv (d_i + k_i)/a_i$ ,  $\alpha_i \equiv D_i/(w_i k_i)$ ,  $\beta_i \equiv a'_i/d'_i$ , and  $\gamma \equiv a'_{12}/d'_{12}$ , ( $i = 1, 2$ ). At steady state, from  $\dot{x}_i = 0$ ,  $\dot{y}_i = 0$ ,  $\dot{z} = 0$ , and  $\dot{C}_i = 0$ , ( $i = 1, 2$ ), we have

$$\begin{cases} x_i = \alpha_i C_i, \\ C_i^{(\text{F})} = K_i \alpha_i C_i (R^{(\text{F})})^{-1}, \\ y_i = \beta_i (K_i \alpha_i C_i)^2 [R^{(\text{F})}]^{-2}, \\ z = \gamma K_1 \alpha_1 K_2 \alpha_2 [R^{(\text{F})}]^{-2} C_1 C_2. \end{cases} \quad (\text{S78})$$

Combined with  $C_i \equiv C_i^{(\text{F})} + x_i + 2y_i + z$ , and since  $C_i > 0$  ( $i = 1, 2$ ), then,

$$\begin{cases} (1 - \alpha_1)(R^{(\text{F})})^2 - K_1 \alpha_1 R^{(\text{F})} = 2\beta_1 (K_1 \alpha_1)^2 C_1 + \gamma K_1 \alpha_1 K_2 \alpha_2 C_2, \\ (1 - \alpha_2)(R^{(\text{F})})^2 - K_2 \alpha_2 R^{(\text{F})} = 2\beta_2 (K_2 \alpha_2)^2 C_2 + \gamma K_1 \alpha_1 K_2 \alpha_2 C_1. \end{cases} \quad (\text{S79})$$

### A. Analytical solutions of species abundances at steady state

If  $R \gg C_1 + C_2$ , then  $R \gg x_1 + x_2$  and thus  $R^{(F)} \approx R$ . Combined with Eq. S79, we obtain

$$\begin{cases} C_1 = R \frac{(2\beta_2 K_2 \alpha_2 (1-\alpha_1) - \gamma K_1 \alpha_1 (1-\alpha_2)) R + (\gamma - 2\beta_2) K_1 \alpha_1 K_2 \alpha_2}{K_1^2 \alpha_1^2 K_2 \alpha_2 (4\beta_1 \beta_2 - \gamma^2)}, \\ C_2 = R \frac{(2\beta_1 K_1 \alpha_1 (1-\alpha_2) - \gamma K_2 \alpha_2 (1-\alpha_1)) R + (\gamma - 2\beta_1) K_1 \alpha_1 K_2 \alpha_2}{K_1 \alpha_1 K_2^2 \alpha_2^2 (4\beta_1 \beta_2 - \gamma^2)}. \end{cases} \quad (\text{S80})$$

For biotic resources, using  $\dot{R} = 0$  and  $R > 0$ , we have

$$R = \frac{\frac{k_1(\gamma - 2\beta_2)}{K_1(4\beta_1\beta_2 - \gamma^2)} + \frac{k_2(\gamma - 2\beta_1)}{K_2(4\beta_1\beta_2 - \gamma^2)} - R_0}{\frac{k_1 2\beta_2(\alpha_1 - 1)}{K_1^2 \alpha_1 (4\beta_1\beta_2 - \gamma^2)} + \frac{k_2 2\beta_1(\alpha_2 - 1)}{K_2^2 \alpha_2 (4\beta_1\beta_2 - \gamma^2)} - \frac{k_1 \gamma(\alpha_2 - 1)}{K_1 K_2 \alpha_2 (4\beta_1\beta_2 - \gamma^2)} - \frac{k_2 \gamma(\alpha_1 - 1)}{K_1 K_2 \alpha_1 (4\beta_1\beta_2 - \gamma^2)} - \frac{R_0}{K_0}}. \quad (\text{S81})$$

For abiotic resources,

$$R = \frac{-\kappa'_2 + \sqrt{(\kappa'_2)^2 + 4\kappa'_1 R_a}}{2\kappa'_1}, \quad (\text{S82})$$

where  $\kappa'_1 = \frac{k_2 \gamma(\alpha_1 - 1)}{K_1 K_2 \alpha_1 (4\beta_1\beta_2 - \gamma^2)} + \frac{k_1 \gamma(\alpha_2 - 1)}{K_1 K_2 \alpha_2 (4\beta_1\beta_2 - \gamma^2)} - \frac{k_1 2\beta_2(\alpha_1 - 1)}{K_1^2 \alpha_1 (4\beta_1\beta_2 - \gamma^2)} - \frac{k_2 2\beta_1(\alpha_2 - 1)}{K_2^2 \alpha_2 (4\beta_1\beta_2 - \gamma^2)}$ , and  $\kappa'_2 = \frac{k_1(\gamma - 2\beta_2)}{K_1(4\beta_1\beta_2 - \gamma^2)} + \frac{k_2(\gamma - 2\beta_1)}{K_2(4\beta_1\beta_2 - \gamma^2)} + \frac{R_a}{K_0}$ . Eqs. S80-S82 are the analytical solutions of the species abundances at steady state when  $R \gg C_1 + C_2$ . As shown in Figure S11, the analytical calculations agree well with the numerical results (the exact solutions).

### B. Stability analysis of the coexisting state

In the scenario involving chasing pair and both intra- and inter-specific interference, the behavior of species coexistence is similar to that without interspecific interference. Evidently, the influence of interspecific interference would be negligible if  $d'_{12}$  is extremely large, and vice versa for intraspecific interference if both  $d'_1$  and  $d'_2$  are tremendous. In the deterministic framework, the two-consumer species can coexist either at constant population densities or with time series dynamics such as oscillations (Figure S10d-f). The fixed points can be globally attracting or there is a stable limit cycle (Figure S10a-c and g-i). Furthermore, there is a non-zero measure of parameter set where both consumer species can coexist at steady state with only one type of resources (Figure S10a-c). In the stochastic framework, just as the scenario involving chasing pair and intraspecific interference, the coexistence state can be maintained along with stochasticity (Figure S12).

## VI. DIMENSIONAL ANALYSIS FOR THE SCENARIO INVOLVING CHASING PAIR AND BOTH INTRA- AND INTER-SPECIFIC INTERFERENCE

The population dynamics of the system involving chasing pair and both intra- and inter-specific interference are shown in Eqs. 1-4. For abiotic resources:

$$\begin{cases} \dot{x}_{il} = a_{il} C_i^{(F)} R_l^{(F)} - (d_{il} + k_{il}) x_{il}, \\ \dot{y}_i = a'_i [C_i^{(F)}]^2 - d'_i y_i, \\ \dot{z}_{ij} = a'_{ij} C_i^{(F)} C_j^{(F)} - d'_{ij} z_{ij} \\ \dot{C}_i = \sum_{l=1}^{S_R} w_{il} k_{il} x_{il} - D_i C_i, \\ \dot{R}_l = R_a^{(l)} (1 - R_l / K_0^{(l)}) - \sum_{i=1}^{S_C} k_{il} x_{il}, \end{cases} \quad (\text{S83})$$

with  $l = 1, \dots, S_R$ ;  $i, j = 1, \dots, S_C$ , and  $i \neq j$ . Here  $C_i = C_i^{(F)} + \sum_l x_{il} + 2y_i + \sum_{j \neq i} z_{ij}$  and  $R_l = R_l^{(F)} + \sum_i x_{il}$  represent the population abundances of the consumers and resources in the system. In fact, there are already several dimensionless variables and parameter in Eq. S83, namely  $x_{il}$ ,  $y_i$ ,  $z_{ij}$ ,  $C_i^{(F)}$ ,  $R_l^{(F)}$ ,  $C_i$ ,  $R_l$ ,  $w_{il}$ ,  $K_0^{(l)}$ . To make all terms dimensionless, we define  $\tilde{t} = t/\tau$ , where  $\tau = \bar{D}_1/D_1$  and  $\bar{D}_1$  is a reducible dimensionless parameter which is freely to take any positive values. Besides, we define dimensionless parameters  $\tilde{a}_{il} = a_{il}\tau$ ,  $\tilde{d}_{il} = d_{il}\tau$ ,  $\tilde{k}_{il} = k_{il}\tau$ ,  $\tilde{a}'_i = a'_i\tau$ ,  $\tilde{d}'_i = d'_i\tau$ ,  $\tilde{a}'_{ij} = a'_{ij}\tau$ ,  $\tilde{d}'_{ij} = d'_{ij}\tau$ ,  $\tilde{D}_i = D_i\tau$  and  $\tilde{R}_a^{(l)} = R_a^{(l)}\tau$ . By substituting all

the dimensionless terms into Eq. S83, we have

$$\begin{cases} \dot{x}_{il} = \tilde{a}_{il} C_i^{(F)} R_l^{(F)} - (\tilde{d}_{il} + \tilde{k}_{il}) x_{il}, \\ \dot{y}_i = \tilde{a}'_i [C_i^{(F)}]^2 - \tilde{d}'_i y_i, \\ \dot{z}_{ij} = \tilde{a}'_{ij} C_i^{(F)} C_j^{(F)} - \tilde{d}'_{ij} z_{ij} \\ \dot{C}_i = \sum_{l=1}^{S_R} w_{il} k_{il} x_{il} - \tilde{D}_i C_i, \\ \dot{R}_l = \tilde{R}_a^{(l)} (1 - R_l/K_0^{(l)}) - \sum_{i=1}^{S_C} \tilde{k}_{il} \tilde{x}_{il}. \end{cases} \quad (\text{S84})$$

Likewise, for biotic resources, by further defining  $\tilde{R}_0^{(l)} = R_0^{(l)} \tau$ , we obtain the population dynamics in the dimensionless form:

$$\begin{cases} \dot{x}_{il} = \tilde{a}_{il} C_i^{(F)} R_l^{(F)} - (\tilde{d}_{il} + \tilde{k}_{il}) x_{il}, \\ \dot{y}_i = \tilde{a}'_i [C_i^{(F)}]^2 - \tilde{d}'_i y_i, \\ \dot{z}_{ij} = \tilde{a}'_{ij} C_i^{(F)} C_j^{(F)} - \tilde{d}'_{ij} z_{ij} \\ \dot{C}_i = \sum_{l=1}^{S_R} w_{il} k_{il} x_{il} - \tilde{D}_i C_i, \\ \dot{R}_l = \tilde{R}_0^{(l)} R_l (1 - R_l/K_0^{(l)}) - \sum_{i=1}^{S_C} \tilde{k}_{il} \tilde{x}_{il}. \end{cases} \quad (\text{S85})$$

For convenience, we omit the notation “ $\sim$ ” and use dimensionless variables and parameters in the simulation studies unless otherwise specified.

## VII. METHODS

### A. Derivation of the encounter rates with the mean-field approximation

In the model depicted in Figure 1a, consumers and resources move randomly in space, which can be regarded as Brownian motions. At moment  $t$ , a consumer individual of species  $C_i$  ( $i = 1, \dots, S_C$ ) moves at speed  $v_{C_i}$  with velocity  $\mathbf{v}_{C_i}(t)$ , while a resource individual of species  $R_l$  ( $l = 1, \dots, S_R$ ) moves at speed  $v_{R_l}$  with velocity  $\mathbf{v}_{R_l}(t)$ . Here  $v_{C_i}$  and  $v_{R_l}$  are two invariants, while the directions of  $\mathbf{v}_{C_i}(t)$  and  $\mathbf{v}_{R_l}(t)$  change constantly. The relative velocity between the two individuals is  $\mathbf{u}_{C_i-R_l}(t) \equiv \mathbf{v}_{R_l}(t) - \mathbf{v}_{C_i}(t)$ , with a relative speed of  $u_{C_i-R_l}(t)$ . Then,  $u_{C_i-R_l}(t)^2 = v_{C_i}^2 + v_{R_l}^2 - 2v_{C_i} \cdot v_{R_l} \cdot \cos \theta_{C_i-R_l}(t)$ , where  $\theta_{C_i-R_l}(t)$  represents the angle between  $\mathbf{v}_{C_i}(t)$  and  $\mathbf{v}_{R_l}(t)$ . This system is homogeneous, thus,  $\overline{\cos \theta_{C_i-R_l}} = 0$ , where the overline stands for the temporal average. Then, we obtain the average relative speed between the  $C_i$  and  $R_l$  individuals:  $\overline{u_{C_i-R_l}} = \sqrt{v_{C_i}^2 + v_{R_l}^2}$ . Likewise, the average relative speed between the  $C_i$  and  $C_j$  individuals is  $\overline{u_{C_i-C_j}} = \sqrt{v_{C_i}^2 + v_{C_j}^2}$ . Evidently,  $\overline{u_{C_i-C_i}} = \sqrt{2}v_{C_i}$ . Meanwhile, the concentrations of species  $C_i$  and  $R_l$  in a squared system with a length of  $L$  are  $n_{C_i} = C_i/L^2$  and  $n_{R_l} = R_l/L^2$ , while those of the freely wandering  $C_i$  and  $R_l$  are  $n_{C_i^{(F)}} = C_i^{(F)}/L^2$  and  $n_{R_l^{(F)}} = R_l^{(F)}/L^2$ .

Then, we use the mean-field approximation to calculate the encounter rates  $a_{il}$  and  $a'_{ij}$  in the well-mixed system. In particular, we estimate  $a_{il}$  by tracking a randomly chosen consumer individual from species  $C_i$  and counting its encounter frequency with the freely wandering individuals from resource species  $R_l$  (Figure S1). At any moment, the consumer individual may form a chasing pair with a  $R_l$  individual within a radius of  $r_{il}^{(C)}$  (Figure 1a). Over a time interval of  $\Delta t$ , the number of encounters between the consumer individual and  $R_l$  individuals can be estimated by the encounter area and the concentration  $n_{R_l}$ , which takes the value of  $2r_{il}^{(C)} n_{R_l} \overline{u_{C_i-R_l}} \Delta t$  (see Figure S1). Combined with  $n_{R_l^{(F)}} = R_l^{(F)}/L^2$ , for all freely wandering  $C_i$  individuals, the number of their encounters with  $R_l^{(F)}$  during interval  $\Delta t$  is  $\frac{2r_{il}^{(C)} \overline{u_{C_i-R_l}} C_i^{(F)} R_l^{(F)}}{L^2} \Delta t$ . Meanwhile, in the ODEs, this corresponds to  $a_i C_i^{(F)} R_l^{(F)} \Delta t$ . Comparing the afore-mentioned two terms above, for chasing pair, we have  $a_{il} = 2r_{il}^{(C)} L^{-2} \overline{u_{C_i-R_l}} = 2r_{il}^{(C)} L^{-2} \sqrt{v_{C_i}^2 + v_{R_l}^2}$ . Likewise, for interference pair, we obtain  $a'_{ij} = 2r_{ij}^{(I)} L^{-2} \overline{u_{C_i-C_j}} = 2r_{ij}^{(I)} L^{-2} \sqrt{v_{C_i}^2 + v_{C_j}^2}$ . In particular,  $a'_{ii} = 2\sqrt{2}v_{C_i} r_{ii}^{(I)} L^{-2}$ .

## B. Stochastic simulations

To investigate the impact of stochasticity on species coexistence, we use stochastic simulation algorithm (SSA) [46] and individual-based modeling (IBM) [47, 48] in simulating the stochastic process. In the SSA studies, we follow the standard Gillespie algorithm and simulation procedures [46].

In the IBM studies, we consider a 2D squared system in a length of  $L$  with periodic boundary conditions. In the case of  $S_C = 2$  and  $S_R = 1$ , consumers of species  $C_i$  ( $i = 1, 2$ ) move at speed  $v_{C_i}$ , while the resources move at speed  $v_R$ . The unit length is  $\Delta l = 1$ , while all individuals move probabilistically. Specifically, when  $\Delta t$  is small so that  $v_{C_i}\Delta t \ll 1$ ,  $C_i$  individuals jump a unit length with the probability  $v_{C_i}\Delta t$ . In practice, we simulate the temporal evolution of the model system following the procedures below.

*Initialization.* We choose the initial position for each individual randomly from a uniform distribution in the squared space, which round to the nearest integer point in the  $x - y$  coordinate.

*Moving.* We choose the destination of a movement randomly from four directions ( $x$ -positive,  $x$ -negative,  $y$ -positive,  $y$ -negative) following a uniform distribution. The consumers and resources jump a unit length with probabilities  $v_{C_i}\Delta t$  and  $v_R\Delta t$ , respectively.

*Forming pairs.* When a  $C_i$  individual and a resource individual get close in space within a distance of  $r^{(C)}$ , they form a chasing pair. Meanwhile, when two consumer individuals  $C_i$  and  $C_j$  stand within a distance of  $r^{(I)}$ , they form an interference pair.

*Dissociation.* We update the system with a small time step  $\Delta t$  so that  $d_i\Delta t, k_i\Delta t, d'_{ij}\Delta t \ll 1$  ( $i, j = 1, 2$ ). In practice, a random number  $\varsigma$  is sampled from a uniform distribution between 0 and 1, i.e.,  $\mathcal{U}(0, 1)$ . If  $\varsigma < d_i\Delta t$  or  $\varsigma < d'_{ij}\Delta t$ , then, the chasing pair or interference pair dissociates into two separated individuals. One occupies the original position, while the other individual gets just out of the encounter radius in a uniformly distributed random angle. For a chasing pair, if  $d_i\Delta t < \varsigma < (d_i + k_i)\Delta t$ , then, the consumer catch the resource, and the biomass of the resource flows into the consumer populations (updated according to the birth procedure), while the consumer individual occupies the original position. Finally, if  $\varsigma > (d_i + k_i)\Delta t$  or  $\varsigma > d'_{ij}\Delta t$ , the chasing pair or interference pair maintain the current status.

*Birth and death.* For each species, we use two separate counters with decimal precision to record the contributions of the birth and death processes, which both accumulate in each time step. The incremental integer part of the counter will trigger updates in this run. Specifically, a newborn would join the system following the initialization procedure in a birth action, while an unfortunate target would be randomly chosen from the living population in a death action.

## VIII. SIMULATION DETAILS OF THE MAIN TEXT FIGURES

In Figure 1c, f:  $a_i = 0.1, d_i = 0.5, w_i = 0.1, k_i = 0.1$  ( $i = 1, 2$ );  $D_1 = 0.002, D_2 = 0.001, K_0 = 5, R_a = 0.05$ . In Figure 1d, g:  $a_i = 0.02, a'_{ij} = 0.021, d_i = 0.5, d'_{ij} = 0.01, w_i = 0.08, k_i = 0.03, i, j = 1, 2, i \neq j, D_2 = 0.001, D_1 = 0.0011, K_0 = 20, R_a = 0.01$ . In Figure 1e, h:  $a_i = 0.5, a'_i = 0.525, d_i = 0.5, d'_i = 0.5, w_i = 0.2, k_i = 0.4$  ( $i = 1, 2$ ),  $D_1 = 0.022, D_2 = 0.020, K_0 = 10, R_0 = 0.1$ . Figure 1c, f were calculated or simulated from Eqs. 1, 4. Figure 1d, g were calculated or simulated from Eqs. 1, 3, 4. Figure 1e, h were calculated or simulated from Eqs. 1, 2, 4.

In Figure 2a:  $a_i = 0.1, a'_i = 0.125, d_i = 0.1, d'_i = 0.05, w_i = 0.1, k_i = 0.1$  ( $i = 1, 2$ );  $D_1 = 0.0035, D_2 = 0.0038, K_0 = 100, R_a = 0.3$ . In Figure 2b-f:  $a_i = 0.1, d_i = 0.1, w_i = 0.1, k_i = 0.1$  ( $i = 1, 2$ );  $K_0 = 100$ . In 2b:  $a'_i = 0.125, d'_i = 0.05$  ( $i = 1, 2$ );  $D_1 = 0.0085, D_2 = 0.0080, R_0 = 0.05$ . In 2c:  $a'_i = 0.125, d'_i = 0.1$  ( $i = 1, 2$ );  $D_1 = 0.0085, D_2 = 0.0080, R_0 = 0.05$ . In Figure 2d:  $D_2 = 0.001, \Delta = (D_1 - D_2)/D_2, K_0 = 100, R_a = 0.1$ . In 2e:  $D_2 = 0.001, \Delta = (D_1 - D_2)/D_2, K_0 = 100, R_0 = 0.05$ . In Figure 2f:  $D_2 = 0.001, \Delta = 1, K_0 = 100, R_0 = 0.05$ . In Figure 2g, j:  $a_i = 0.02, a'_i = 0.025, d_i = 0.7, d'_i = 0.7, w_i = 0.4, k_i = 0.05$  ( $i = 1, 2$ );  $D_1 = 0.0160, D_2 = 0.0171, K_0 = 2000, R_a = 5.5$ . In Figure 2h-i:  $a_i = 0.06, a'_i = 0.075, d_i = 2, d'_i = 2, w_i = 0.32, k_i = 0.22$  ( $i = 1, 2$ );  $D_1 = 0.0550, D_2 = 0.0551, K_0 = 5000, R_0 = 0.13$ . In Figure 2k-l:  $L = 120, r^{(C)} = 5, r^{(I)} = 5, v_C = 1, v_R = 1, a_i = 0.195, a'_i = 0.195, d'_i = 0.4, d_i = 0.4, w_i = 0.3, k_i = 0.1$  ( $i = 1, 2$ );  $D_1 = 0.0080, D_2 = 0.0085, K_0 = 200, R_0 = 0.5$ . Figure 2a-l were calculated or simulated from Eqs. 1, 2, 4.

In Figure 3a-b:  $a_i = 0.3, a'_i = 0.33, w_i = 0.018, k_i = 4.8, d'_i = 5, d_i = 5.5$  ( $i = 1, 2$ );  $D_2 = 0.010, R_a = 35, K_0 = 10000$ . In Figure 3a:  $D_1 = 0.011$ . In Figure 3b:  $D_1 = 0.0132$ . In Figure 3c-d:  $w_i = 0.02, k_i = 4.5, d'_i = 4, d_i = 4.5$  ( $i = 1, 2$ );  $D_2 = 0.010, R_a = 35, K_0 = 10000$ . In Figure 3c:  $a_i = 0.2, a'_i = 0.24$  ( $i = 1, 2$ );  $D_1 = 0.0120$ . In Figure 3d:  $a_i = 0.3, a'_i = 0.36$  ( $i = 1, 2$ );  $D_1 = 0.0122$ . In Figure 3a-d:  $\tau = 0.4\text{Day}$  (see Sec. VI). Figure 3a-d were simulated from Eqs. 1, 2, 4. See Figure S15 for the long-term time series of all species.

In Figure 4a:  $a_i = 0.001, a'_i = 0.00125, d_i = 0.95, d'_i = 0.02, w_i = 0.2, k_i = 0.3, K_0 = 2000, R_a = 15.65, D_1 = 0.0260, D_2 = 0.0274, D_3 = 0.0250, D_4 = 0.0200, D_5 = 0.0230$ . Model settings in Figure 4b, d (bird):  $a_i = 0.1, a'_i = 0.125, d_i = 0.5, d'_i = 0.5, w_i = 0.3, k_i = 0.2, D_i = 0.02 \times \mathcal{N}(1, 0.28)$  ( $i = 1, \dots, S_C$ );  $R_a = 110, K_0 = 10^5, S_C = 250$  and  $S_R = 1$ . Model settings in Figure 4c, f (plankton(PS)):  $a_{il} = 0.1, a'_i = 0.125, d_{il} = 0.5, d'_i = 0.2, w_{il} = 0.3, k_{il} = 0.2, K_0^{(1)} = 8 \times 10^4, K_0^{(2)} = 5 \times 10^4, K_0^{(3)} = 3 \times 10^4, R_a^{(1)} = 280, R_a^{(2)} = 200, R_a^{(3)} = 150, D_i = 0.03 \times \mathcal{N}(1, 0.25)$  ( $i = 1, \dots, S_C, l = 1, \dots, S_R$ ),  $S_C = 150$  and  $S_R = 3$ . Model settings in Figure 4d (fish):  $a_i =$

$0.1, a'_i = 0.14, d_i = 0.5, d'_i = 0.5, w_i = 0.2, k_i = 0.1, D_i = 0.015 \times \mathcal{N}(1, 0.32)$  ( $i = 1, \dots, 45$ );  $R_a = 550, K_0 = 10^6, S_C = 45$  and  $S_R = 1$ . Model settings in Figure 4d (butterfly):  $a_i = 0.1, a'_i = 0.125, d_i = 0.5, d'_i = 0.3, w_i = 0.3, k_i = 0.2, D_i = 0.034 \times \mathcal{N}(1, 0.35)$  ( $i = 1, \dots, S_C$ );  $R_a = 300, K_0 = 10^5, S_C = 150$  and  $S_R = 1$ . Model settings in Figure 4e (bat):  $a_i = 0.1, a'_i = 0.125, d_i = 0.5, d'_i = 0.5, w_i = 0.2, k_i = 0.1, D_i = 0.013 \times \mathcal{N}(1, 0.34)$  ( $i = 1, \dots, S_C$ );  $R_a = 250, K_0 = 10^6, S_C = 40$  and  $S_R = 1$ . Model settings in Figure 4e (lizard):  $a_i = 0.1, a'_i = 0.125, d_i = 0.5, d'_i = 0.5, w_i = 0.2, k_i = 0.1, D_i = 0.014 \times \mathcal{N}(1, 0.34)$  ( $i = 1, \dots, S_C$ );  $R_a = 250, K_0 = 10^6, S_C = 55$  and  $S_R = 1$ . Model settings in Figure 4f (plankton(NS)):  $a_i = 0.1, a'_i = 0.125, d_i = 0.3, d'_i = 0.3, w_i = 0.3, k_i = 0.2, R_a = 350, K_0 = 10^4, D_i = 0.03 \times \mathcal{N}(1, 0.27)$  ( $i = 1, \dots, S_C$ ),  $S_C = 50$  and  $S_R = 1$ .  $\mathcal{N}(\mu, \sigma)$  represents the Gaussian distribution, where  $\mu$  and  $\sigma$  are the mean and standard deviation of the distribution. Figure 4a-f were simulated from Eqs. 1, 2, 4. See Figures 4b, S21k, c, d, h, i, j, S25e, f, g, h (the same as Figure 4c) for the time series of Figures 4d (ODEs $_{\text{bird}}^{S_R=1}$ ), 4d (ODEs $_{\text{butterfly}}^{S_R=1}$ ), 4d (ODEs $_{\text{fish}}^{S_R=1}$ ), 4e (ODEs $_{\text{bat}}^{S_R=1}$ ), 4e (SSA $_{\text{bat}}^{S_R=1}$ ), 4e (ODEs $_{\text{lizard}}^{S_R=1}$ ), 4e (SSA $_{\text{lizard}}^{S_R=1}$ ), 4f (ODEs $_{\text{plankton(NS)}}^{S_R=1}$ ), 4f (SSA $_{\text{plankton(NS)}}^{S_R=1}$ ), 4f (ODEs $_{\text{plankton(PS)}}^{S_R=3}$ ) and 4f (SSA $_{\text{plankton(PS)}}^{S_R=3}$ ), respectively. The Shannon entropies of the experimental data and simulation results for each ecological community are:  $H_{\text{Exp(ODEs)}}^{\text{bird(1982)}} = 5.67(6.79)$ ,  $H_{\text{Exp(ODEs)}}^{\text{bird(2018)}} = 6.63(6.79)$ ,  $H_{\text{Exp(ODEs)}}^{\text{butterfly}} = 4.78(4.12)$ ,  $H_{\text{Exp(ODEs)}}^{\text{fish}} = 3.78(3.40)$ ;  $H_{\text{Exp(ODEs,SSA)}}^{\text{bat}} = 3.00(2.95, 2.84)$ ,  $H_{\text{Exp(ODEs,SSA)}}^{\text{lizard}} = 4.05(3.57, 3.50)$ ;  $H_{\text{Exp(ODEs,SSA)}}^{\text{plankton(NS)}} = 4.67(4.74, 4.64)$ ,  $H_{\text{Exp(ODEs,SSA)}}^{\text{plankton(PS)}} = 4.68(6.43, 6.48)$ . Here the Shannon entropy  $H = - \sum_{i=1}^{S_C} \mathcal{P}_i \log_2(\mathcal{P}_i)$ , where  $\mathcal{P}_i$  is the probability that a consumer individual belongs to species  $C_i$ .

## IX. SUPPLEMENTAL FIGURES

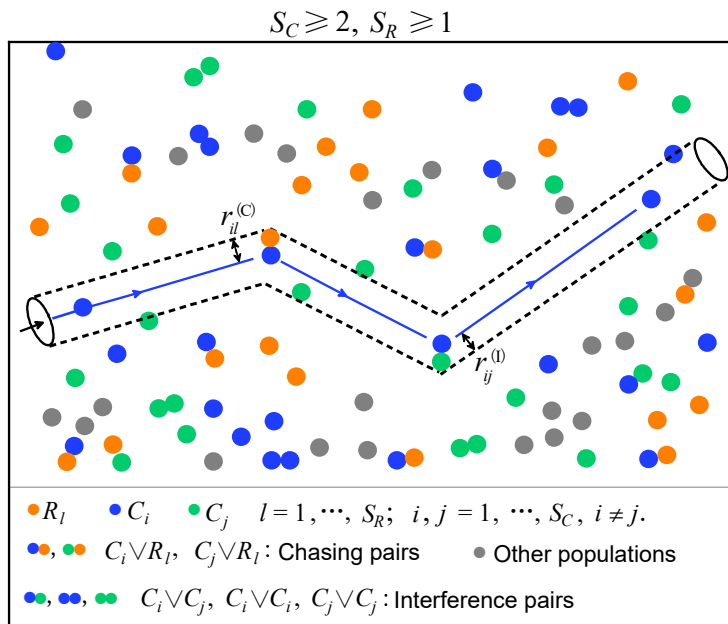


Figure S1. Estimation of the encounter rates with the mean-field approximations. To calculate  $a_{il}$  in the chasing pair, we suppose that all individuals of species  $R_l$  stand still while a  $C_i$  individual moves at the speed of  $\overline{u_{C_i-R_l}}$  (the relative speed). Over a time interval of  $\Delta t$ , the length of zigzag trajectory of the  $C_i$  individual is approximately  $\overline{u_{C_i-R_l}} \Delta t$ , while the encounter area (marked with dashed lines) is estimated to be  $2r_{il}^{(C)} \overline{u_{C_i-R_l}} \Delta t$ . Then, we can estimate the encounter rate  $a_{il}$  using the encounter area and concentrations of the species (see SI Sec. VII A for details). Similarly, we can estimate  $a'_{ij}$  in the interference pair.

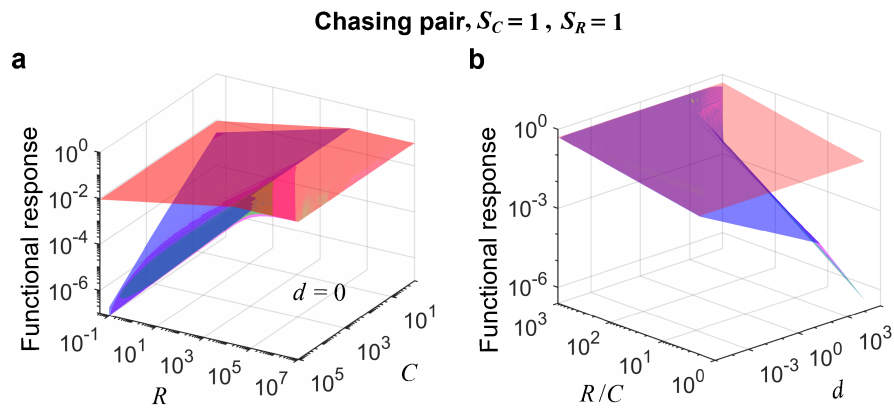


Figure S2. Functional response in the scenario involving only chasing pair. (a-b) The red surface corresponds to the B-D model (calculated from Eq.S10), while the green surface represents the exact solutions to our mechanistic model (calculated from Eq. S7). The magenta (calculated from Eq. S8) and blue (calculated from Eq. S9) surfaces represent the approximate solutions to our model. In (a-b):  $k = 0.1, a = 0.25$ . In (a):  $d = 0$ . (see SI Sec. II B).

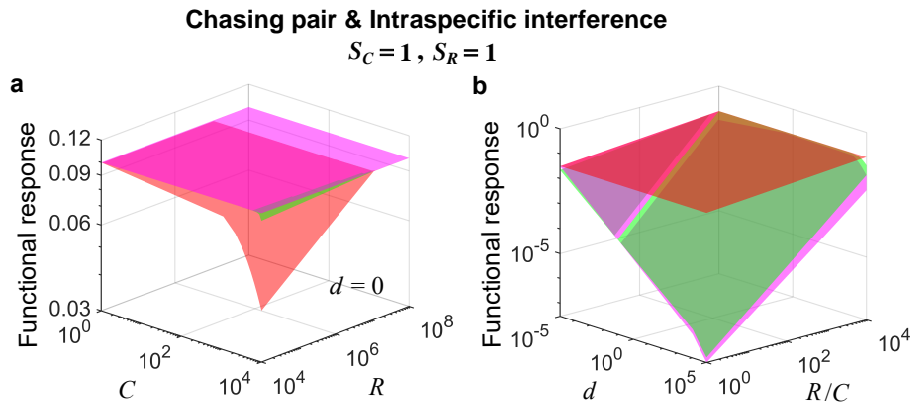


Figure S3. Functional response in the scenario involving chasing pair and intraspecific interference. (a-b) The red surface corresponds to the B-D model (calculated from Eq.S24), while the green surface represents the exact solutions to our mechanistic model (calculated from Eq. S17). The blue surface (calculated from Eq. S19) and the magenta surface (calculated from Eq. S21) represent the quasi-rigorous and the approximate solutions to our model, respectively. In (a-b):  $a = 0.1, k = 0.1, d' = 0.1, a' = 0.12$ . In (a):  $d = 0$  (see SI Sec. II C).

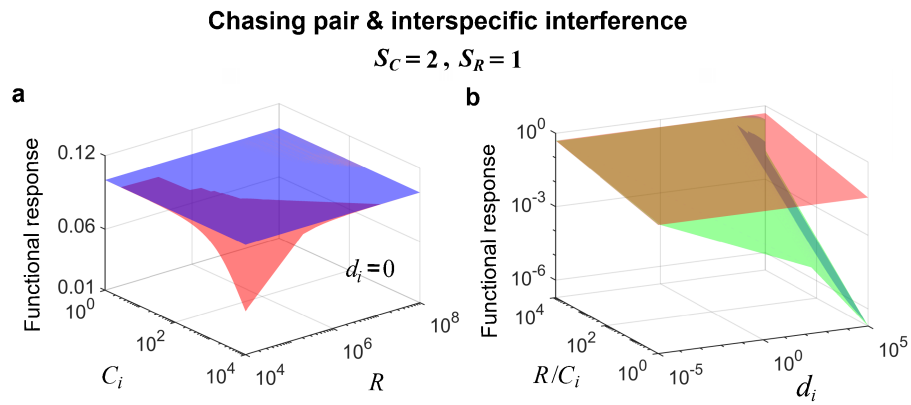


Figure S4. Functional response in the scenario involving chasing pair and interspecific interference. (a-b) The red surface corresponds to the B-D model (calculated from Eq. S31), while the green surface represents the quasi-rigorous solutions to our mechanistic model (calculated from Eq. S27). The blue surface (calculated from Eq. S29) represents the approximate solutions to our model. In (a-c):  $a_1 = a_2 = 0.1, k_1 = k_2 = 0.1, d'_{12} = 0.1, a'_{12} = 0.12$ . In (a):  $d_i = 0$  ( $i = 1, 2$ ) (see SI Sec. IID).

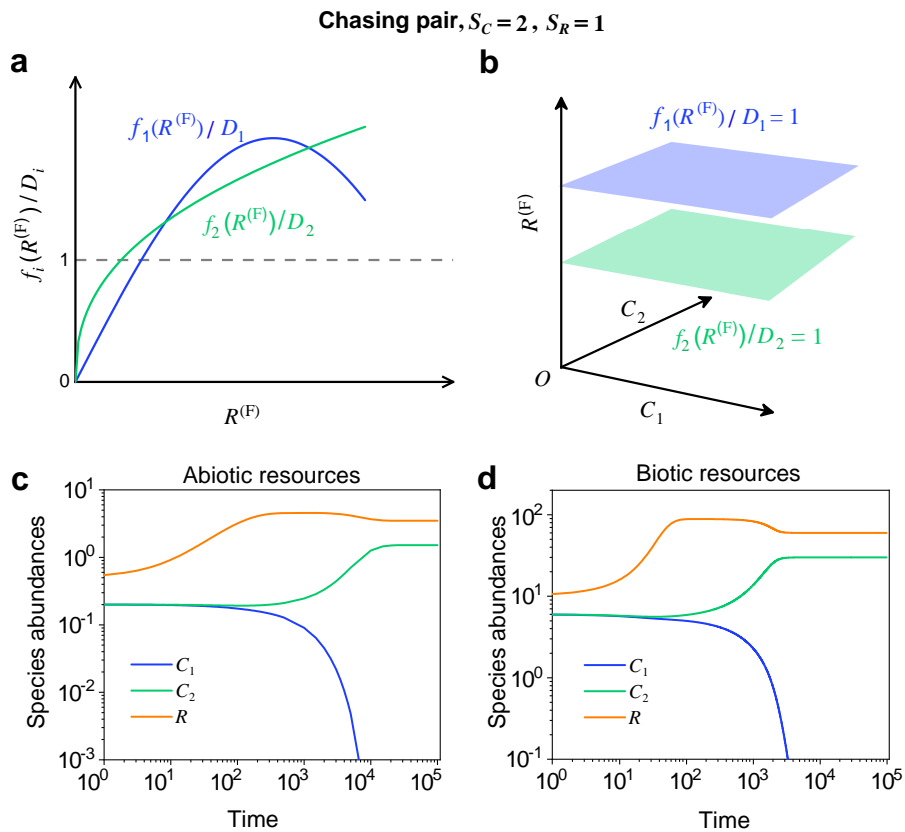


Figure S5. Forming chasing pair cannot break the constraint of competitive exclusion. (a) If all consumer species coexist at steady state, then  $f_i(R^{(F)})/D_i = 1$  ( $i = 1, 2$ ), where  $f_i(R^{(F)}) \equiv R^{(F)}/(R^{(F)} + K_i)$  and  $K_i \equiv (d_i + k_i)/a_i$ . This requires that the three lines  $y = f_i(R)/D_i$  ( $i = 1, 2$ ) and  $y = 1$  share a common point, which is generally impossible. (b) The blue plane is parallel to the green one, and hence they do not have a common point. (c-d) Time courses of the species abundances in the scenario involving only chasing pair. (c) and (d) were simulated from Eqs. 1, 4. In (c):  $a_1 = a_2 = 0.1, k_1 = k_2 = 0.1, w_1 = w_2 = 0.1, d_1 = d_2 = 0.5, D_1 = 0.002, D_2 = 0.001, K_0 = 5, R_a = 0.05$ . In (d):  $a_1 = a_2 = 0.1, k_1 = k_2 = 0.1, w_1 = w_2 = 0.1, d_1 = d_2 = 0.8, D_1 = 0.01, D_2 = 0.008, R_0 = 0.1, K_0 = 100$ .

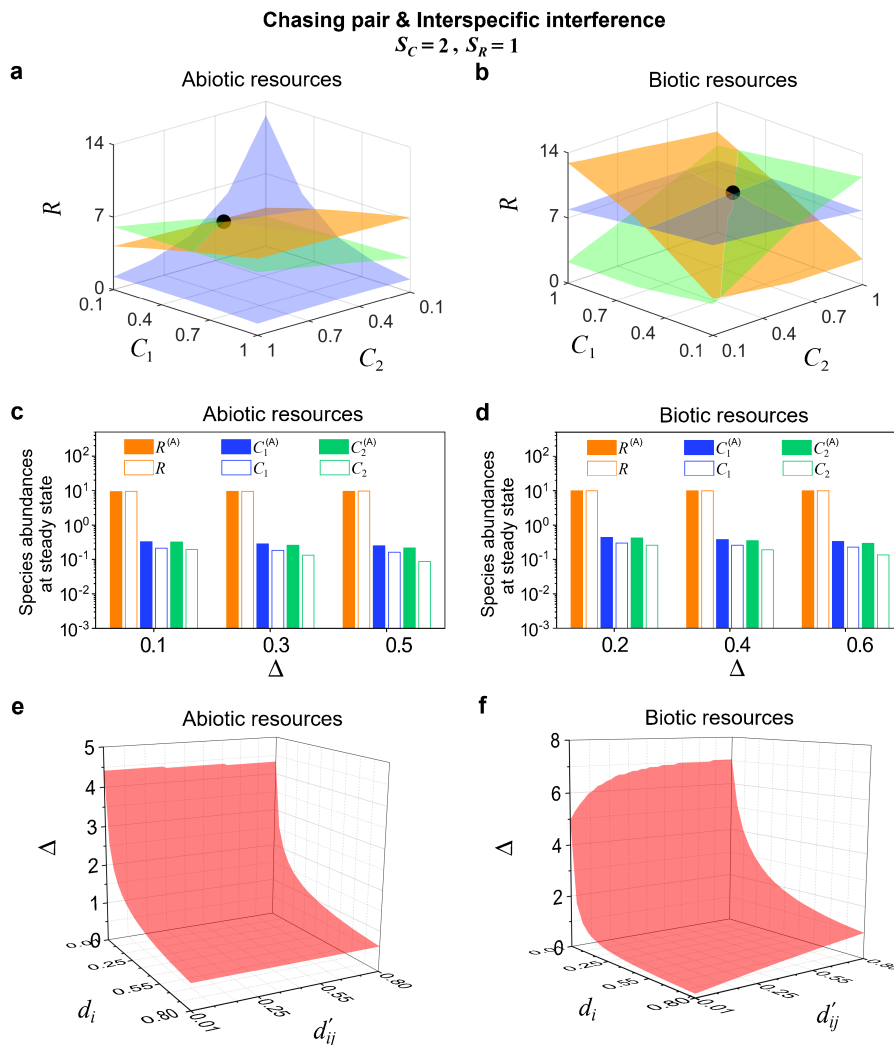


Figure S6. Fixed point solutions in the scenario involving chasing pair and interspecific interference. Here,  $S_C = 2$  and  $S_R = 1$ .  $D_i$  ( $i = 1, 2$ ) is the only parameter that varies with the consumer species (with  $D_1 > D_2$ ), and  $\Delta = (D_1 - D_2)/D_2$  represents the competitive difference between the two species. (a-b) Positive solutions to the steady-state equations:  $R_1 = 0$  (orange surface),  $C_1 = 0$  (blue surface),  $C_2 = 0$  (green surface). The intersection points marked by black dots are unstable fixed points. (c-d) Comparisons between the numerical results and analytical solutions of the species abundances at fixed points. Color bars are analytical solutions while hollow bars are numerical results. The analytical solutions (marked with superscript “A”) were calculated from Eqs. S72, S74, S76. (e-f) In this scenario, there is no parameter region for stable coexistence. The region below the red surface and above  $\Delta = 0$  represents unstable fixed points, which may end in a limit cycle (Figure S7e, g), a torus (Figure S7f, h), or  $C_1$  extinction (Figure S7c-d). The numerical results in (a)-(f) were calculated from Eqs. S42, S65. In (a):  $a_1 = a_2 = 0.05, d_1 = d_2 = 0.05, K_0 = 20, a'_{12} = 0.06, d'_{12} = 0.01, k_1 = k_2 = 0.02, w_1 = w_2 = 0.08, D_1 = 0.0011, D_2 = 0.001, R_a = 0.01$ . In (b):  $a_1 = a_2 = 0.05, d_1 = d_2 = 0.05, K_0 = 10, a'_{12} = 0.06, d'_{12} = 0.001, k_1 = k_2 = 0.02, w_1 = w_2 = 0.1, D_1 = 0.0011, D_2 = 0.001, R_0 = 0.01$ . In (c):  $a_1 = a_2 = 0.04, d_1 = d_2 = 0.2, K_0 = 10, a'_{12} = 0.048, d'_{12} = 0.001, k_1 = k_2 = 0.1, w_1 = w_2 = 0.3, D_2 = 0.0008, R_a = 0.2$ . In (d):  $a_1 = a_2 = 0.05, d_1 = d_2 = 0.2, K_0 = 10, a'_{12} = 0.07, d'_{12} = 0.001, k_1 = k_2 = 0.1, w_1 = w_2 = 0.2, D_2 = 0.0005, R_0 = 0.2$ . In (e-f):  $a_1 = a_2 = 0.1, K_0 = 100, k_1 = k_2 = 0.1, w_1 = w_2 = 0.1, D_2 = 0.001, a'_{12} = 0.12$ . In (e):  $R_a = 0.1$ . In (f):  $R_0 = 0.05$ .

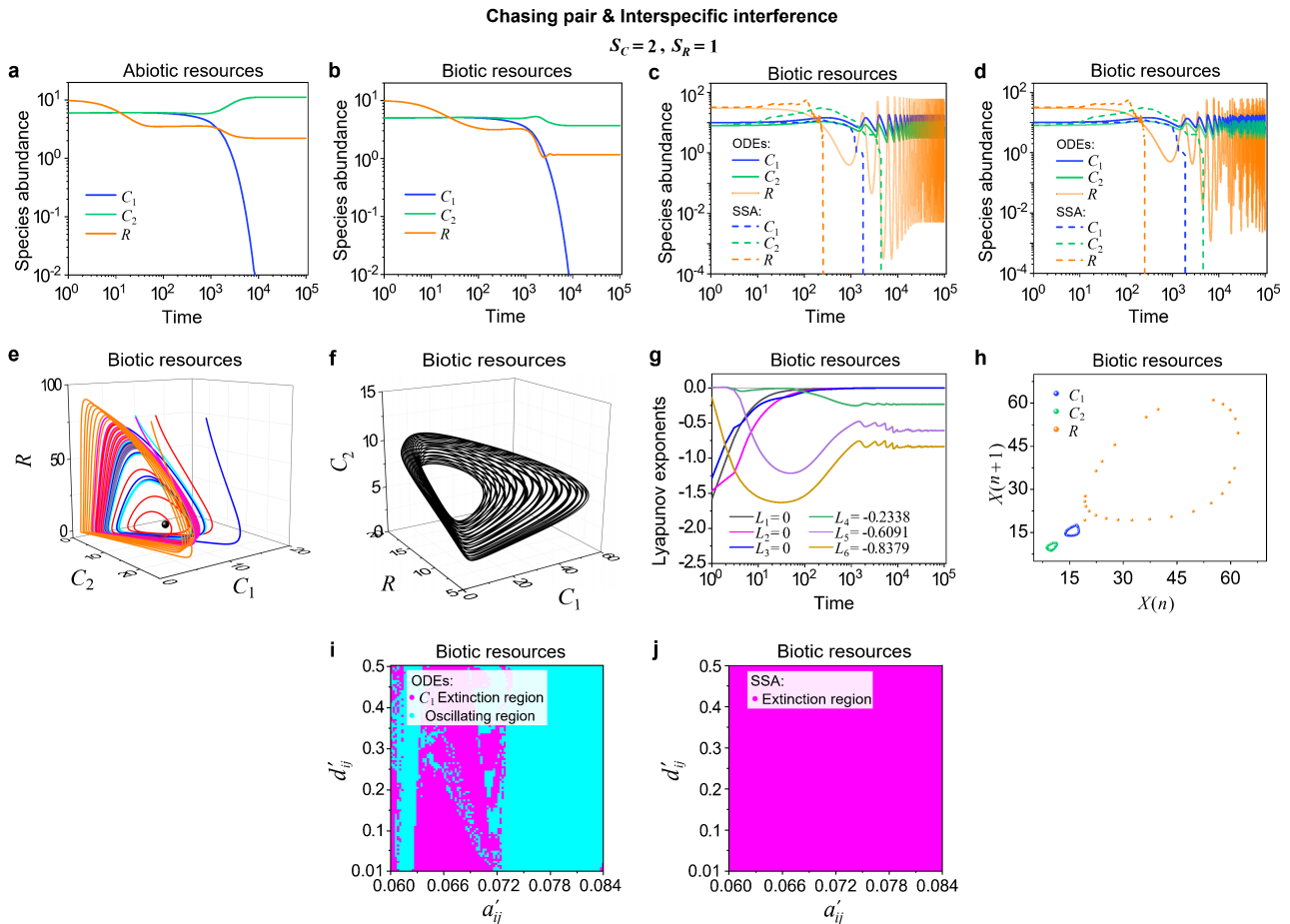


Figure S7. Numerical results in the scenario involving chasing pairs and interspecific interference. Here,  $S_C = 2$  and  $S_R = 1$ . (a-d) Time courses of the species abundances simulated with ODEs or SSA. (a-b) Consumer species cannot coexist at steady state. (c-d) Consumer species may coexist with time series dynamics in the ODEs simulations, yet all the coexistence states are vulnerable to stochasticity. (e-f) In a 3D phase space, the ODEs results in (c) and (d) correspond to a limit cycle and a quasi-periodic torus, respectively. (g-h) The Lyapunov exponents and Poincaré map further suggest that the dynamics in (d) is a quasi-periodic oscillation. (g) In the Lyapunov spectrum, three exponents are zeros while the rest are all negative, suggesting a 3-D torus. Here  $L_1, L_2, \dots, L_6$  represent the Lyapunov exponents. (h) The loops in the Poincaré map indicate a quasi-periodic oscillation. (i) In the ODEs studies, the cyan region represents oscillating coexistence while the magenta region represents  $C_1$  extinction. (j) In the SSA studies, there is no parameter region for species coexistence. The numerical results in (a)-(j) were calculated or simulated from Eqs. 1, 3, 4. In (a-b):  $a_1 = a_2 = 0.05$ ,  $d_1 = d_2 = 0.1$ ,  $k_1 = k_2 = 0.1$ ,  $w_1 = w_2 = 0.05$ ,  $D_1 = 0.0009$ ,  $a'_{12} = 0.06$ ,  $D_2 = 0.0007$ ,  $d'_{12} = 0.02$ ,  $K_0 = 10$ . In (a):  $R_a = 0.2$ . In (b):  $R_0 = 0.05$ . In (c-j):  $a_1 = a_2 = 0.06$ ,  $d_1 = d_2 = 0.2$ ,  $k_1 = k_2 = 0.1$ ,  $w_1 = w_2 = 0.06$ ,  $D_1 = 0.0009$ ,  $K_0 = 100$ ,  $R_0 = 0.05$ . In (c, e):  $D_2 = 0.00075$ ,  $a'_{12} = 0.063$ ,  $d'_{12} = 0.05$ . In (d, f, g, h):  $D_2 = 0.00071$ ,  $a'_{12} = 0.063$ ,  $d'_{12} = 0.05$ . In (i-j):  $D_2 = 0.00075$ .

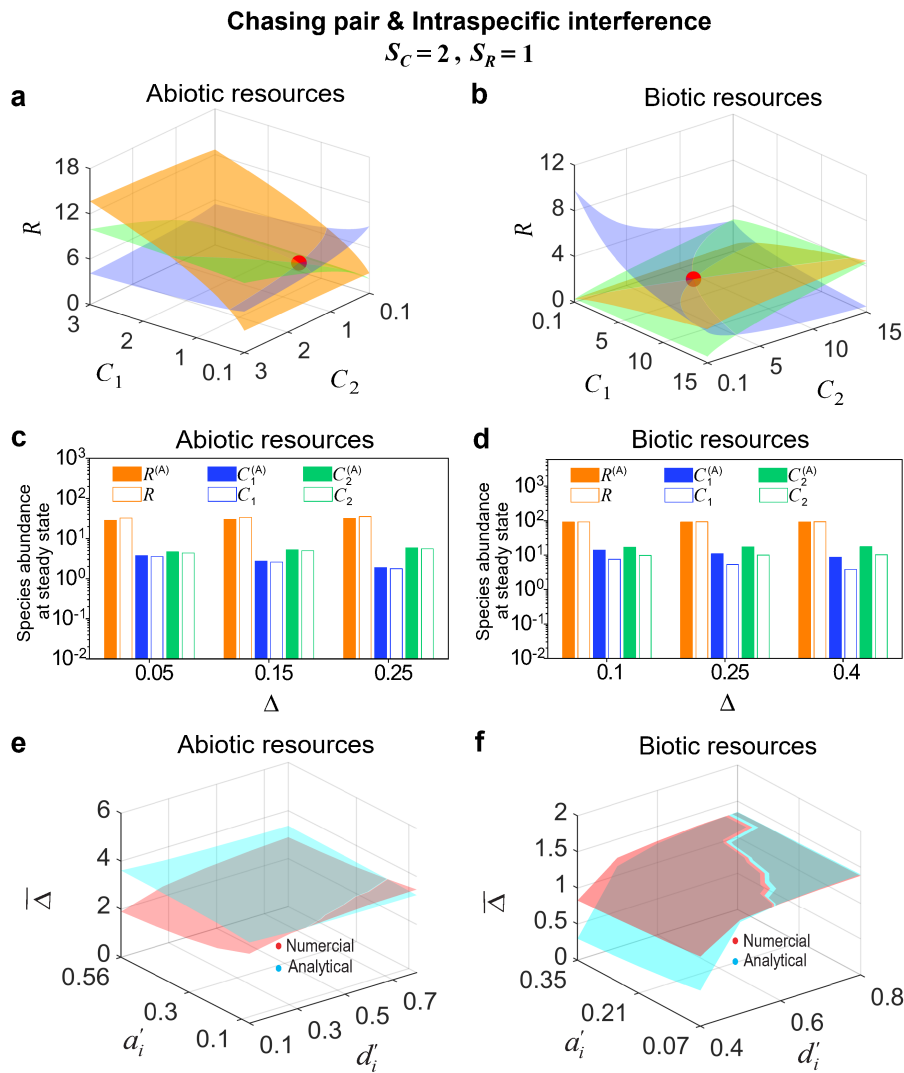


Figure S8. Fixed point solutions in the scenario involving chasing pair and intraspecific interference. Here,  $S_C = 2$  and  $S_R = 1$ .  $D_i$  ( $i = 1, 2$ ) is the only parameter varying with the consumer species (with  $D_1 > D_2$ ), and  $\Delta = (D_1 - D_2)/D_2$  represents the competitive difference between the two species. (a-b) Positive solutions to the steady-state equations:  $\dot{R}_1 = 0$  (orange surface),  $\dot{C}_1 = 0$  (blue surface),  $\dot{C}_2 = 0$  (green surface). The intersection points marked by red dots are stable fixed points. (c-d) Comparisons between the numerical results and analytical solutions of the species abundances at fixed points. Color bars are analytical solutions while hollow bars are numerical results. The analytical solutions (marked with superscript “(A)”) were calculated from Eqs. S41, S43 and S44. (e-f) Comparisons between the numerical results and analytical solutions of the coexistence region. Here  $\bar{\Delta}$  represents the maximum competitive difference tolerated for species coexistence. The red and cyan surfaces represent the analytical solutions (calculated from Eqs. S47, S48) and numerical results, respectively. The numerical results in (a)-(f) were calculated from Eqs. S33 and S42. In (a-b)  $a_1 = a_2 = 0.5, a'_1 = a'_2 = 0.625, d_1 = d_2 = 0.5, d'_1 = d'_2 = 0.5, k_1 = k_2 = 0.4, D_2 = 0.02, w_1 = w_2 = 0.5, K_0 = 10$ . In (a):  $D_1 = 1.2D_2, R_a = 0.1$ . In (b):  $D_1 = 1.05D_2, R_0 = 0.3$ . In (c):  $a_1 = a_2 = 0.1, a'_1 = a'_2 = 0.12, k_1 = k_2 = 0.12, w_1 = w_2 = 0.3, D_2 = 0.02, K_0 = 100, R_a = 0.8, d_1 = d_2 = 0.5, d'_1 = d'_2 = 0.05$ . In (d):  $a_1 = a_2 = 0.05, a'_1 = a'_2 = 0.06, k_1 = k_2 = 0.12, w_1 = w_2 = 0.2, D_2 = 0.008, K_0 = 100, R_0 = 0.1, d_1 = d_2 = 0.8, d'_1 = d'_2 = 0.01$ . In (e):  $a_1 = a_2 = 0.5, k_1 = k_2 = 0.2, w_1 = w_2 = 0.2, D_2 = 0.008, K_0 = 60, R_a = 0.8, d_1 = d_2 = 0.8$ . In (f):  $a_1 = a_2 = 0.5, k_1 = k_2 = 0.1, w_1 = w_2 = 0.2, D_2 = 0.008, K_0 = 100, R_0 = 0.2, d_1 = d_2 = 0.8$ .

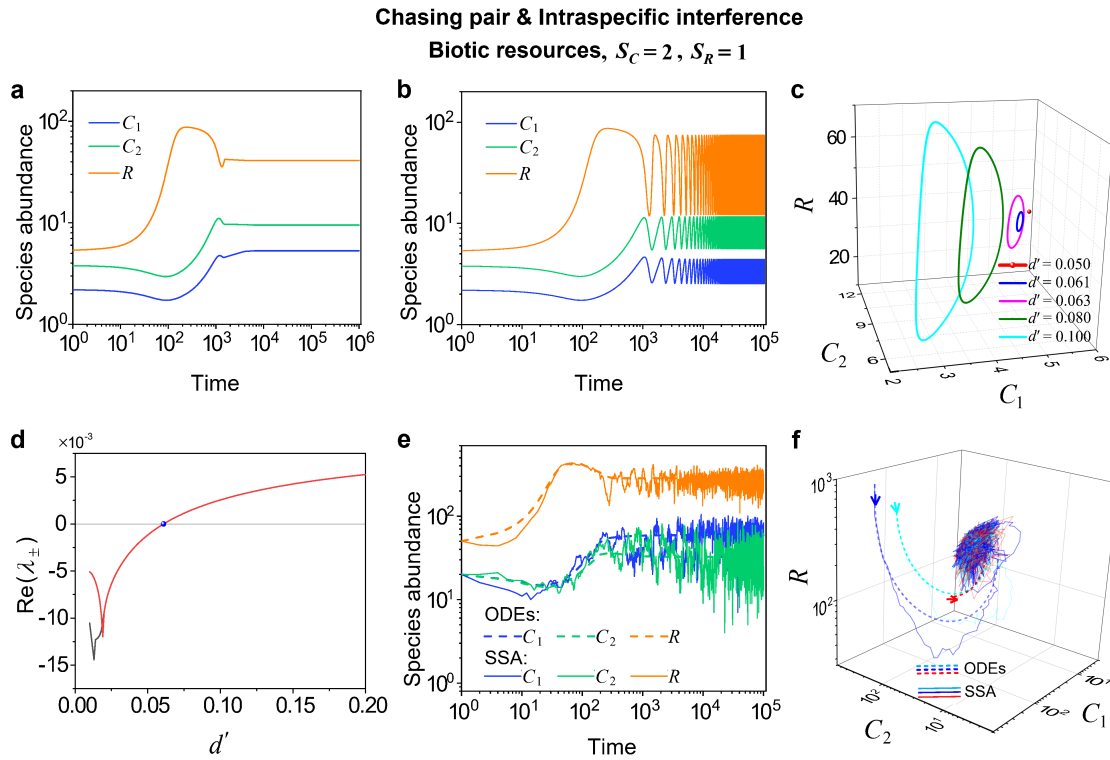


Figure S9. Numerical results in the scenario involving chasing pair and intraspecific interference. Here,  $S_C = 2$  and  $S_R = 1$ . (a-b) Time courses of the species abundances simulated with ODEs. The consumer species may coexist at steady state or with time series dynamics. (c) The phase diagram of a Hopf bifurcation by varying the parameter  $d'$  ( $d' \equiv d'_1 = d'_2$ ). (d) The Hopf bifurcation curve. (e-f) The two consumer species may coexist indefinitely along with stochasticity. (f) The coexistence state is stable and globally attractive (see (e) for the time courses). The numerical results in (a)-(f) were calculated or simulated from Eqs. 1, 2, 4. In (a-d):  $a_1 = a_2 = 0.1, a'_1 = a'_2 = 0.125, d_1 = d_2 = 0.1, k_1 = k_2 = 0.1, w_1 = w_2 = 0.1, K_0 = 100, D_1 = 0.0085, D_2 = 0.008, R_0 = 0.05$ . In (a):  $d'_1 = d'_2 = 0.05$ . In (b):  $d'_1 = d'_2 = 0.1$ . In (e-f):  $a_1 = a_2 = 0.06, a'_1 = a'_2 = 0.075, d_1 = d_2 = 2, d'_1 = d'_2 = 2, k_1 = k_2 = 0.22, w_1 = w_2 = 0.32, K_0 = 500, D_1 = 0.055, D_2 = 0.057, R_0 = 0.13$ .

## Chasing pair &amp; Interspecific and intraspecific interference

$$S_C = 2, S_R = 1$$

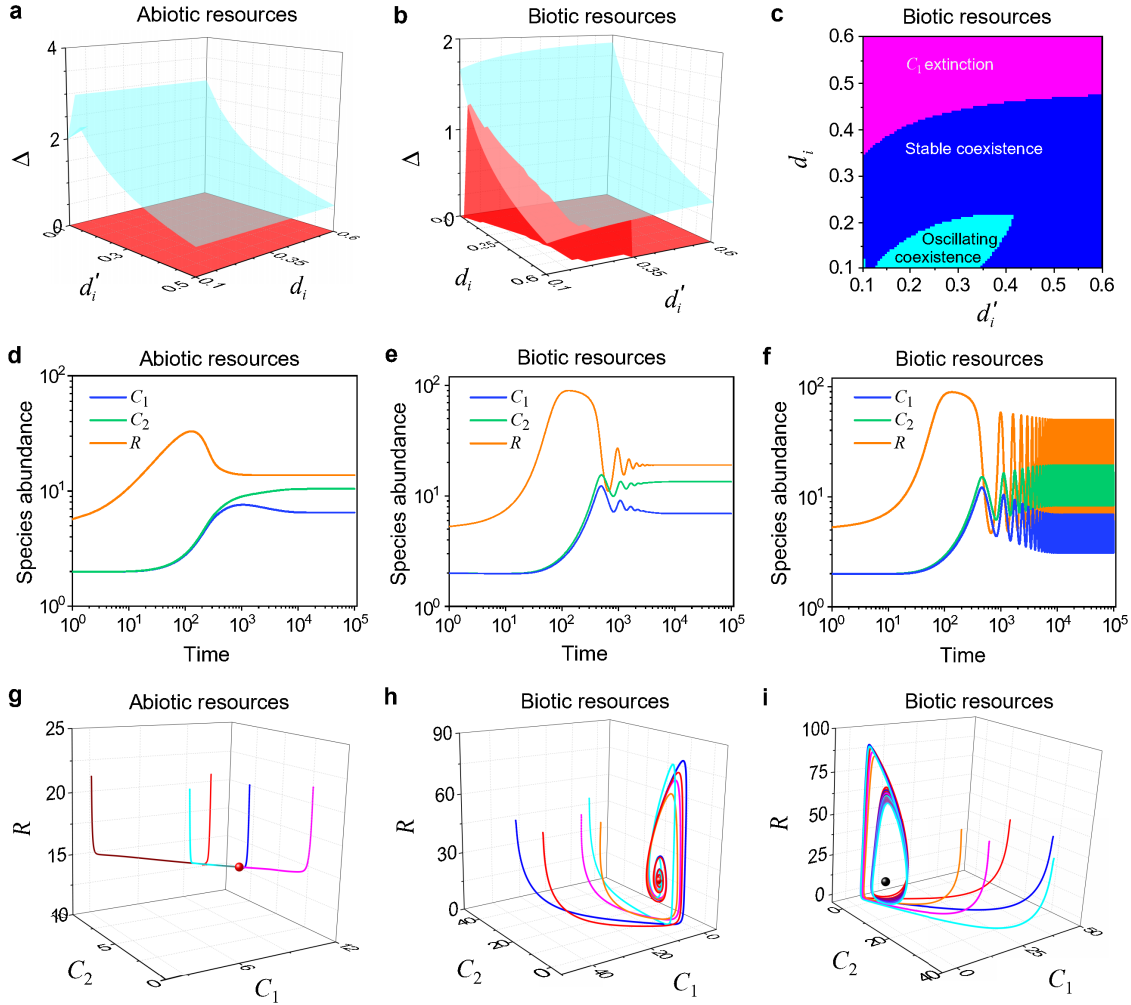


Figure S10. ODEs results in the scenario involving chasing pair and both intra- and inter-specific interference. Here,  $S_C = 2$  and  $S_R = 1$ . (a-c) 3D Phase diagrams.  $D_i$  ( $i = 1, 2$ ) is the only parameter that varies with the consumer species (with  $D_1 > D_2$ ), and  $\Delta = (D_1 - D_2)/D_2$  measures the competitive difference between the two species. The parameter region below the blue surface yet above the red surface represents stable coexistence, while that below the red surface and above  $\Delta = 0$  represents unstable fixed points. (c) A transection that corresponds to the plane  $\Delta = 0.25$  in (b). (d-f) Time courses of the species abundances. Consumer species may coexist at steady state or in an oscillating way. (g-h) The fixed points (shown in red) are stable and globally attractive. (i) The fixed point is unstable, and trajectories end in a limit cycle. The numerical results in (a)-(i) were calculated or simulated from Eqs. 1-4. In (a, d, g):  $a_1 = a_2 = 0.1, a'_1 = a'_2 = 0.12, k_1 = k_2 = 0.1, w_1 = w_2 = 0.1, D_2 = 0.004, K_0 = 100, a'_{12} = 0.12, R_a = 0.8, d'_{12} = 0.5$ . In (d, g):  $d_1 = d_2 = 0.3, d'_1 = d'_2 = 0.5, D_1 = 0.0042$ . In (b-c, e-f, h-i):  $a_1 = a_2 = 0.15, a'_1 = a'_2 = 0.165, k_1 = k_2 = 0.11, w_1 = w_2 = 0.1, D_2 = 0.0055, d'_{12} = 0.6, K_0 = 100, a'_{12} = 0.165, R_0 = 0.075$ . In (c):  $D_1 = 0.00688$ . In (e, h):  $d_1 = d_2 = 0.3, d'_1 = d'_2 = 0.4, D_1 = 0.006$ . In (f, i):  $d_1 = d_2 = 0.2, d'_1 = d'_2 = 0.4, D_1 = 0.006$ .

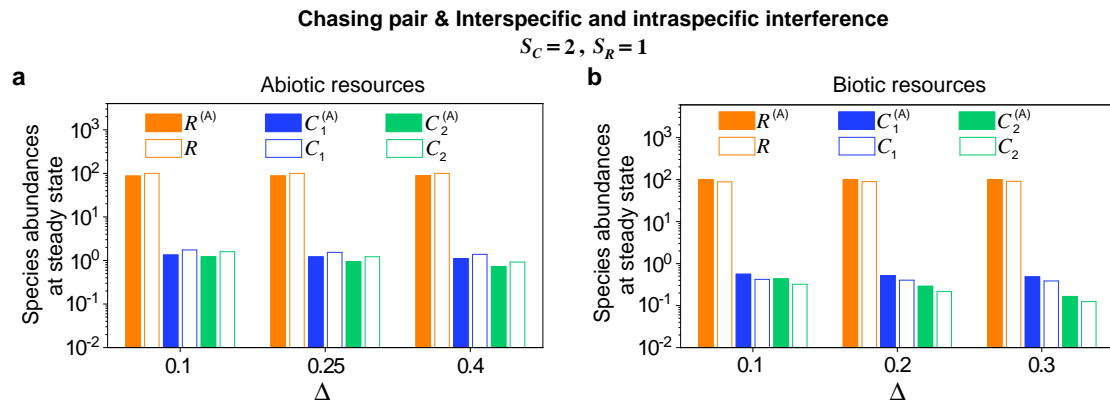


Figure S11. Comparisons between numerical results and analytical solutions of the species abundances at fixed points in the scenario involving chasing pair and both intra- and inter-specific interference. Here,  $S_C = 2$  and  $S_R = 1$ .  $D_i$  ( $i = 1, 2$ ) is the only parameter that varies with the consumer species, and  $\Delta = (D_1 - D_2)/D_2$  measures the competitive difference between the two species. Color bars are analytical solutions while hollow bars are numerical results. The numerical results were calculated from Eqs. 1-4, while the analytical solutions (marked with superscript “(A)”) were calculated from Eqs. S80-S82. In (a):  $a_1 = a_2 = 0.05, a'_1 = a'_2 = 0.06, k_1 = k_2 = 0.1, w_1 = w_2 = 0.2, D_2 = 0.008, K_0 = 100, R_a = 0.8, d_1 = d_2 = 0.5, d'_1 = d'_2 = 0.15, a'_{12} = 0.06, d'_{12} = 0.0005$ . In (b):  $a_1 = a_2 = 0.05, a'_1 = a'_2 = 0.06, k_1 = k_2 = 0.05, w_1 = w_2 = 0.2, D_2 = 0.006, K_0 = 100, R_0 = 0.2, d_1 = d_2 = 0.5, d'_1 = d'_2 = 0.02, a'_{12} = 0.06, d'_{12} = 0.0005$ .

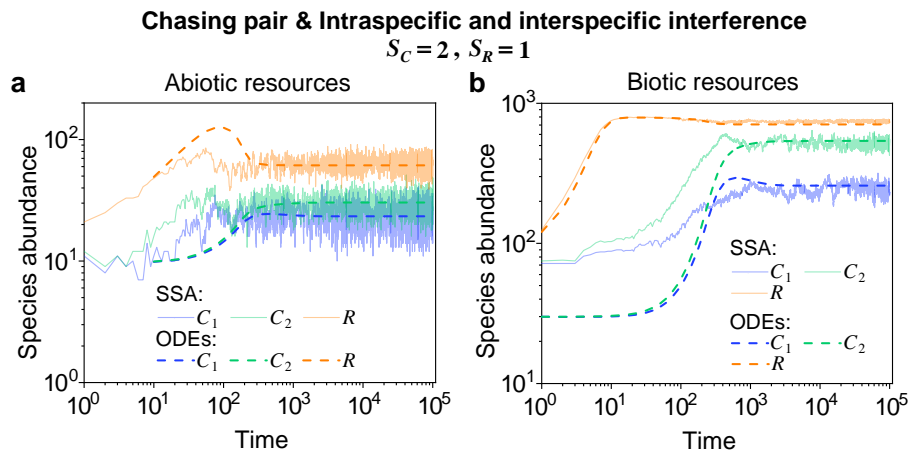


Figure S12. Outcomes of two consumers species competing for one resource species involving chasing pair and intra- and inter-specific interference. Here,  $S_C = 2$  and  $S_R = 1$ . (a-b) Both consumer species may coexist indefinitely with either lifeform of the resources regardless of stochasticity. The numerical results were calculated or simulated from Eqs. 1-4. In (a):  $a_1 = a_2 = 0.1, a'_1 = a'_2 = 0.14, k_1 = k_2 = 0.12, w_1 = w_2 = 0.15, D_1 = 0.0125, D_2 = 0.012, K_0 = 300, R_a = 5.5, d_1 = d_2 = 0.3, d'_1 = d'_2 = 0.5, a'_{12} = 0.14, d'_{12} = 5$ . In (b):  $a_1 = a_2 = 0.05, a'_1 = a'_2 = 0.07, k_1 = k_2 = 0.1, w_1 = w_2 = 0.2, D_1 = 0.011, D_2 = 0.01, K_0 = 800, R_0 = 0.5, d_1 = d_2 = 0.3, d'_1 = d'_2 = 0.5, a'_{12} = 0.07, d'_{12} = 0.02$ .

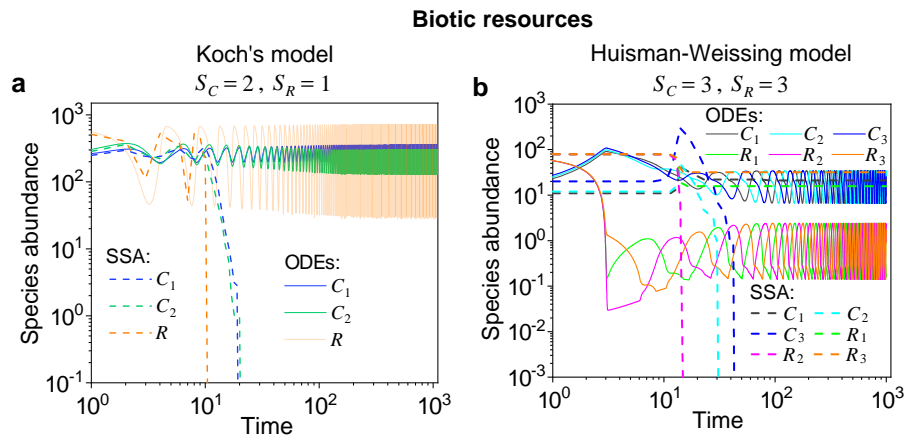


Figure S13. Stochasticity jeopardizes species coexistence. (a-b) Koch's model [13] and Huisman-Weissing model [14] were simulated with SSA using the same parameter settings as their deterministic model. Nevertheless, both cases of oscillating coexistence are vulnerable to stochasticity. See Ref. [13] and [14] for the parameters.

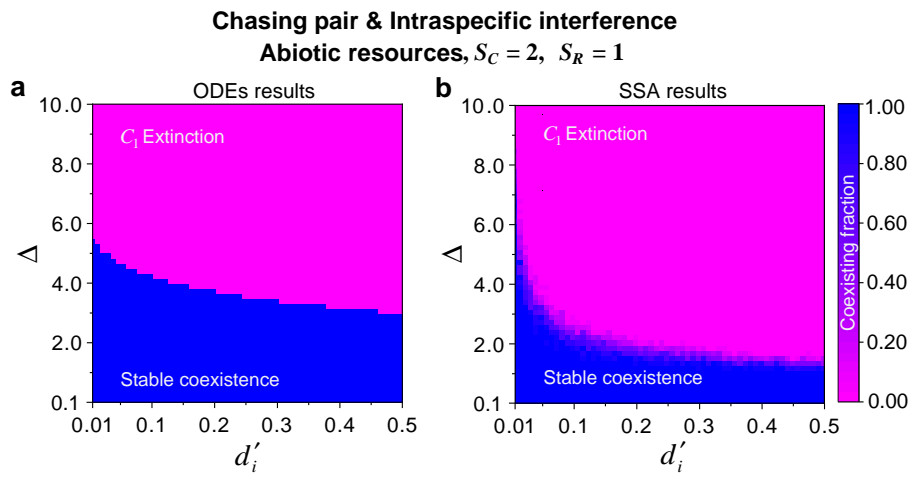


Figure S14. Phase diagrams in the scenario involving chasing pair and intraspecific interference. Here,  $S_C = 2$  and  $S_R = 1$ .  $D_i$  ( $i = 1, 2$ ) is the only parameter varying with the consumer species (with  $D_1 > D_2$ ), and  $\Delta = (D_1 - D_2)/D_2$  represents the competitive difference between the two species. (a) The ODEs results. (b) The SSA results (with the same parameter region as (a)). The species' coexisting fraction in each pixel was calculated from 16 random repeats. (a) and (b) were calculated from Eqs. 1, 2, 4. In (a-b):  $a_i = 0.1, a'_i = 0.125, d_i = 0.5, w_i = 0.1, k_i = 0.1$  ( $i = 1, 2$ );  $K_0 = 100, R_a = 5, D_2 = 0.0014$ .

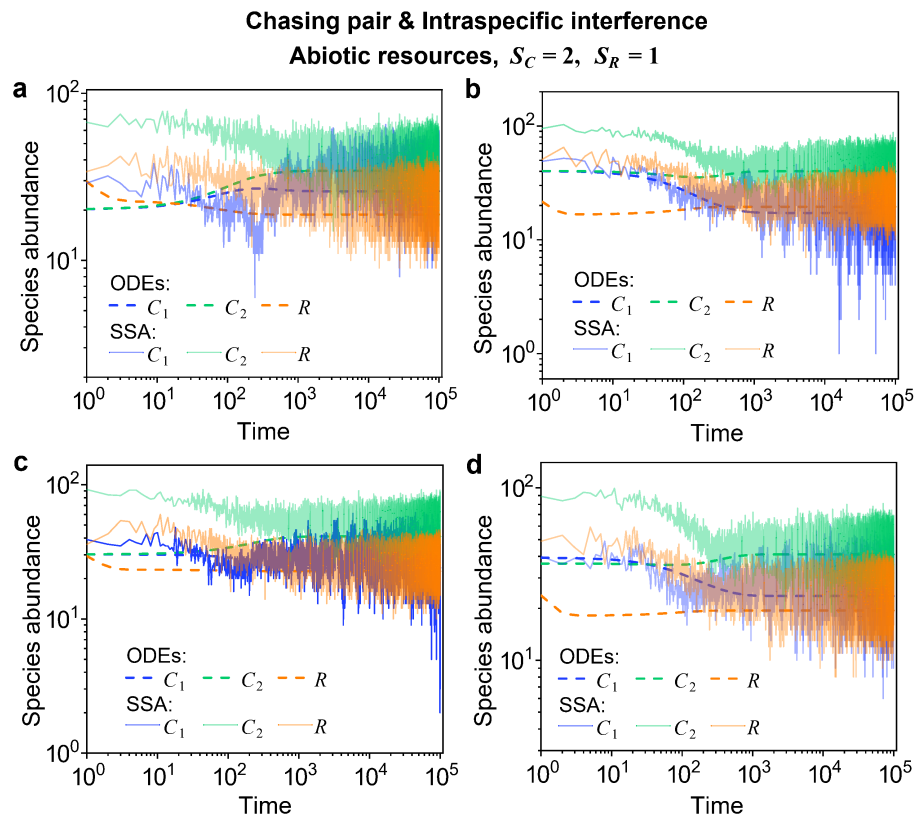


Figure S15. Time courses of the species abundances in the scenario involving chasing pair and intraspecific interference. Here,  $S_C = 2$  and  $S_R = 1$ . The time series in (a)-(d) correspond to the long-term version of that shown in Figure 3a-d.

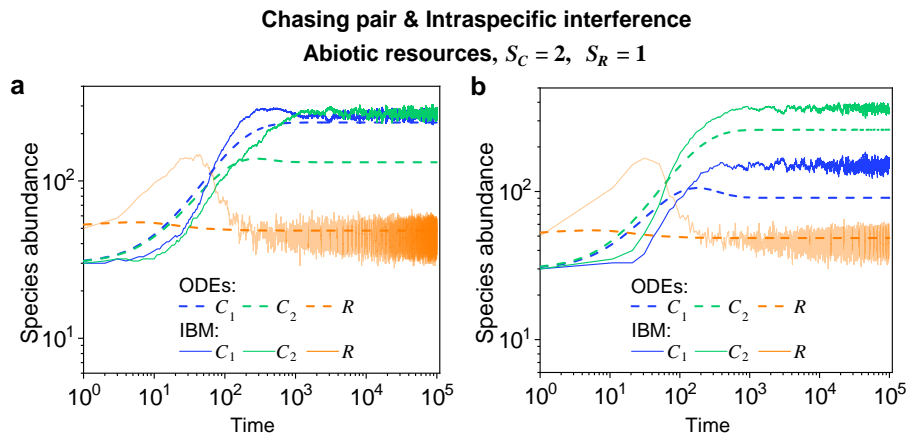


Figure S16. Time courses of the species abundances in the scenario involving chasing pair and intraspecific interference. In the stochastic simulations with IBM, two consumer species may coexist indefinitely with one type of resources. (a) and (b) were simulated from Eqs. 1, 2, 4. In (a-b):  $L = 50$ ,  $r^{(C)} = 4.5$ ,  $r^{(I)} = 4.5$ ,  $v_C = 1$ ,  $v_R = 1$ ,  $a_i = 0.765$ ,  $a'_i = 1.071$ ,  $k_i = 0.2$ ,  $d_i = 0.4$ ,  $d'_i = 0.6$ ,  $w_i = 0.45$ ,  $D_2 = 0.010$ ,  $K_0 = 500$ ,  $R_a = 10$ . In (a):  $D_1 = 0.013$ . In (b):  $D_1 = 0.016$ .

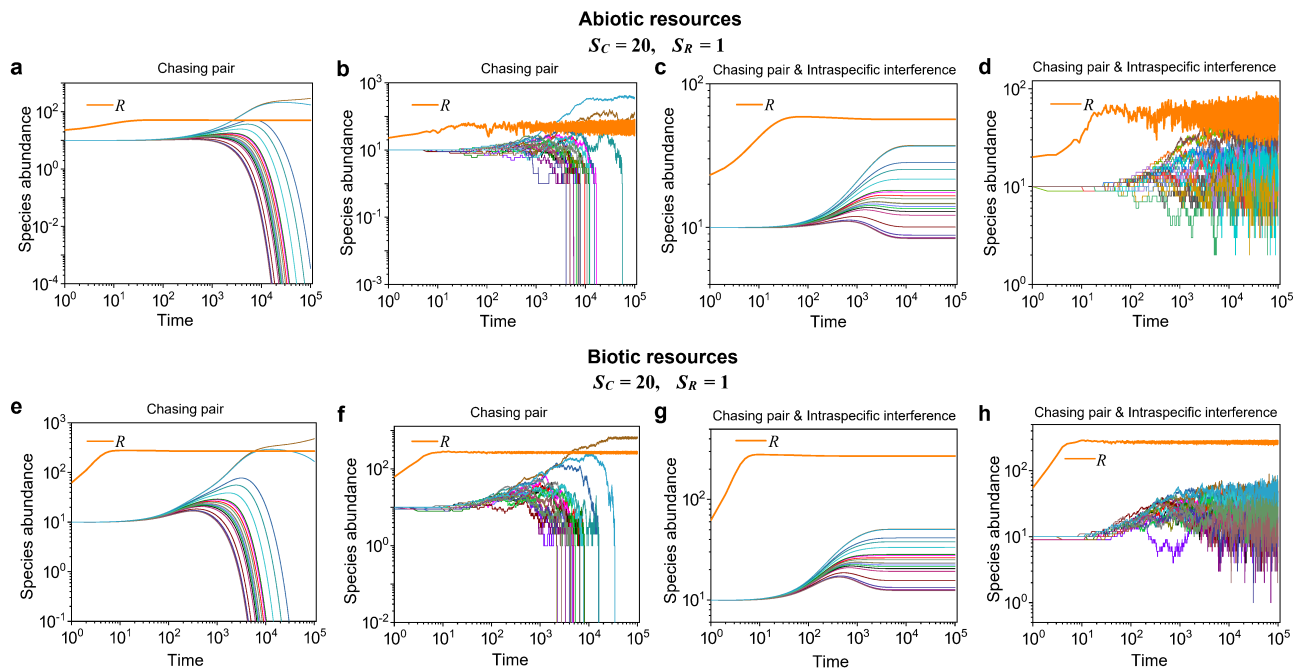


Figure S17. Intraspecific interference enables many consumers species to coexist with one type of resources. Here,  $S_C = 20$  and  $S_R = 1$ .  $D_i$  is the only parameter varying with the consumer species ( $i = 1, \dots, S_C$ ), which was randomly drawn from a uniform distribution  $\mathcal{U}(0, 1)$ . (a, c, e, g) Time courses of the species abundances simulated with ODEs. (b, d, f, h) Time courses of the species abundances simulated with SSA. (c, d, g, h) Intraspecific interference facilitates species coexistence regardless of stochasticity. (a),(b), (e) and (f) were simulated from Eqs. 1, 4.. (c), (d), (g) and (h) were simulated from Eqs. 1, 2, 4. In (a-d):  $a_i = 0.1, d_i = 0.5, w_i = 0.1, k_i = 0.1, D_i = 0.001 + 0.001 \times \mathcal{U}(0, 1)$  ( $i = 1, \dots, 20$ );  $K_0 = 10000, R_a = 5$ . In (a-b):  $a'_i = 0, d'_i = 0$ . In (c-d):  $a'_i = 0.125, d'_i = 0.1$ . In (e-h):  $a_i = 0.1, d_i = 0.3, R_0 = 0.95, w_i = 0.1, k_i = 0.1, D_i = 0.004 + 0.002 \times \mathcal{U}(0, 1)$  ( $i = 1, \dots, 20$ );  $K_0 = 300$ . In (e-f):  $a'_i = 0, d'_i = 0$ . In (g-h):  $a'_i = 0.125, d'_i = 0.3$ .

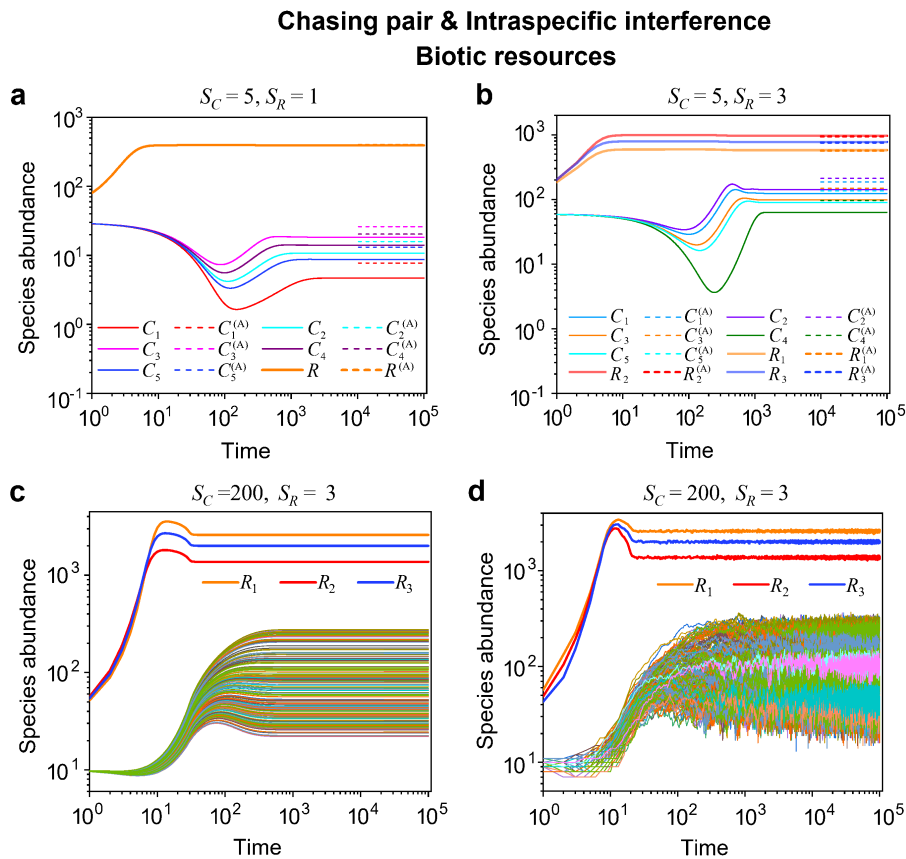


Figure S18. Intraspecific interference enables a wide range of consumers species to coexist with a handful type of resources. Here,  $D_i$  ( $i = 1, \dots, S_C$ ) is the only parameter that varies with the consumer species, which was randomly drawn from a uniform distribution  $\mathcal{U}(0, 1)$ . (a-c) Time courses of the species abundances simulated with ODEs. The dotted lines in (a-b) are the analytical steady-state solutions (marked with superscript “A”), which were calculated from Eqs. S55-S64. (d) Time courses of the species abundances simulated with SSA. The numerical results in (a)-(d) were simulated from Eqs. 1, 2, 4. In (a):  $a_i = 0.04, a'_i = 0.056, d_i = 0.6, d'_i = 0.04, w_i = 0.45, k_i = 0.15, D_1 = 0.062, D_2 = 0.059, D_3 = 0.057, D_4 = 0.058, D_5 = 0.060, K_0 = 400, R_a = 0.9$ . In (b):  $a_{il} = 0.05, a'_i = 0.07, d_{il} = 1.05, d'_i = 0.018, w_{il} = 0.45, k_{il} = 0.16$  ( $i = 1, \dots, 5, l = 1, 2, 3$ );  $K_0^{(1)} = 600, K_0^{(2)} = 1000, K_0^{(3)} = 800, R_0^{(1)} = R_0^{(2)} = 0.9, R_0^{(3)} = 0.95, D_1 = 0.062, D_2 = 0.0615, D_3 = 0.0639, D_4 = 0.066, D_5 = 0.0644$ . In (c-d):  $a_{il} = 0.2, a'_i = 0.25, d_{il} = 0.4, d'_i = 0.2, w_{il} = 0.3, k_{il} = 0.3, R_0^{(1)} = 0.85, R_0^{(2)} = 0.95, R_0^{(3)} = 0.9, K_0^{(1)} = 4000, K_0^{(2)} = 2000, K_0^{(3)} = 3000, D_i = 0.02 + 0.03 \times \mathcal{U}(0, 1)$  ( $i = 1, \dots, 200, l = 1, 2, 3$ ).

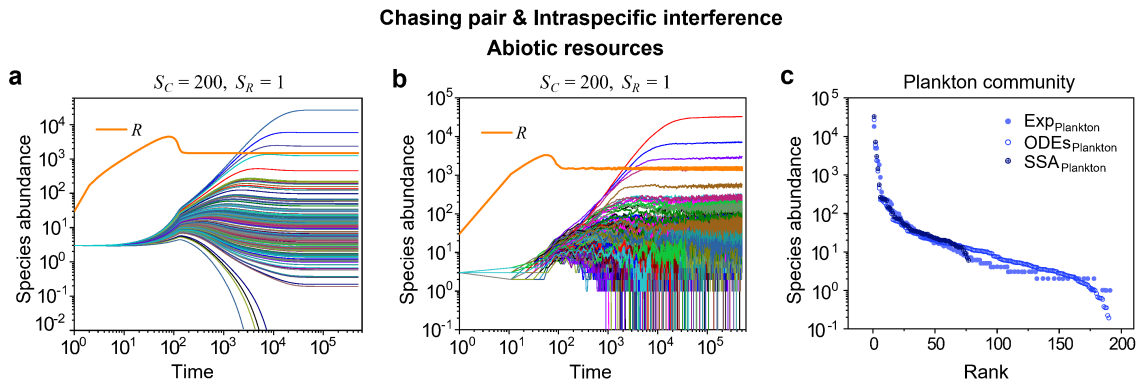


Figure S19. A model of intraspecific interference semi-quantitatively illustrates the rank-abundance curve of a plankton community ( $S_C \gg S_R$ ). (a-b) Intraspecific interference enables a wide range of consumer species to coexist with one type of resources. (a) Time courses of the species abundances simulated with ODEs. (b) Time series of the species abundances simulated with SSA (with the same parameter settings as (a)). (c) The rank-abundance curve of a plankton community. The solid dots represent the experimental data (marked with “Exp”) reported in a recent study [36] (TARA\_139.SUR.180.2000.DNA), while the hollow dots and those with “+” center are the ODEs and SSA results constructed from timestamp  $t = 5.0 \times 10^5$  in the time series (see (a) and (b)), respectively. The Shannon entropies of the experimental data and simulation results for the plankton community are:  $H_{\text{Exp(ODEs,SSA)}}^{\text{Plankton}} = 2.85(2.18, 2.00)$ . In the model settings,  $S_C = 200$  and  $S_R = 1$ .  $D_i$  ( $i = 1, \dots, S_C$ ) is the only parameter that varies with the consumer species, which was randomly drawn from a Gaussian distribution  $\mathcal{N}(\mu, \sigma)$ . Here,  $\mu$  and  $\sigma$  are the mean and standard deviation of the distribution. The numerical results in (a)-(c) were simulated from Eqs. 1, 2, 4. In (a-c):  $a_i = 0.1, a'_i = 0.125, d'_i = 0.5, d_i = 0.2, w_i = 0.2, k_i = 0.1, K_0 = 10^5, D_i = \mathcal{N}(1, 0.38) \times 0.008$  ( $i = 1, \dots, 200$ ),  $R_a = 150$ .

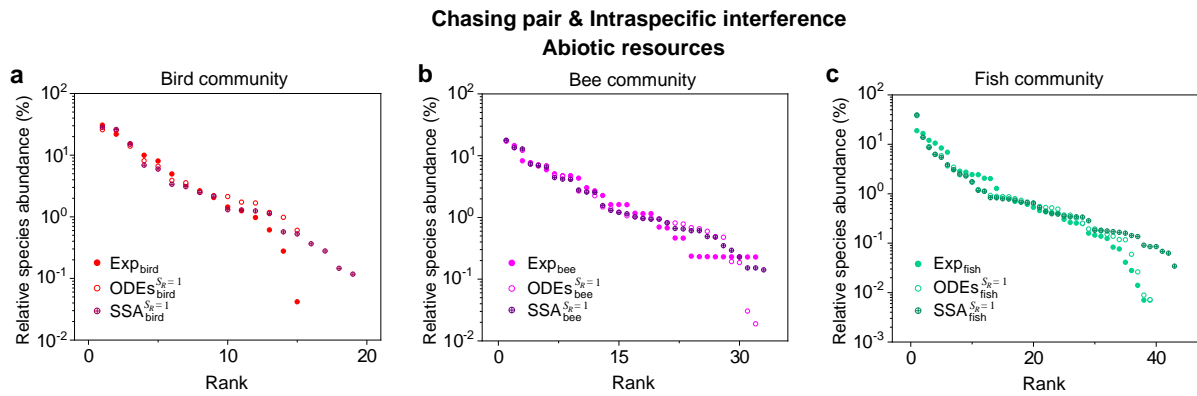


Figure S20. A model of intraspecific interference illustrates the rank-abundance curves across different ecological communities ( $S_C \gg S_R$ ). The solid dots represent the experimental data (marked with “Exp”) reported in existing studies [37, 42, 53], while the hollow dots and those with “+” center are the ODEs and SSA results constructed from timestamp  $t = 1.0 \times 10^5$  in the time series (see Figure S21a-g), respectively. In the model settings,  $S_R = 1$ ,  $S_C = 20$  (in (a)), 35 (in (b)) or 45 (in (c)).  $D_i$  ( $i = 1, \dots, S_C$ ) is the only parameter varying with the consumer species, which was randomly drawn from a Gaussian distribution. The Shannon entropies of the experimental data and simulation results for each ecological community are:  $H_{\text{Exp}(\text{ODEs,SSA})}^{\text{bird}} = 2.98(3.06, 2.98)$ ,  $H_{\text{Exp}(\text{ODEs,SSA})}^{\text{bee}} = 4.04(4.02, 4.02)$ ,  $H_{\text{Exp}(\text{ODEs,SSA})}^{\text{fish}} = 3.78(3.40, 3.41)$ . In the Kolmogorov-Smirnov (K-S) test, the probabilities ( $p$  values) that the simulation results and the corresponding experimental data come from identical distributions are:  $p_{\text{ODEs}}^{\text{bird}} = 0.89$ ,  $p_{\text{SSA}}^{\text{bird}} = 0.88$ ;  $p_{\text{ODEs}}^{\text{bee}} = 0.47$ ,  $p_{\text{SSA}}^{\text{bee}} = 0.75$ ;  $p_{\text{ODEs}}^{\text{fish}} = 0.88$ ,  $p_{\text{SSA}}^{\text{fish}} = 0.77$ . With a significance threshold of 0.05, none of the  $p$  values suggest there exists a statistically significant difference. The numerical results in (a)-(c) were simulated from Eqs. 1, 2, 4. In (a):  $a_i = 0.1$ ,  $a'_i = 0.125$ ,  $d_i = 0.5$ ,  $d'_i = 0.6$ ,  $w_i = 0.22$ ,  $k_i = 0.1$ ,  $D_i = 0.016 \times \mathcal{N}(1, 0.35)$  ( $i = 1, \dots, 20$ );  $R_a = 350$ ,  $K_0 = 10^6$ . In (b):  $a_i = 0.1$ ,  $a'_i = 0.125$ ,  $d_i = 0.5$ ,  $d'_i = 0.6$ ,  $w_i = 0.22$ ,  $k_i = 0.1$ ,  $D_i = 0.012 \times \mathcal{N}(1, 0.35)$  ( $i = 1, \dots, 35$ );  $R_a = 350$ ,  $K_0 = 10^6$ . In (c):  $a_i = 0.1$ ,  $a'_i = 0.14$ ,  $d_i = 0.5$ ,  $d'_i = 0.5$ ,  $w_i = 0.2$ ,  $k_i = 0.1$ ,  $D_i = 0.015 \times \mathcal{N}(1, 0.32)$  ( $i = 1, \dots, 45$ );  $R_a = 550$ ,  $K_0 = 10^6$ .

**Chasing pair & Intraspecific interference**  
**Abiotic resources**

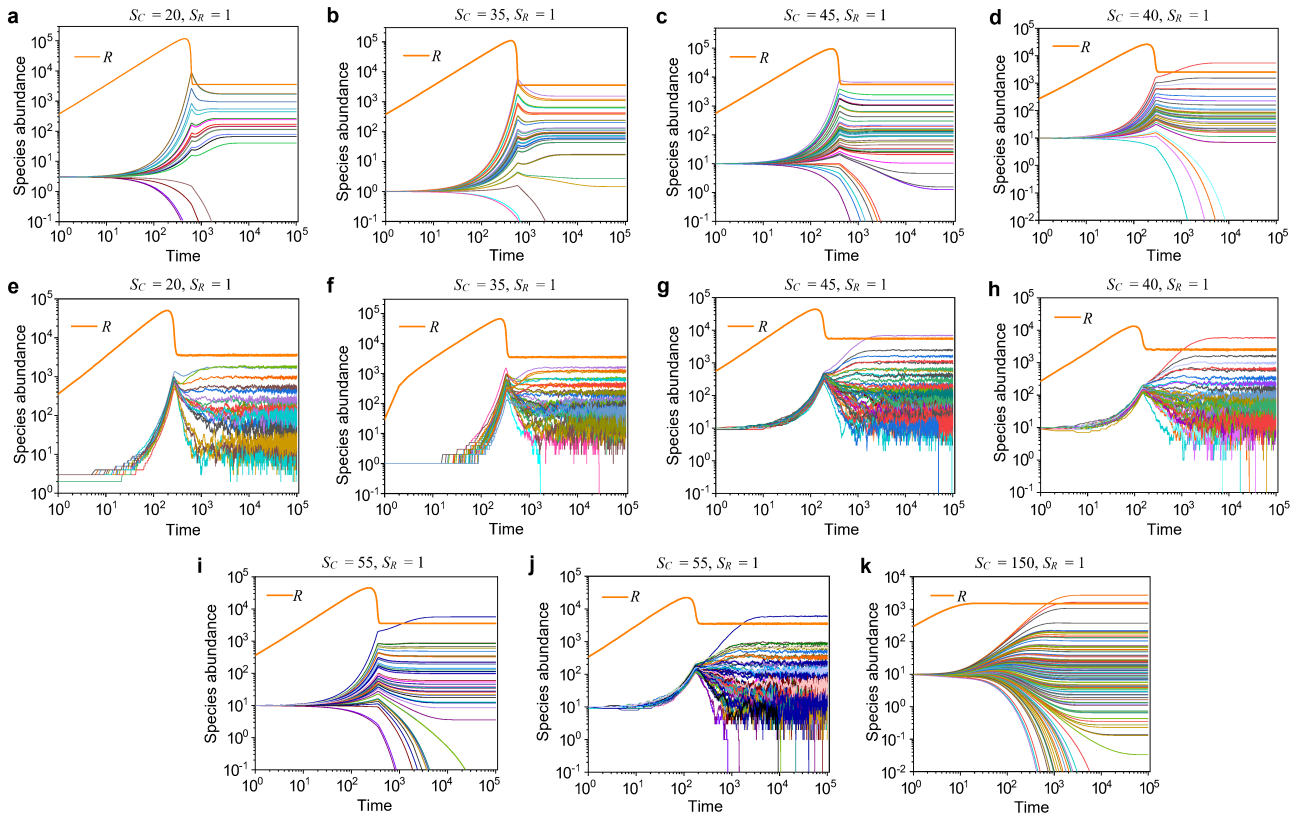


Figure S21. Time courses of the species abundances in the scenario involving chasing pair and intraspecific interference. The time series in (a, e), (b, f), (c, g), (d, h), (i, j) and (k) correspond to that shown in Figures S20a-c, 4e (bat), 4e (lizard) and 4d (butterfly), respectively.

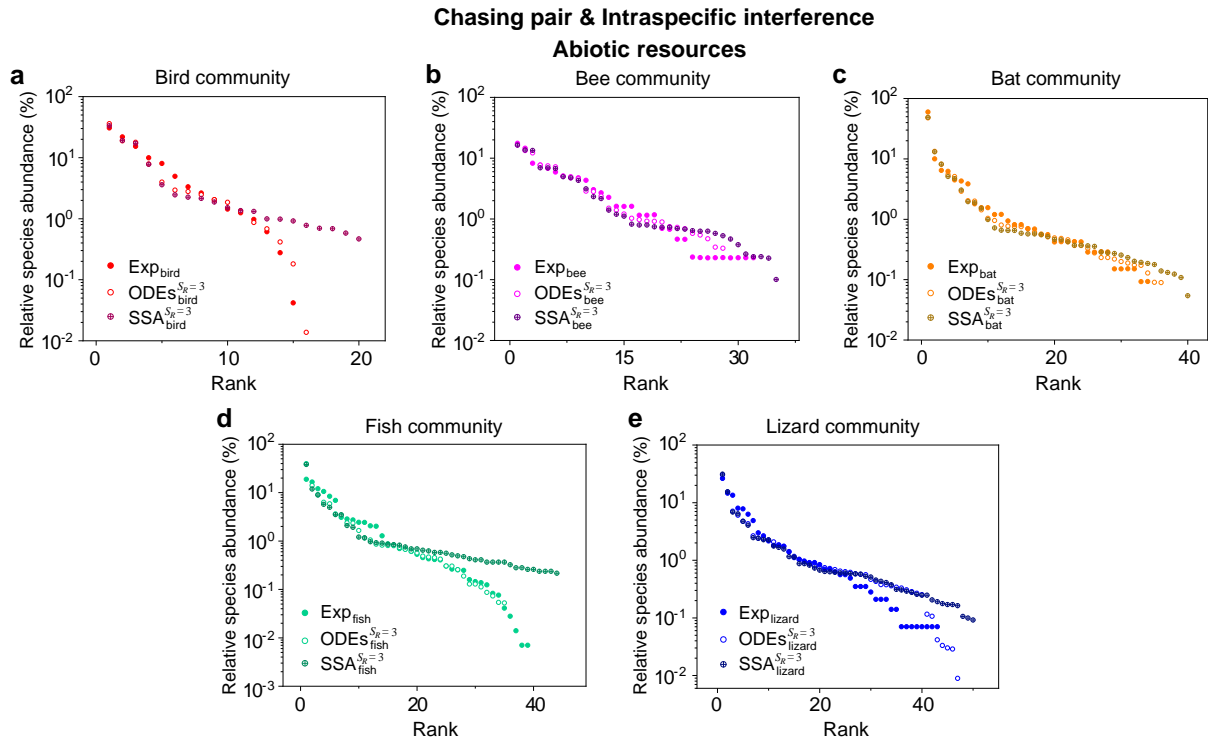


Figure S22. A model of intraspecific interference illustrates the rank-abundance curves across different ecological communities ( $S_C \gg S_R$ ). The solid dots represent the experimental data (marked with “Exp”) reported in existing studies [37, 40, 42, 53], while the hollow dots and those with “+” center are the ODEs and SSA results constructed from timestamp  $t = 1.0 \times 10^5$  in the time series (see Figure S23), respectively. In the model settings,  $S_R = 3$ ,  $S_C = 20$  (in (a)), 35 (in (b)), 40 (in (c)), 45 (in (d)) or 50 (in (e)).  $D_i$  ( $i = 1, \dots, S_C$ ) is the only parameter varying with the consumer species, which was randomly drawn from a Gaussian distribution. The Shannon entropies of the experimental data and simulation results for each ecological community are:  $H_{\text{Exp(ODEs,SSA)}}^{\text{Bird}} = 2.98(2.98, 3.26)$ ,  $H_{\text{Exp(ODEs,SSA)}}^{\text{Bee}} = 4.04(4.34, 4.35)$ ,  $H_{\text{Exp(ODEs,SSA)}}^{\text{Bat}} = 3.00(3.00, 3.00)$ ,  $H_{\text{Exp(ODEs,SSA)}}^{\text{Fish}} = 3.78(3.28, 3.64)$ ,  $H_{\text{Exp(ODEs,SSA)}}^{\text{Lizard}} = 4.05(3.94, 3.94)$ . In the K-S test, the  $p$  values that the simulation results and the corresponding experimental data come from identical distributions are:  $p_{\text{Exp vs ODEs}}^{\text{Bird}} = 0.59$ ,  $p_{\text{Exp vs SSA}}^{\text{Bird}} = 0.43$ ,  $p_{\text{Exp vs ODEs}}^{\text{Bee}} = 0.47$ ,  $p_{\text{Exp vs SSA}}^{\text{Bee}} = 0.33$ ,  $p_{\text{Exp vs ODEs}}^{\text{Bat}} = 0.42$ ,  $p_{\text{Exp vs SSA}}^{\text{Bat}} = 0.27$ ,  $p_{\text{Exp vs ODEs}}^{\text{Fish}} = 0.22$ ,  $p_{\text{Exp vs SSA}}^{\text{Fish}} = 0.06$ ,  $p_{\text{Exp vs ODEs}}^{\text{Lizard}} = 0.56$ ,  $p_{\text{Exp vs SSA}}^{\text{Lizard}} = 0.36$ . With a significance threshold of 0.05, none of the  $p$  values suggest there exists a statistically significant difference. The numerical results in (a)-(e) were simulated from Eqs. 1, 2, 4. In (a-e):  $a_{il} = 0.1$ ,  $a'_i = 0.125$ ,  $d_{il} = 0.5$ . In (a):  $d'_i = 0.3$ ,  $w_{il} = 0.2$ ,  $k_{il} = 0.12$ ,  $K_0^{(1)} = 8 \times 10^4$ ,  $K_0^{(2)} = 5 \times 10^4$ ,  $K_0^{(3)} = 3 \times 10^4$ ,  $D_i = 0.021 \times \mathcal{N}(1, 0.28)$  ( $i = 1, \dots, 20$ ,  $l = 1, 2, 3$ );  $R_a^{(1)} = 180$ ,  $R_a^{(2)} = 160$ ,  $R_a^{(3)} = 140$ . In (b):  $d'_i = 0.6$ ,  $w_{il} = 0.2$ ,  $k_{il} = 0.12$ ,  $K_0^{(1)} = 8 \times 10^4$ ,  $K_0^{(2)} = 5 \times 10^4$ ,  $K_0^{(3)} = 3 \times 10^4$ ,  $D_i = 0.017 \times \mathcal{N}(1, 0.3)$  ( $i = 1, \dots, 35$ ,  $l = 1, 2, 3$ );  $R_a^{(1)} = 180$ ,  $R_a^{(2)} = 160$ ,  $R_a^{(3)} = 110$ . In (c):  $d'_i = 0.4$ ,  $w_{il} = 0.3$ ,  $k_{il} = 0.12$ ,  $K_0^{(1)} = 10^5$ ,  $K_0^{(2)} = 5 \times 10^4$ ,  $K_0^{(3)} = 3 \times 10^4$ ,  $D_i = 0.023 \times \mathcal{N}(1, 0.34)$  ( $i = 1, \dots, 40$ ,  $l = 1, 2, 3$ );  $R_a^{(1)} = 180$ ,  $R_a^{(2)} = 120$ ,  $R_a^{(3)} = 40$ . In (d):  $d'_i = 0.3$ ,  $w_{il} = 0.3$ ,  $k_{il} = 0.12$ ,  $K_0^{(1)} = 8 \times 10^4$ ,  $K_0^{(2)} = 5 \times 10^4$ ,  $K_0^{(3)} = 3 \times 10^4$ ,  $D_i = 0.027 \times \mathcal{N}(1, 0.32)$  ( $i = 1, \dots, 45$ ,  $l = 1, 2, 3$ );  $R_a^{(1)} = 80$ ,  $R_a^{(2)} = 60$ ,  $R_a^{(3)} = 40$ . In (e):  $d'_i = 0.3$ ,  $w_{il} = 0.3$ ,  $k_{il} = 0.2$ ,  $K_0^{(1)} = 3 \times 10^5$ ,  $K_0^{(2)} = 10^5$ ,  $K_0^{(3)} = 3 \times 10^4$ ,  $D_i = 0.034 \times \mathcal{N}(1, 0.34)$  ( $i = 1, \dots, 50$ ,  $l = 1, 2, 3$ );  $R_a^{(1)} = 380$ ,  $R_a^{(2)} = 260$ ,  $R_a^{(3)} = 140$ .

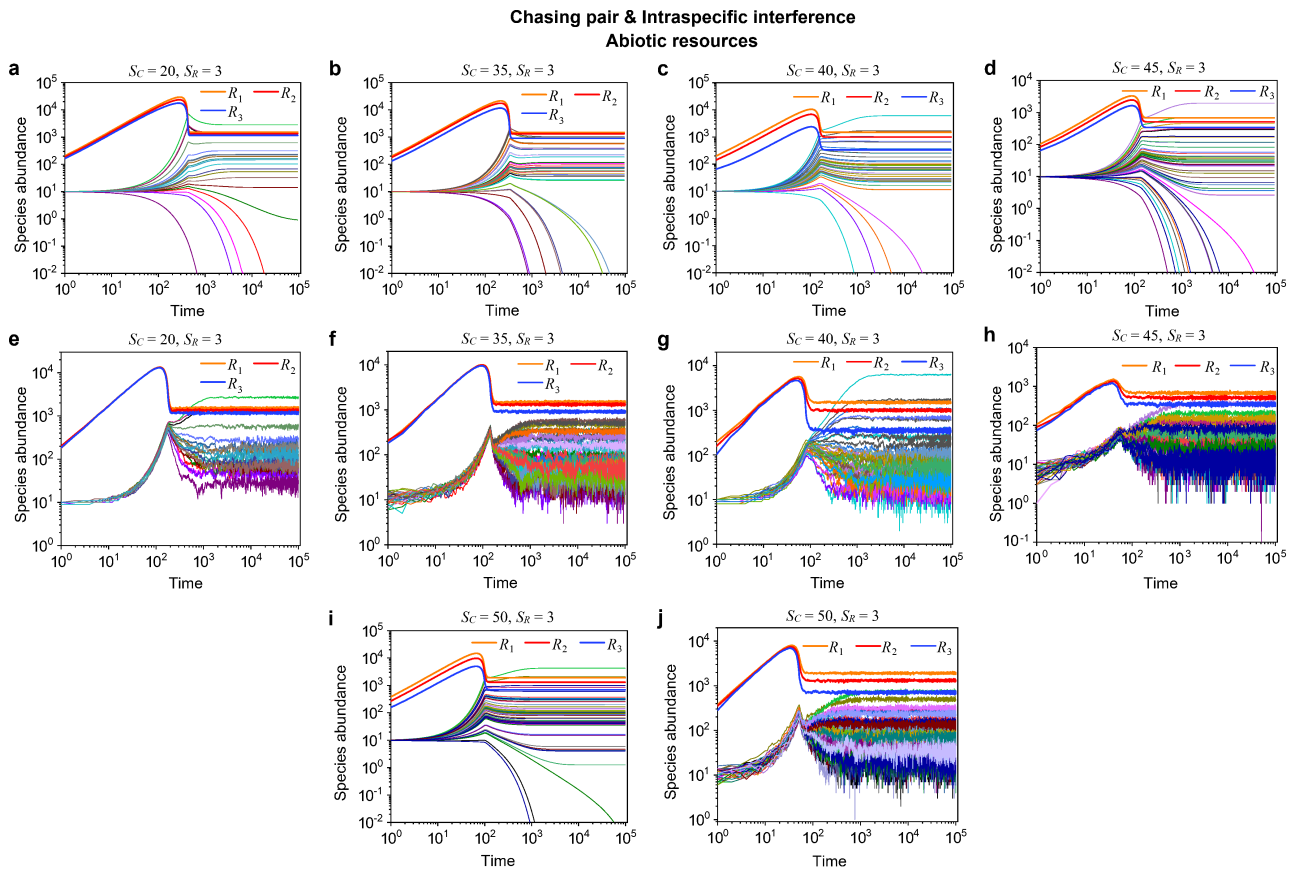


Figure S23. Time courses of the species abundances in the scenario involving chasing pair and intraspecific interference. The time series in (a, e), (b, f), (c, g), (d, h), and (i, j) correspond to that shown in Figure S22a-e, respectively.

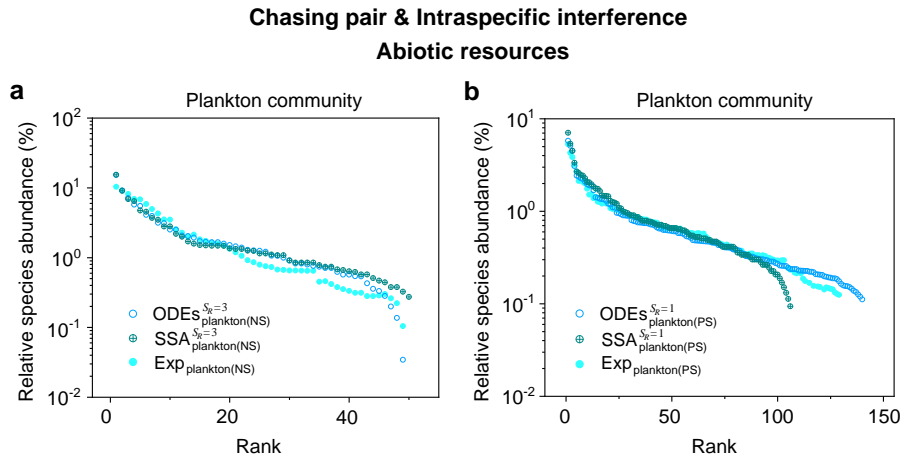


Figure S24. A model of intraspecific interference illustrates the rank-abundance curves across different plankton communities ( $S_C \gg S_R$ ). The solid dots represent the experimental data (marked with “Exp”) reported in a recent study[35], while the hollow dots and those with “+” center are the ODEs and SSA results constructed from timestamp  $t = 1.0 \times 10^5$  in the time series (see Figure S23), respectively. The plankton community data were obtained separately from the Norwegian Sea (NS) and Pacific Station (PS). In the model settings,  $S_R = 1$  (in (b)), 3 (in (a));  $S_C = 50$  (in (a)), 150 (in (b)).  $D_i$  ( $i = 1, \dots, S_C$ ) is the only parameter varying with the consumer species, which was randomly drawn from a Gaussian distribution. The Shannon entropies of the experimental data and simulation results for each plankton community are:  $H_{\text{Exp}(\text{ODEs,SSA})}^{\text{plankton(NS)}} = 4.67(4.85, 4.90)$ ,  $H_{\text{Exp}(\text{ODEs,SSA})}^{\text{plankton(PS)}} = 4.68(6.53, 6.16)$ . In the K-S test, the  $p$  values that the simulation results and the corresponding experimental data come from identical distributions are:  $p_{\text{ODEs}}^{\text{plankton(NS)}} = 0.31$ ,  $p_{\text{SSA}}^{\text{plankton(NS)}} = 0.14$ ;  $p_{\text{ODEs}}^{\text{plankton(PS)}} = 0.08$ ,  $p_{\text{SSA}}^{\text{plankton(PS)}} = 0.28$ . With a significance threshold of 0.05, none of the  $p$  values suggest there exists a statistically significant difference. The numerical results in (a)-(b) were simulated from Eqs. 1, 2, 4. In (a):  $a_{il} = 0.1$ ,  $a'_i = 0.125$ ,  $d_{il} = 0.5$ ,  $d'_i = 0.2$ ,  $w_{il} = 0.3$ ,  $k_{il} = 0.2$ ,  $K_0^{(1)} = 8 \times 10^4$ ,  $K_0^{(2)} = 5 \times 10^4$ ,  $K_0^{(3)} = 3 \times 10^4$ ,  $R_a^{(1)} = 280$ ,  $R_a^{(2)} = 200$ ,  $R_a^{(3)} = 150$ ,  $D_i = 0.035 \times \mathcal{N}(1, 0.25)$  ( $i = 1, \dots, 50$ ,  $l = 1, 2, 3$ ). In (b):  $a_i = 0.1$ ,  $a'_i = 0.125$ ,  $d_i = 0.3$ ,  $d'_i = 0.3$ ,  $w_i = 0.3$ ,  $k_i = 0.2$ ,  $D_i = 0.025 \times \mathcal{N}(1, 0.25)$  ( $i = 1, \dots, 150$ ,  $l = 1, 2, 3$ );  $R_a = 350$ ,  $K_0 = 10^4$ .

**Chasing pair & Intraspecific interference**  
**Abiotic resources**

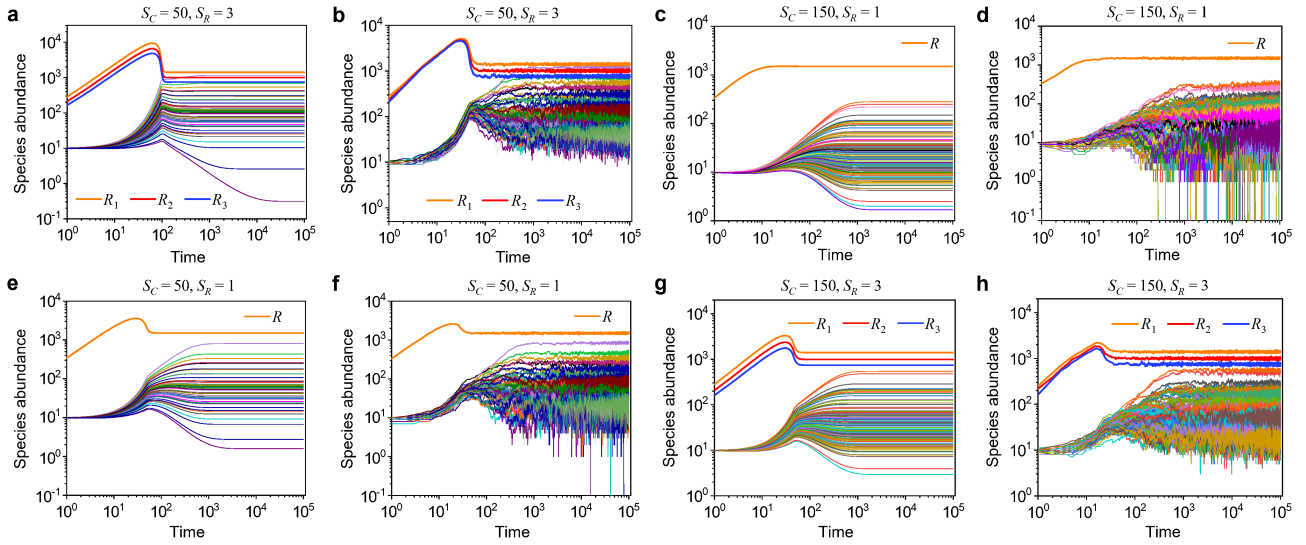


Figure S25. Time courses of the species abundances in the scenario involving chasing pair and intraspecific interference. The time series in (a-b), (c-d), (e-f), and (g-h) correspond to that shown in Figures S24a, S24b, 4f (NS), and 4f (PS), respectively.

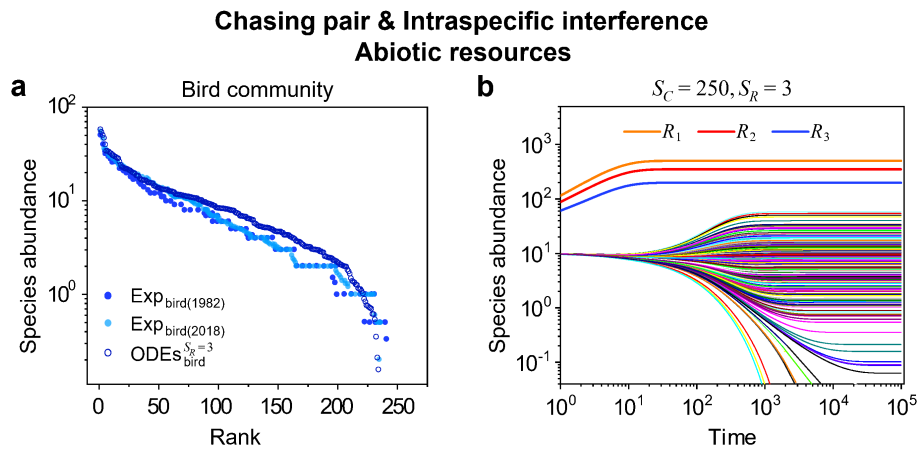


Figure S26. A model of intraspecific interference illustrates the rank-abundance curve of a bird community ( $S_C \gg S_R$ ). (a) The rank-abundance curve. The solid dots represent the bird community data (marked with “Exp”) collected longitudinally within the same Amazonian region in 1982 (blue) and 2018 (cyan) [38, 39]. The hollow dots are the ODEs results constructed from timestamp  $t = 1.0 \times 10^5$  in the time series (see (b)). (b) Time courses of the species abundances simulated with ODEs. In the model settings,  $S_R = 3$  and  $S_C = 250$ .  $D_i$  ( $i = 1, \dots, S_C$ ) is the only parameter varying with the consumer species, which was randomly drawn from a Gaussian distribution. The Shannon entropies of the experimental data and simulation results for the bird community are  $H_{\text{Exp(ODEs)}}^{\text{bird(1982/2018)}} = 5.67/6.63(7.31)$ . In the K-S test, the  $p$  values that the simulation results and the corresponding experimental data come from identical distributions are:  $p_{\text{ODEs}}^{\text{bird(1982)}} = 0.28$ ,  $p_{\text{ODEs}}^{\text{bird(2018)}} = 0.46$ . With a significance threshold of 0.05, none of the  $p$  values suggest there exists a statistically significant difference. The numerical results in (a)-(b) were simulated from Eqs. 1, 2, 4. In (a-b):  $a_{il} = 0.1$ ,  $a'_i = 0.125$ ,  $d_{il} = 0.5$ ,  $d'_i = 0.6$ ,  $w_{il} = 0.3$ ,  $k_{il} = 0.2$ ,  $D_i = 0.032 \times \mathcal{N}(1, 0.17)$  ( $i = 1, \dots, 250, l = 1, 2, 3$ );  $K_0^{(1)} = 5 \times 10^4$ ,  $K_0^{(2)} = 3 \times 10^4$ ,  $K_0^{(3)} = 10^4$ ,  $R_a^{(1)} = 100$ ,  $R_a^{(2)} = 70$ ,  $R_a^{(3)} = 40$ .

## Chasing pair &amp; Intraspecific interference

$$S_C = 40, S_R = 1$$

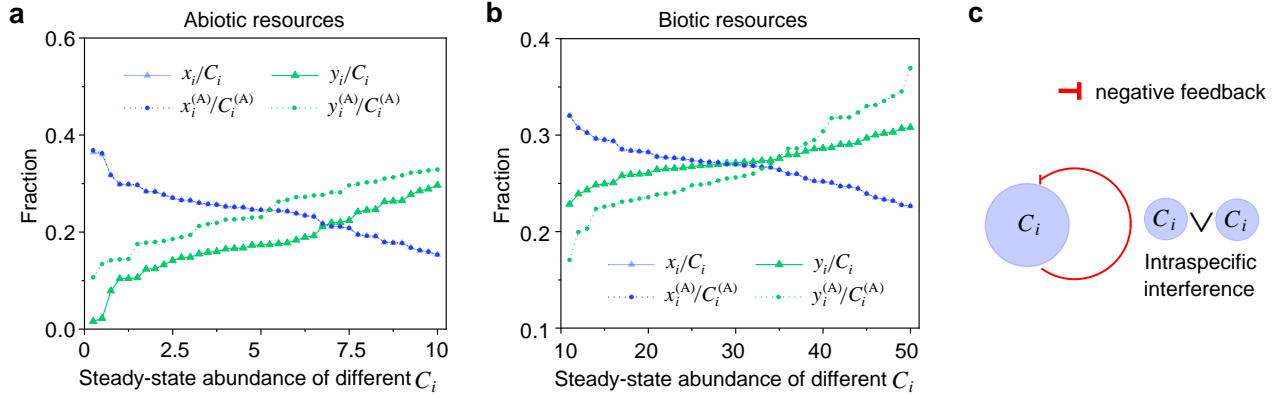


Figure S27. Intraspecific interference results in a negative feedback loop and promotes biodiversity. Here,  $S_C = 40$  and  $S_R = 1$ . (a-b) The fraction of individuals engaged in pairwise encounters for each consumer species within a model system. Here,  $x_i$  represents  $C_i^{(P)} \vee R^{(P)}$  and  $y_i$  represents  $C_i^{(P)} \vee C_i^{(P)}$ .  $x_i/C_i$  and  $y_i/C_i$  stand for the fractions of consumers within a chasing pair or an interference pair. The icons are the numerical results (triangles) or analytical solutions (dots) to the steady-state abundances of different consumer species  $C_i$  ( $i = 1, \dots, 40$ ). (c) The formation of intraspecific interference effectively results in a self-inhibiting negative feedback loop. As the population size of  $C_i$  increases, a larger portion of the  $C_i$  individuals are then trapped in the interference pair which are temporarily absent from hunting. This lead to a smaller  $x_i/C_i$ , and effectively forms a self-inhibiting negative feedback loop. The numerical results in (a) and (b) were calculated from Eqs. 1, 2, 4, while the analytical solutions (marked with superscript “(A)”) were calculated from Eqs. S50, S63, S64. In (a):  $a_i = 0.4, a'_i = 0.48, d_i = 0.6, d'_i = 0.7, w_i = 0.14, k_i = 0.12, R_a = 2.2, K_0 = 1000, D_i = 0.004 \times \mathcal{N}(1, 0.2)$  ( $i = 1, \dots, 40$ ). In (b):  $a_i = 0.04, a'_i = 0.056, d_i = 0.6, d'_i = 0.2, w_i = 0.4, k_i = 0.15, R_0 = 0.8, K_0 = 400, D_i = 0.016 \times \mathcal{N}(1, 0.1)$  ( $i = 1, \dots, 40$ ).